

**DESIGN AND SYNTHESIS OF RHODAMINE  
BASED FLUORESCENT AND COLORIMETRIC  
SENSORS FOR THE DETECTION OF GOLD IONS**

**A Thesis Submitted to  
the Graduate School of Engineering and Sciences of  
İzmir Institute of Technology  
in Partial Fulfillment of the Requirements for the Degree of**

**DOCTOR OF PHILOSOPHY**

**in Chemistry**

**by  
Erman KARAKUŞ**

**July, 2017  
İZMİR**

We approve the thesis of **Erman KARAKUŞ**

**Examining Committee Members:**

---

**Assoc. Prof. Dr. Mustafa EMRULLAHOĞLU**

Department of Chemistry, İzmir Institute of Technology

---

**Prof. Dr. Mehtap EMİRDAĞ EANES**

Department of Chemistry, İzmir Institute of Technology

---

**Assoc. Prof. Dr. Yaşar AKDOĞAN**

Department of Materials Science and Engineering, İzmir Institute of Technology

---

**Assoc. Prof. Dr. Murat IŞIK**

Department of Materials Science and Engineering, Bingöl University

---

**Assist. Prof. Dr. Nesrin HORZUM POLAT**

Department of Engineering Science, İzmir Katip Çelebi University

**25 July 2017**

---

**Assoc. Prof. Dr. Mustafa EMRULLAHOĞLU**

Supervisor, Department of Chemistry,  
İzmir Institute of Technology

---

**Prof. Dr. Ahmet Emin EROĞLU**

Head of the Department of Chemistry

---

**Prof. Dr. Aysun SOFUOĞLU**

Dean of the Graduate School of  
Engineering and Science

## ACKNOWLEDGEMENTS

During my PhD studies, there are many people to thank. I would like to express my deepest appreciation to the people who provide help, support and guidance through my graduate study at İzmir Institute of Technology. I am heartily thankful to my supervisor Assoc. Prof. Dr. Mustafa Emrulloğlu for his patient guidance, encouragement and excellent advice throughout this study. This thesis could not have been written without his astute guidance. It was honor to study with him.

Also, I would like to thank all old and new members of İYTE Emrulloğlu research group. I would like to extend special thanks to Muhammed Üçüncü for his support, help and friendship for thirteen years.

I would like to thank to Ayşenur Çataler Karakuş, Muhammed Üçüncü, Melek Özkan and Dane Rusçuklu for cell imaging studies, Assist. Prof. Dr. Tuna Subaşı for HRMS analyses.

Special thanks to Prof. Dr. Mehtap Emirdağ Eanes, Assoc. Prof. Dr. Yaşar Akdoğan, Assoc. Prof. Dr. Murat Işık and Assist. Prof. Dr. Nesrin Horzum Polat for participating as committee member and for reviewing my work.

I would like to thank to TUBITAK for fellowship support (2211-A) during this project.

Endless gratitude is also extended to my parents and all my friends for providing love and support every time.

Finally, I would especially like to thank my wife, Ayşenur ÇATALER KARAKUŞ for loving me unconditionally and for her everlasting encouragement. I would like to thank my little daughter, Arya KARAKUŞ for being my motivation source. I love her more than anything in my life.

# ABSTRACT

## DESIGN AND SYNTHESIS OF RHODAMINE BASED FLUORESCENT AND COLORIMETRIC SENSORS FOR THE DETECTION OF GOLD IONS

The usage of chemosensors for the detection of heavy and transition metal ions is prevalent. Because these metal ions play crucial roles in living systems and have extremely toxic effects on the environment. Among these metal ions, gold species have interesting biological properties and uses. They play important roles in biological systems and often have significant impacts on human health. For instance, gold based drugs have long been used in the treatment of rheumatoid arthritis and other autoimmune diseases. In addition, gold nanoparticles function as carriers for drugs and gene delivery systems. Gold ions, on the other hand, are potentially toxic to humans. Because of their reactive nature, ionic gold species can interact with proteins, DNA and other biomolecules and disturb a series of cellular processes, leading to serious health problems.

Detection of gold ions can be performed by spectroscopic methods such as atomic absorption and atomic emission spectroscopy and inductively-coupled plasma spectrometry that required complicated sample preparation steps, and sophisticated instrumentation. In contrast to these highly expensive and time consuming methods, fluorogenic or chromogenic methods can be good alternatives for the detection of these species that provides high analyte sensitivity and selectivity, visual simplicity, instantaneous response, as well as real time monitoring. The rhodamine scaffold is an ideal template for the construction of metal ion chemosensors because they have large molar extinction coefficient, long excitation and emission wavelengths, high fluorescence quantum yields, good water solubility, and the potential for colorimetric and turn-on fluorescent detection.

In this thesis work, we focus on design and synthesis of novel rhodamine based molecules for the detection of gold ions. Moreover, we investigate the photophysical properties of synthesized molecules in the absence and presence of gold ions in both synthetic samples and living cells.

## ÖZET

### ALTIN İYONLARININ TAYİNİ İÇİN RODAMİN BAZLI FLORESAN VE KOLORİMETRİK SENSÖRLERİN TASARIMI VE SENTEZİ

Ağır ve geçiş metal iyonlarının tespiti için kemosensörlerin kullanımı yaygın bir yöntemdir. Çünkü bu metal iyonları canlı sistemlerde çok önemli rol oynar ve çevre üzerinde aşırı derecede toksik etkilere sahiptir. Bu metal iyonları arasında altın türleri değişik biyolojik özelliklere ve kullanım alanlarına sahiptir. Biyolojik sistemlerde önemli rollere sahiptirler ve genelde insan sağlığı üzerinde pozitif etkilere sahiptirler. Örneğin, altın bazlı ilaçlar romatoid artrit ve diğer otoimmün hastalıkların tedavisinde uzun süredir kullanılmaktadır. Buna ek olarak, altın nanopartiküller ilaç ve gen dağıtım sistemleri için taşıyıcı olarak işlev görür. Altın iyonları, diğer yandan insanlar için potansiyel olarak toksik etkiye sahiptir. İyonik altın türleri, reaktif özelliklerinden dolayı proteinler, DNA ve diğer biyomoleküller ile etkileşime girebilir ve bir dizi hücresel işlemi sekteye uğratar ve ciddi sağlık sorunlarına yol açabilir.

Bu iyonların tayini için atomik absorpsiyon ve atomik emisyon spektroskopisi, indüktif olarak eşleşmiş plazma spektrometresi gibi spektroskopik yöntemler kullanılabilir, ancak bu yöntemler karmaşık örnek hazırlama aşamaları ve sofistike cihazlar gerektirmektedir. Bu son derece pahalı ve zaman alıcı yöntemlerin yerine, yüksek analit duyarlılığı ve seçiciliği olan, kolay gözlemlenebilen, anlık yanıt verme ve gerçek zamanlı izlenebilme sağlayan floresan ve kromojenik yöntemler bu türlerin saptanması için iyi bir alternatif olabilir. Rodamin iskeleti yüksek molar sönmülme katsayısı, uzun eksitasyon ve emisyon dalga boyları, yüksek floresan kuantum verimi ve suda iyi çözünbilme gibi özellikleri dolayısıyla altın iyon kemosensörünün oluşturulması için iyi bir örnektir.

Bu tez çalışmasında altın iyonlarının saptanması için rodamine bazlı yeni moleküllerin dizaynı ve sentezi üzerinde duruyoruz. Aynı zamanda tasarladığımız sensör moleküllerinin hem sulu çözeltilerde hem de canlı hücre içerisinde analit varlığında ve yokluğunda foto-fiziksel değişimlerini inceliyoruz.

# TABLE OF CONTENT

LIST OF FIGURES .....	viii
LIST OF ABBREVIATIONS.....	xiv
CHAPTER 1. INTRODUCTION .....	1
1.1. An Overview .....	1
1.2. Fluorescence Theory.....	3
1.3. Organic Fluorescent Dyes.....	5
1.4. Xanthene Based Fluorescent Dyes.....	9
1.4.1. Fluorescein .....	9
1.4.2. Rhodamine .....	12
1.5. Fluorescent Chemosensors.....	15
1.6. Rhodamine as Molecular Sensor .....	22
1.6.1. Detection of Metal Ions by Spiroring-Opening of Rhodamine Derivatives .....	23
1.6.2. Detection of Anions based on Rhodamine and Related Derivatives .....	26
1.6.3. Detection of Reactive Oxygen and Nitrogen Species and Thiols based on Rhodamine Derivatives.....	28
CHAPTER 2. SPIRO RING OPENING REACTION BASED MOLECULAR SENSORS FOR GOLD ION DETECTION.....	31
2.1. Literature Studies .....	31
2.2. Rhodamine Based Fluorescent and Colorimetric Sensors for Gold Ions Detection.....	40
2.2.1. Gold Ion Sensing Properties of <b>RH-1</b> .....	41
2.2.2. Gold Ion Sensing Properties of <b>RH-2</b> .....	52
2.2.3. Gold Ion Sensing Properties of <b>RH-3</b> .....	63
CHAPTER 3. EXPERIMENTAL STUDY .....	74
3.1. General Methods.....	74

3.2. Determination of Detection Limit.....	74
3.3. Detection of Residual Au <sup>3+</sup> Content using Inductively-Coupled Plasma Mass Spectroscopy (ICP-MS).....	75
3.4. Kinetic Study .....	75
3.5. Cell Imaging.....	75
3.6. Synthesis of Probe Molecules .....	76
3.6.1. Synthesis of Rhodamine Hydrazide .....	77
3.6.2. Synthesis of <b>RH-1</b> .....	77
3.6.3. Synthesis of <b>RH-O-BOD</b> and <b>RH-2</b> .....	78
3.6.4. Synthesis of <b>RH-3</b> .....	80
3.6.5. Synthesis of <b>RH-1P</b> .....	80
3.6.6. Synthesis of Rhodamine B from <b>RH-3</b> .....	81
 CHAPTER 4. CONCLUSION .....	 83
 REFERENCES .....	 85
 APPENDICES	
APPENDIX A. <sup>1</sup> H-NMR AND <sup>13</sup> C-NMR SPECTRA OF COMPOUNDS .....	93
APPENDIX B. MASS SPECTRA OF COMPOUNDS .....	108

## LIST OF FIGURES

<b><u>Figure</u></b>	<b><u>Page</u></b>
Figure 1.1. The Perrin-Jablonski diagram .....	3
Figure 1.2. Stoke's shift .....	4
Figure 1.3. Distribution of common dyes in the UV-vis region .....	5
Figure 1.4. BODIPY core structure .....	6
Figure 1.5. BODIPY structures with different absorption and emission wavelengths .....	6
Figure 1.6. Pyrene and perylene core structures .....	7
Figure 1.7. Molecular structures of DAPI and Hoechst .....	7
Figure 1.8. General structure of cyanine dyes .....	8
Figure 1.9. Common examples of coumarin derivatives of 4-MU and AMC .....	8
Figure 1.10. Molecular structures of xanthene, rhodamine and fluorescein .....	9
Figure 1.11. Synthesis of fluorescein fluorophore .....	9
Figure 1.12. pH dependence of fluorescein equilibrium .....	10
Figure 1.13. Electrophilic aromatic substitution on fluorescein .....	11
Figure 1.14. Selected fluorescein dyes with different reactive groups .....	11
Figure 1.15. Synthesis scheme for Rhodamine core .....	12
Figure 1.16. General structure of rhodamine dye .....	12
Figure 1.17. Molecular structures of Rhodamine 101 and Rhodamine B in acidic and basic medium .....	13
Figure 1.18. Synthesis of rhodamines via direct nucleophilic substitution from halogenated fluoresceins .....	14
Figure 1.19. Commercially available rhodamine derivatives .....	14
Figure 1.20. Schematic representation of design concept for the construction fluorescent chemosensors .....	15
Figure 1.21. Photo induced electron transfer mechanism .....	16
Figure 1.22. Intermolecular charge transfer mechanism .....	17
Figure 1.23. Fluorescence resonance energy transfer mechanism .....	17
Figure 1.24. Reaction based approaches to construct molecular sensors .....	18
Figure 1.25. Examples of fluorescent molecular sensors classify by reaction based approach .....	18



Figure 1.26.Examples of fluorescent molecular sensors classify by hydrolysis reaction based approach.....	19
Figure 1.27.Coordination based approaches to construct molecular sensors .....	20
Figure 1.28.Examples of coordination based fluorescent sensors .....	20
Figure 1.29.Examples of cation exchange reaction based fluorescent sensors .....	21
Figure 1.30.Spirolactam ring-opening process of rhodamine derivative.....	22
Figure 1.31.Cu <sup>2+</sup> -assisted hydrolysis of Czarnik's rhodamine B hydrazide .....	23
Figure 1.32. Hg <sup>2+</sup> induced ring opening and cyclization of Tae's chemodosimeter .....	24
Figure 1.33.Proposed binding mode of Yoon's chemosensors with Pb <sup>2+</sup> .....	25
Figure 1.34.Chemosensor and chemodosimeter examples by utilizing spiroring-opening reaction of rhodamine derivatives.....	25
Figure 1.35.Binding site-signaling subunit and displacement approaches for the anion sensing.....	26
Figure 1.36.Chemodosimeter approach for the anion sensing.....	27
Figure 1.37.Some important anion sensor examples of spirolactam derivatives.....	27
Figure 1.38.Some important ROS/RNS sensor examples of xanthene derivatives .....	29
Figure 1.39.Some important thiol probes based on rhodamine derivatives.....	30
Figure 2.1.First example of gold ion selective and sensitive molecular sensor.....	31
Figure 2.2.Rhodamine-propargylamide based fluorescent sensor for gold ions .....	32
Figure 2.3.Fluorescent molecular sensor works via hydrolysis of acylsemicarbazide ...	33
Figure 2.4.The first example of reversible gold (III) ion sensor.....	33
Figure 2.5.Approach involving anchoring-unanchoring of a fluorophore.....	34
Figure 2.6.Synthesis of fluorescein based gold ion probe .....	34
Figure 2.7.Mechanistic pathway of gold ion sensing .....	35
Figure 2.8.Turn-on sensing mechanism of the probe by gold (III) ion .....	35
Figure 2.9.Proposed mechanism for the response of probe to gold (III) ion.....	36
Figure 2.10.A proposed mechanism of the cyclization of the rhodol based probe induced by gold (III) ion .....	37
Figure 2.11.Synthesis of fluorescein based gold (III) ion probe .....	38
Figure 2.12.Mechanism for the formation of non-separable isomer products of <b>FL-1</b> ..	38
Figure 2.13.Proposed mechanism of <b>FL-2</b> in the presenece of gold (III) ion .....	39
Figure 2.14. Rhodamine based gold ion selective novel probes.....	40
Figure 2.15.Synthesis of probe <b>RH-1</b> .....	41

Figure 2.16. Effect of water content on the fluorescence intensity of probe <b>RH-1</b> (20 $\mu\text{M}$ ) in the presence of $\text{Au}^{3+}$ (20 $\mu\text{M}$ ) at pH = 7.0 .....	42
Figure 2.17. Effect of different pH values (pH: 6.0, 6.2, 6.4, 6.6, 6.8, 7.0, 7.2, 7.4, 7.6, 7.8 and 8.0) on the fluorescence intensity of probe <b>RH-1</b> (20 $\mu\text{M}$ ) in the presence of $\text{Au}^{3+}$ (60 $\mu\text{M}$ ) .....	43
Figure 2.18. (a) Absorption and (b) Emission spectra of probe <b>RH-1</b> (20 $\mu\text{M}$ ) and $\text{Au}^+$ and $\text{Au}^{3+}$ (60 $\mu\text{M}$ , 3.0 equiv.) in 1:1 $\text{CH}_3\text{CN}/\text{HEPES}$ buffer at pH = 7.0; ( $\lambda_{\text{ex}}$ = 500 nm, at 25 $^\circ\text{C}$ ). .....	44
Figure 2.19. Emission titration curve of probe <b>RH-1</b> (20 $\mu\text{M}$ ) and $\text{Au}^{3+}$ (0 to 10 equiv) in 1:1 $\text{CH}_3\text{CN}/\text{HEPES}$ buffer at pH = 7.0; Inset: plot of fluorescence intensity depending on the number of equivalents of $\text{Au}^{3+}$ . .....	44
Figure 2.20. Fluorescence intensity changing of probe <b>RH-1</b> (20 $\mu\text{M}$ ) upon addition of $\text{AuCl}_3$ (2.0 to 10.0 $\mu\text{M}$ , 0.1 to 0.5 equiv.) in 1:1 $\text{CH}_3\text{CN}/\text{HEPES}$ buffer at pH = 7.0. ....	45
Figure 2.21. Fluorescence spectrum of probe <b>RH-1</b> (20 $\mu\text{M}$ ) upon addition of $\text{AuCl}_3$ (2.0 $\mu\text{M}$ / 0.6 ppm) in 1:1 $\text{CH}_3\text{CN}/\text{HEPES}$ buffer at pH = 7.0 .....	45
Figure 2.22. Time-dependent fluorescence change of probe <b>RH-1</b> (20 $\mu\text{M}$ ) in the presence of 60 $\mu\text{M}$ of (a) $\text{AuCl}$ and (b) $\text{AuCl}_3$ measured in 1:1 $\text{CH}_3\text{CN}/\text{HEPES}$ buffer at pH = 7.0.....	46
Figure 2.23. Fluorescence intensities of probe <b>RH-1</b> (20 $\mu\text{M}$ ) in 1:1 $\text{CH}_3\text{CN}/\text{HEPES}$ buffer at pH=7.0 emission at 580 nm ( $\lambda_{\text{ex}}$ = 500 nm): in the presence of metal ions (5 equiv). All data were taken after 60 min.....	47
Figure 2.24. Fluorescence intensities of probe <b>RH-1</b> (20 $\mu\text{M}$ ) in 1:1 $\text{CH}_3\text{CN}/\text{HEPES}$ buffer at pH = 7.0 at $\lambda_{\text{max}}$ : 580 nm in the presence $\text{Au}^{3+}$ (100 $\mu\text{M}$ , 5.0 equiv.) and 200 $\mu\text{M}$ of the metal ions .....	48
Figure 2.25. Proposed mechanism for the product formation with gold (III) ion .....	49
Figure 2.26. Synthesis of oxazole derivative in the presence of gold (III) ion.....	49
Figure 2.27. Fluorescence images of HCT-116 cells : (a) fluorescence image of HCT-116 cells treated with probe <b>RH-1</b> (20 $\mu\text{M}$ ) in the absence of $\text{Au}^{3+}$ (control); (b) fluorescence image of HCT-116 cells treated with Hoechst -34580 (2 $\mu\text{M}$ ) (control); (c) fluorescence image of HCT-116 cells treated with $\text{Au}^{3+}$ (10 $\mu\text{M}$ ) and probe <b>RH-1</b> (20 $\mu\text{M}$ ); (d) merge image of frames b and c. ....	50
Figure 2.28. Molecular structure of <b>RH-2</b> .....	52
Figure 2.29. Synthetic pathway of <b>RH-2</b> .....	53

Figure 2.30. Effect of water content on the fluorescence intensity of <b>RH-2</b> (5 $\mu\text{M}$ ) in $\text{CH}_3\text{CN}/\text{HEPES}$ buffer (pH = 7.0) in the presence $\text{Au}^{3+}$ (1 equiv.) ( $\lambda_{\text{ex}} = 590$ nm).	54
Figure 2.31. Effect of pH on the fluorescence intensity of <b>RH-2</b> (5 $\mu\text{M}$ ) in 10 mM HEPES buffer/ $\text{CH}_3\text{CN}$ in the absence and presence $\text{Au}^{3+}$ (1 equiv.) ( $\lambda_{\text{ex}} = 590$ nm).	54
Figure 2.32. Absorption spectra of <b>RH-2</b> (5 $\mu\text{M}$ ) and $\text{Au}^{3+}$ (1 equiv.) in 1:1 $\text{CH}_3\text{CN}/\text{HEPES}$ buffer at pH = 7.0	55
Figure 2.33. Emission spectra of <b>RH-2</b> (5 $\mu\text{M}$ ) and $\text{Au}^{3+}$ (1 equiv.) in 1:1 $\text{CH}_3\text{CN}/\text{HEPES}$ buffer at pH = 7.0	56
Figure 2.34. Fluorescence titration spectra of <b>RH-2</b> (5.0 $\mu\text{M}$ ) in 1:1 $\text{CH}_3\text{CN}/\text{HEPES}$ buffer (pH=7.0) the presence of $\text{Au}^{3+}$ (0-10 equivalent) $\lambda_{\text{ex}} = 525$ nm	56
Figure 2.35. Fluorescence intensity changes of <b>RH-2</b> vs equivalents of $\text{Au}^{3+}$ $\lambda_{\text{ex}} = 525$ nm	57
Figure 2.36. (a) Fluorescence changes of <b>RH-2</b> (5.0 $\mu\text{M}$ ) upon addition of $\text{Au}^{3+}$ (0.05 to 0.3 $\mu\text{M}$ , 0.01 to 0.05 equiv.) (b) Fluorescence spectra of <b>RH-2</b> (5.0 $\mu\text{M}$ ) in the presence of $\text{Au}^{3+}$ (0.05 $\mu\text{M}$ , 0.01 equiv.) in 1:1 $\text{CH}_3\text{CN}/\text{HEPES}$ buffer at pH = 7.0	58
Figure 2.37. Fluorescence intensities of <b>RH-2</b> (5 $\mu\text{M}$ ) in 1:1 $\text{CH}_3\text{CN}/\text{HEPES}$ buffer at pH = 7.0 at $\lambda_{\text{max}}$ : 590 nm in the presence of 10.0 equivalent of the cations interest,	58
Figure 2.38. Fluorescence intensities of <b>RH-2</b> (5 $\mu\text{M}$ ) in 1:1 $\text{CH}_3\text{CN}/\text{HEPES}$ buffer at pH = 7.0 at $\lambda_{\text{max}}$ : 590 nm in the presence $\text{Au}^{3+}$ (1.0 equiv.) and 10.0 equiv the metal ions.	59
Figure 2.39. Proposed mechanism of <b>RH-2</b> towards the addition of $\text{Au}^{3+}$ ions.	60
Figure 2.40. Job's plot for the rhodamine derivative and $\text{Au}^{3+}$ in 1:1 $\text{CH}_3\text{CN}/\text{HEPES}$ buffer at $\lambda_{\text{ex}} = 525$ nm.	60
Figure 2.41. Structure of control probe of <b>RH-2</b>	61
Figure 2.42. a) Fluorescence image of A549 cells treated with only <b>RH-2</b> (5 $\mu\text{M}$ ); b) Image of cells treated with $\text{Au}^{3+}$ (5 $\mu\text{M}$ ) and probe (5 $\mu\text{M}$ ) ( $\lambda_{\text{ex}} = 470$ nm); c) Cells treated with $\text{Au}^{3+}$ (5 $\mu\text{M}$ ) and probe (5 $\mu\text{M}$ ) ( $\lambda_{\text{ex}} = 525$ nm); d and h) Cells treated with DAPI for 15 min (control); d) Merged image of frame b and d; f) merged image of frame c and d; g) Cells treated with $\text{Hg}^{2+}$ (5 $\mu\text{M}$ ) and probe (5 $\mu\text{M}$ ) ( $\lambda_{\text{ex}} = 525$ nm); i) merged image of frame g and h.	61

Figure 2.43. Molecular structure of <b>RH-3</b> .....	63
Figure 2.44. Synthetic scheme of <b>RH-3</b> .....	64
Figure 2.45. Effect of pH on the fluorescence intensity of <b>RH-3</b> (10 $\mu$ M) in phosphate buffer in the absence (a) and presence (b) of $\text{Au}^{3+}$ (5.0 equiv.).....	65
Figure 2.46. Absorbance spectra <b>RH-3</b> (10 $\mu$ M) in the absence (black line) and presence (red line) of 5 equiv. of $\text{Au}^{3+}$ and fluorescence spectra of <b>RH-3</b> (10 $\mu$ M) in the absence (green line) and presence (blue line) of 5 equiv. of $\text{Au}^{3+}$ in Phosphate buffer (0.1 M). .....	66
Figure 2.47. Emission titration curve of <b>RH-3</b> (10 $\mu$ M) and $\text{Au}^{3+}$ (0 to 10 equiv.) in Phosphate buffer (0.1 M) at pH = 7.0 (After 5 min.).....	66
Figure 2.48. A Pseudo-first-order kinetic plot of the reaction between <b>RH-3</b> (10 $\mu$ M) in the presence of 1.0 equivalent of $\text{AuCl}_3$ measured in phosphate buffer at pH = 7.0. $k_{\text{obs}} = 1.37 \times 10^{-2} \text{ sec}^{-1}$ .....	67
Figure 2.49. Time-dependent fluorescence change of <b>RH-3</b> (10 $\mu$ M) in the presence of 1.0 equivalent of $\text{AuCl}_3$ measured in phosphate buffer at pH = 7.0 .....	67
Figure 2.50. (a) Fluorescence changes of <b>RH-3</b> (10 $\mu$ M) upon addition of $\text{Au}^{3+}$ (0.05 to 0.3 $\mu$ M, 0.005 to 0.025 equiv.) (b) Fluorescence spectra of <b>RH-3</b> (10 $\mu$ M) in the presence of $\text{Au}^{3+}$ (0.05 $\mu$ M, 0.005 equiv.) in phosphate buffer at pH = 7.0 .....	68
Figure 2.51. Fluorescence intensities of <b>RH-3</b> (10 $\mu$ M) in phosphate buffer at pH = 7.0 at $\lambda_{\text{max}} = 580 \text{ nm}$ in the presence of 10.0 equivalent of the cations interest. .	69
Figure 2.52. Fluorescence intensities of <b>RH-3</b> (10 $\mu$ M) in phosphate buffer at pH = 7.0 at $\lambda_{\text{max}} = 580 \text{ nm}$ in the presence $\text{Au}^{3+}$ (1.0 equiv.) and 10.0 equivalent of the cations interest. ....	70
Figure 2.53. Proposed mechanism for the detection of $\text{Au}^{3+}$ ions.....	71
Figure 2.54. Images of A-549 cells: (a) Cells treated with <b>RH-3</b> (10 $\mu$ M) in the absence of $\text{Au}^{3+}$ (control) did not have any fluorescent signal (b) Cells were detected with DAPI nuclear counter-stain (c) Cells treated with <b>RH-3</b> (10 $\mu$ M) and $\text{Au}^{3+}$ (10 $\mu$ M) displayed strong red fluorescence (d) The fluorescent signal appeared in and around of the nucleus judged by the DAPI counterstain in the merged image; <b>DAPI</b> blue, <b>RH-3</b> red.....	72
Figure 2.55. Brightfield microscopic images of zebrafish embryos treated with (a) <b>RH-3</b> (10 $\mu$ M) in the absence of $\text{Au}^{3+}$ , (b) <b>RH-3</b> (10 $\mu$ M) and $\text{Au}^{3+}$ (20 $\mu$ M). Fluorescence images of zebrafish embryos treated with (c) <b>RH-3</b> (10 $\mu$ M)	

(control) (d) <b>RH-3</b> (10 $\mu\text{M}$ ) and $\text{Au}^{3+}$ (20 $\mu\text{M}$ ) showing that <b>RH-3</b> fluoresces in the embryo only in presence of $\text{Au}^{3+}$ .....	73
Figure 3.1.Synthetic routes of probe molecules .....	76
Figure 4.1.Summary of synthesized probe molecules .....	83

## LIST OF ABBREVIATIONS

Rhodamine B	2-(3,6-bis(diethylamino)-9H-xanthen-9-yl)benzoic acid
Fluorescein	3',6'-dihydroxy-3H-spiro[isobenzofuran-1,9'-xanthen]-3-one
BODIPY	4, 4-difluoro-4-bora-3a, 4a-diaza-s-indacene
PET	Photoinduced Electron Transfer
ICT	Intramolecular Charge Transfer
FRET	Fluorescence Resonance Energy Transfer
TICT	Twisted Intramolecular/Intermediate Charge Transfer
PICT	Planar Intramolecular Charge Transfer
ROS	Reactive Oxygen Species
RNS	Reactive Nitrogen Species
DDQ	2,3-Dichloro-5,6-dicyano-1,4-benzoquinone
TFA	Trifluoroacetic Acid
THF	Tetrahydrofuran
DCM	Dichloromethane
DMF	Dimethyl Formamide
DCE	Dichloroethane
DMAP	4-Dimethylaminopyridine
EDC	1-Ethyl-3-(3-dimethylaminopropyl) carbodiimide
NEt <sub>3</sub>	Triethylamine
DMSO	Dimethyl Sulfoxide
EtOH	Ethanol
MeOH	Methanol
RT	Room Temperature
EtOAc	Ethyl Acetate
HEPES	2-[4-(2-hydroxyethyl)piperazin-1-yl]ethanesulfonic acid
DAPI	4',6-diamidino-2-phenylindole
LOD	Limit of Detection

# CHAPTER 1

## INTRODUCTION

### 1.1.An Overview

Being one of the most significant noble metals, gold is widely spread in nature and its concentration in soil and rocks has been estimated 1 and 4 ng g<sup>-1</sup> respectively, and 50 and 200 pg mL<sup>-1</sup> have been found in sea water and river water. (Vasimalai et al., 2014). Due to its unparalleled physical, mechanical and chemical properties, gold and gold salts have been extensively employed in chemistry, medicine, biology and industry. In chemistry, gold-based catalysts have been greatly used for chemical transformations due to having the characteristic alkynophilicity towards the gold ion (Arcadi, 2008; Gorin and Toste, 2007; Jiménez-Núñez and Echavarren, 2008; Z. Li et al., 2008) . In medicine, gold-based drugs, such as solganol, sanocrysin and auranofin, are important for the treatment of different diseases including rheumatic arthritis, asthma, malaria, cancer, and HIV and brain lesions (Gabbiani et al., 2007; Messori and Marcon, 2004; Ott, 2009) . In biology, gold nanoparticles (AuNPs) have been widely used as drug and gene delivery systems, biosensors, and bioimaging probes (Duncan et al., 2010; Hong et al., 2006; Y. Li et al., 2010). In industry, gold has many practical usages such as pollution control, mobile phones, laptops, space travel and dentistry (Chakraborty et al., 2000; Corti et al., 2002, 2007; P. Goodman, 2002). For instance, since gold can reflect the infrared, visible light and radio waves, it is utilized as a coating material of many satellites and planes. Despite the widespread usage of gold, it can cause adverse effects to the environment as well as biological systems. Because of their reactive nature, ionic gold species can interact with proteins, DNA and other biomolecules and disturb a series of cellular processes, leading to serious health problems (C. M. Goodman et al., 2004; Habib and Tabata, 2004). Moreover, gold (III) ion, one of the most powerful sensitizer, can causes severe allergic reactions like contact dermatitis, rhinitis, conjunctivitis, asthma and urticarial. Soluble gold salts such as gold chloride is known to cause damage to the liver, kidneys, and the peripheral nervous system (Nam et al., 2014). Therefore, it is significant to determine gold species in both environment and biological systems. There are several methods for

the determination of trace levels of metal ions such as inductively coupled plasma atomic-emission spectroscopy (ICP-AES), inductively coupled plasma mass spectroscopy (ICP-MS) and anodic stripping voltammetry (Cao et al., 2011). However, most of these methods have different disadvantages such as complicated sample preparation steps and time consuming and requiring expensive instrumentation. Also, these methods do not allow real time monitoring gold species in biological systems. As an alternative way, fluorometric and colorimetric techniques are preferable approaches for the detection of trace amount of metal ions, because these techniques are very rapid, easy to use, highly sensitive, inexpensive and non-destructive. More importantly, they allow visualization analysis of metal ions *in vivo/vitro* (Chen et al., 2012; Eun Jun et al., 2011; Singha et al., 2015). To date, several types of fluorophores have been employed as a signal units of chemosensors such as rhodamine and fluorescein (Beija et al., 2009; Chen et al., 2012; Kim et al., 2008; Zheng et al., 2013), boron dipyrromethene difluoride (BODIPY), (Noel Boens et al., 2012; Kowada et al., 2015; Loudet and Burgess, 2007) cyanine (Mishra et al., 2000) etc. Among these fluorophores, rhodamine is very favorable because of bearing outstanding photophysical features such as, high absorption and emission coefficient, high fluorescence quantum yield, great photostability and relatively long emission wavelength.

In this thesis work, design and synthesis of new Rhodamine B based fluorescent molecular probes for the detection of gold ions in synthetic samples and living system is aimed. Gold ions display a high affinity to fluorescent molecules bearing heteroatoms like sulfur and nitrogen (Singha et al., 2015). Also, gold ions and their complexes show high reactivity towards unsaturated systems such as alkenes and alkynes. There are many fluorescent probes that are designed and synthesized making use of this reactivity (Singha et al., 2015). The content of this thesis involves Rhodamine B based fluorescent sensors that exploit alkynophilicity and the strong heteroatom coordination ability of gold ions. Also, new reactive patterns and strategies are designed and carried out to determine gold ions successfully.



## 1.2. Fluorescence Theory

Photoluminescence is a process in which an atom or a molecule absorbs a light of a given wavelength (excitation) and emits a light of a different, longer wavelength. Based on the nature of the excited state photoluminescence can be split into two categories as fluorescence and phosphorescence. The Perrin-Jablonski diagram clearly explains the relationship between photoluminescence and molecular energy states (Lakowicz, 2006). In this diagram, first transition is the absorbance of a photon with a certain energy. Absorbance is the process by which an electron is excited from a lower energy state to a higher energy state. After the absorption of a certain wavelength of light, the molecules will go into their excited state such as  $S_1$  and  $S_2$ . The absorbed energy is strongly related to excitation of molecules from ground state to excited state and relates to emission of light via a fluorescence or phosphorescence mechanism.

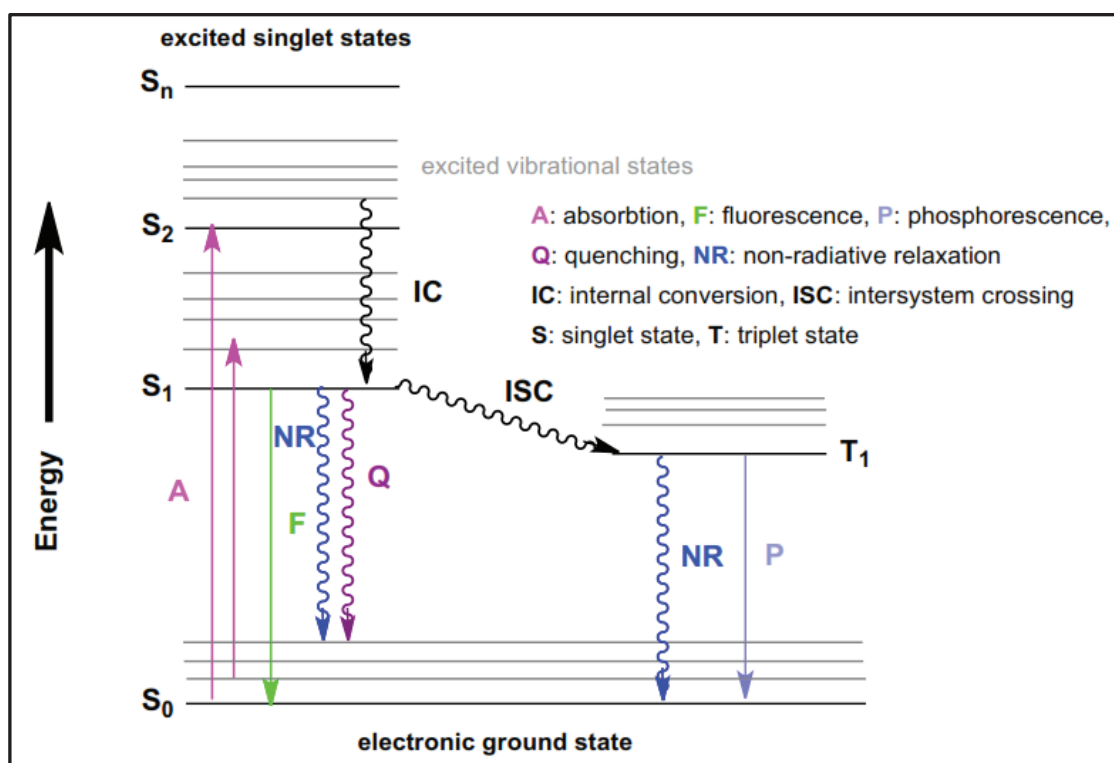


Figure 1.1. The Perrin-Jablonski diagram  
(Source: Lakowicz, 2006)

Excitation of a molecule to  $S_1$  mostly cause the quick promotion of an electron from the highest occupied molecular orbital (HOMO) to the lowest unoccupied molecular

orbital (LUMO). After excitation process the molecule then undergoes a rapid relaxation called internal conversion to the lowest vibrational energy level of the first excited state,  $S_1$  and it produces radiative emission in the form of fluorescence. This process is a spin allowed process because excited electron has opposite spin to the electron in the ground state. However, the excited electron at  $S_1$  state may undergo intersystem crossing to the triplet state,  $T_1$  with different mechanism in which the electron in the excited orbital has the same spin orientation as the ground-state electron which is called as spin-prohibited process. The nonradiative transition from  $S_1$  to  $T_1$  induces phosphorescence.

First recorded observation of the fluorescence was made by the Spanish physician and botanist Nicolas Monardes in 1565. He realized a strange blue shining from water containing a cup made from special wood (*Ligirium nephiticem*). In the 17<sup>th</sup> century Robert Boyle and Issac Newton greatly described fluorescence theory. In 1845, John Herschel achieved first crude fluorescence emission spectrum for quinine sulfate solution under sunlight illumination (Herschel, 1845). Intense work was expended for understanding fluorescence theory in the late 19<sup>th</sup> century by George Stokes. He found the technique of observing fluorescence with two separate colored filters, one for the excitation beam, and other one emission observation. Stokes also explored that emission takes places at longer wavelengths than absorption, which bears his name ‘Stokes Shift’, is the difference between maximum of first absorption band and maxima of emission spectrum (Stokes, 1852)

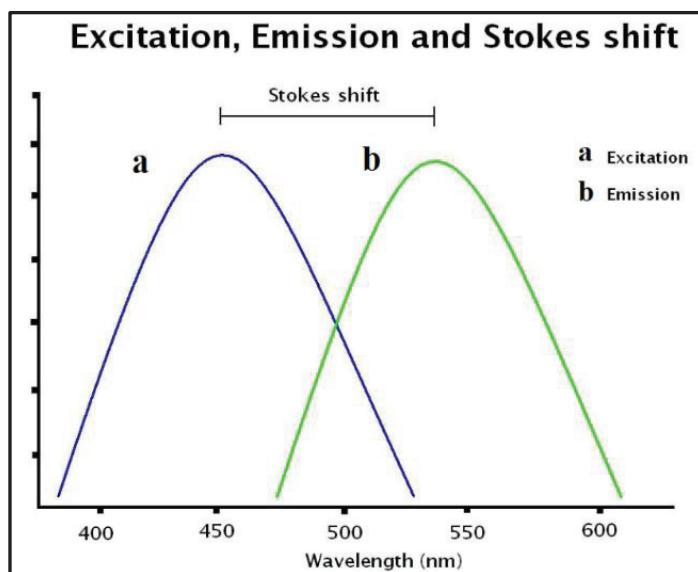


Figure 1.2. Stoke's shift  
(Source: Stokes, 1852)

### 1.3.Organic Fluorescent Dyes

Fluorescent molecules, also called as fluorophores, always contain chromophore whose characteristic property is to absorb specific wavelength of the visible light and reflects or transmits others and they are seen as color by the observers. Chromophores usually seem in conjugated  $\pi$ -systems such as various food colorings, fabric dyes, pH indicators, lycopene,  $\beta$ -carotene and anthocyanin. In contrast to chromophores, fluorophores not only absorb the light but also re-emit part of the light as radiation.

Organic fluorescent molecules that transmit ultraviolet (UV), visible (Vis) and near infrared (near-IR) region are widely used for many applications such as metal ion, anion, or ROS/RNS detection; the labeling agents; and the visualization of biological processes (Bates et al., 2007; Marks and Nolan, 2006). The most common dyes and their emission band are shown in figure below.

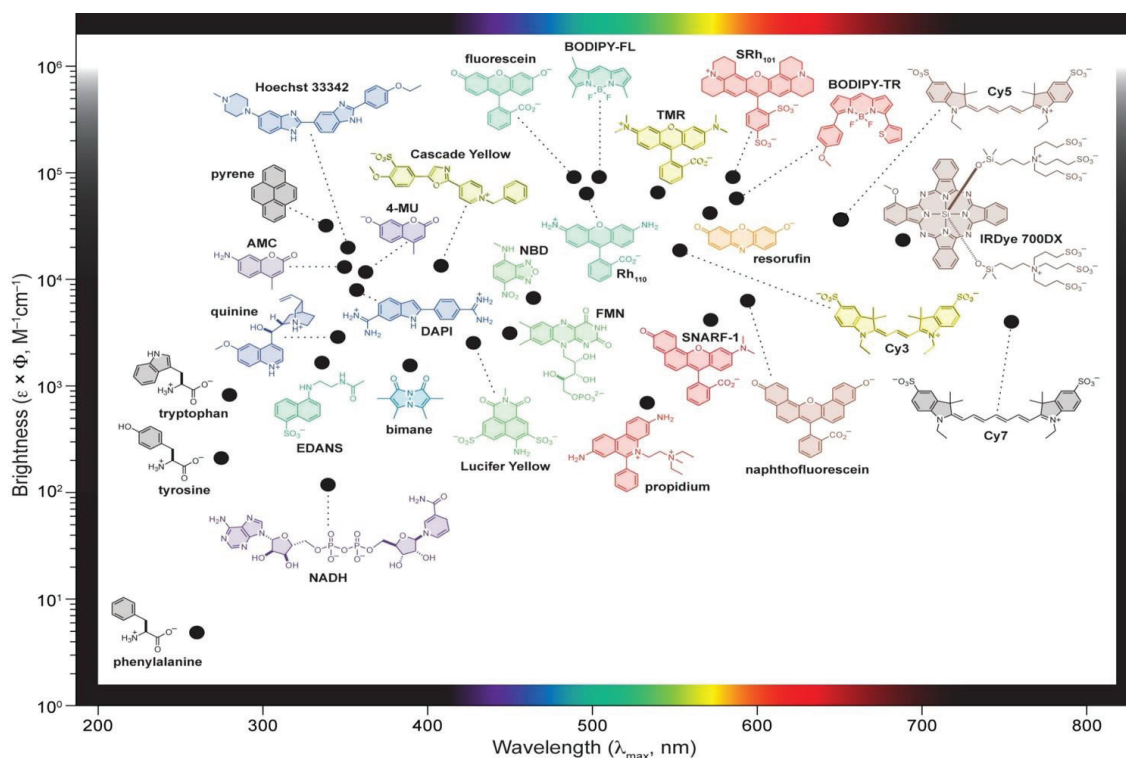


Figure 1.3.Distribution of common dyes in the UV-vis region (Source: Marks et al., 2006)

The boron-dipyrromethene (BODIPY) dyes have been used for many chemical and biological applications such as fluorescent molecular sensors for metal ions or biologically important species, photodynamic therapy agents, solar cells, laser dyes and labeling agents thanks to bearing specific photophysical characteristics such as great photostability, good quantum yields and long emission/absorption wavelength in the visible region.

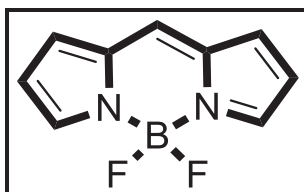


Figure 1.4. BODIPY core structure  
(Source: Ulrich et al., 2008)

Moreover, another crucial point of BODIPY dye is that chemical modification can easily be applied for switching spectroscopic properties. Diversity of photochemical features enables to choose a specific dye for particular applications (Noel Boens et al., 2012; Noël Boens et al., 2015; Ulrich et al., 2008).

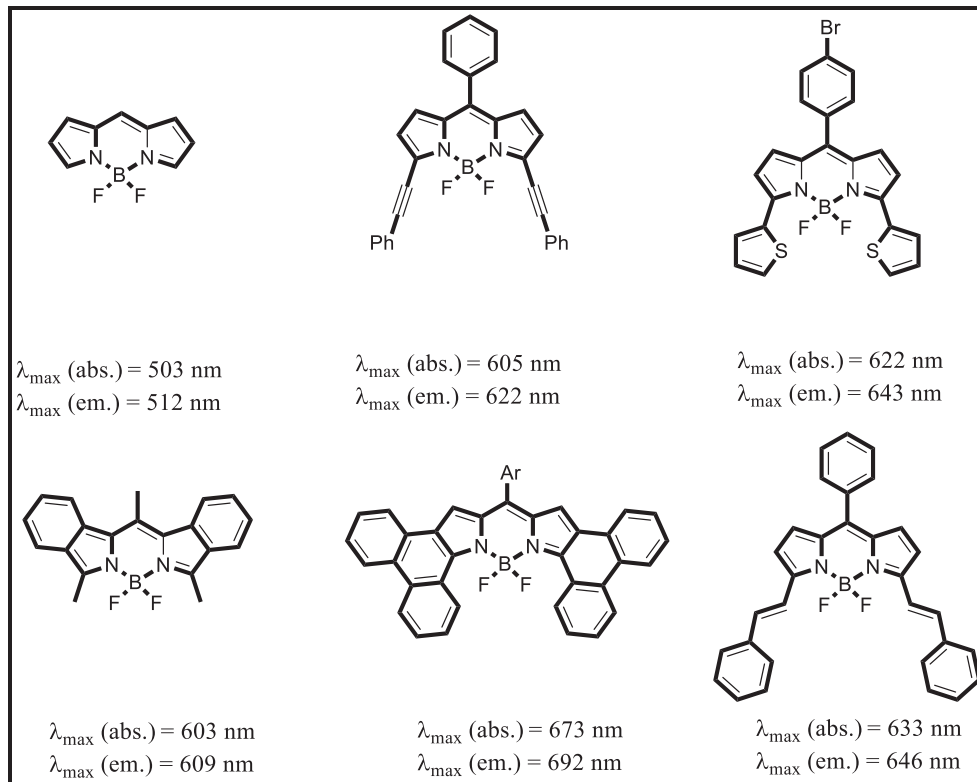


Figure 1.5. BODIPY structures with different absorption and emission wavelengths  
(Source: Ni and Wu, 2014)

For example, BODIPY core is excited and emitted at relatively lower wavelengths about 450-500 nm, however, after some chemical changing is performed like increasing conjugation, halogenation etc. emission wavelength shifts longer up to 700 nm (Figure 1.5) (Ni and Wu, 2014).

Pyrene consists of four fused benzene rings and they are used to evaluate significant biomolecular processes such as protein conformation and reporting DNA folding (Smalley and Silverman, 2006). Perylene derivatives are also another class of fluorophores which show remarkably high quantum yields. For example; quinine, one of the first discovered fluorescent dye, is still used as fluorescent standard (Schulman et al., 1974; Süßmeier and Langhals, 2001).

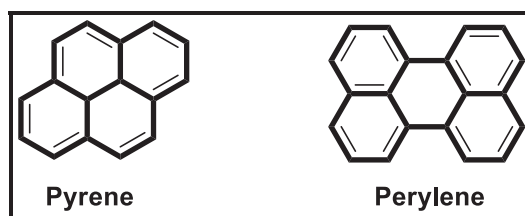


Figure 1.6. Pyrene and perylene core structures  
(Source: Smalley et al., 2006; Schulman et al., 1974)

Imidazoles and indoles have also fluorescent properties. 4',6'-diamidino-2-phenylindole (DAPI), a popular nuclear and chromosome counterstain that binds A-T rich areas in DNA. This binding causes large fluorescence increase; therefore, it is often used in cellular imaging. The benzimidazoles known as Hoechst dyes which are another staining dyes similar to DAPI extensively used for fluorescence microscopy and flowcytometry (Haugland, 2005)

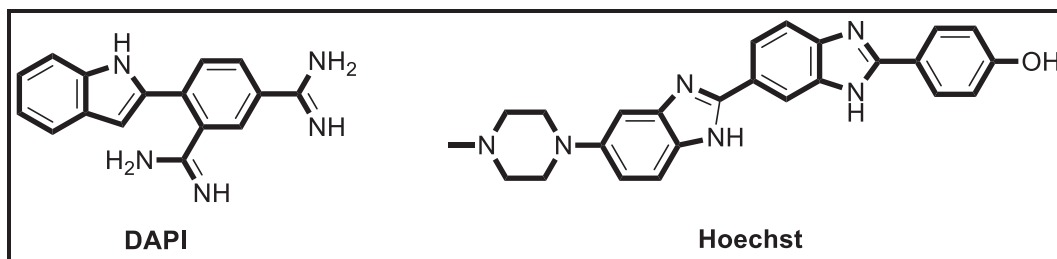


Figure 1.7. Molecular structures of DAPI and Hoechst  
(Source: Haugland, 2005)

Cyanine dyes contain two connected nitrogen centers by a polymethine chain bridge. Each nitrogen can be a piece of different heteroaromatic compounds such as pyrrole, imidazole, indole, pyridine etc. Cyanine dyes are known as near IR emitting dyes and maximum absorption and emission wavelength of which can be easily changed by varying both the length of the polymethine bridge and the heterocyclic structure. They are used for many biological processes such as labeling in nucleic acids and proteins, DNA staining, dead-cell staining, *in vivo* imaging, and proteomics (Narayanan and Patonay, 1995). In addition to their biological usefulness, cyanine molecules are often used for designing fluorescent sensors (Guo et al., 2012; Yin et al., 2015; Zhao et al., 2014).

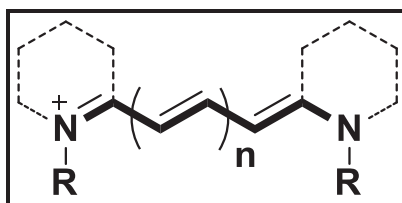


Figure 1.8. General structure of cyanine dyes  
(Source: Narayanan et al., 1995)

Coumarin dyes are member of the benzopyrone family having significant properties such as low molecular weight, water solubility, excitation in UV region and blue fluorescent. These dyes are found in more than thousands of natural products and also used in different fields such as laser dye and organic light-emitting diode (LED) applications, profiling enzymatic activities in cells and fluorescent sensors (Aulsebrook et al., 2015; Liu et al., 2015). Common examples of coumarin derivatives are 7-hydroxy-4-methylcoumarin (4-MU) and 7-amino-4-methyl coumarin (AMC).

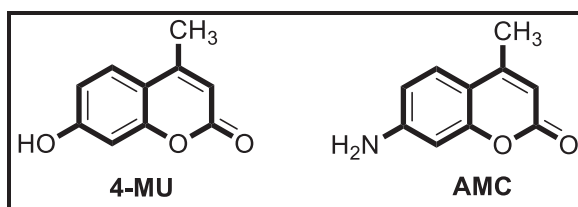


Figure 1.9. Common examples of coumarin derivatives of 4-MU and AMC

## 1.4.Xanthene Based Fluorescent Dyes

Xanthene is a yellow heterocyclic organic compound having molecular formula of  $C_{13}H_{10}O$  and used to kill fungi or fungal spores. Also, it is a practical intermediate in organic synthesis. Fluorescent dyes containing xanthene ring are known as xanthene based fluorescent dyes. Rhodamine and fluorescein dyes are highly favorable xanthene based dyes and they receive intense interest due to their excellent photophysical properties such as high extinction coefficients, high fluorescence quantum yield, great photostability, and relatively long emission wavelength (Chen et al., 2012).

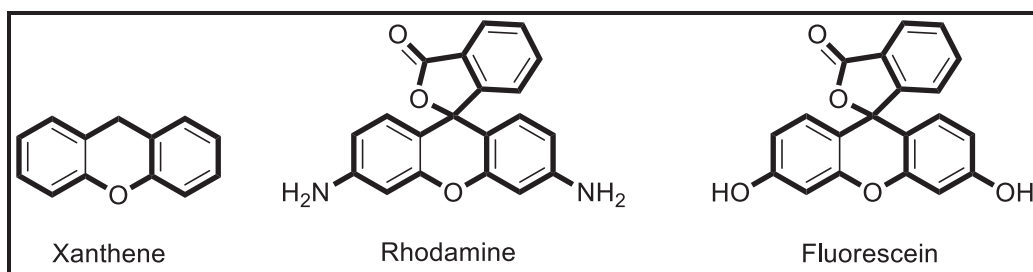


Figure 1.10.Molecular structures of xanthene, rhodamine and fluorescein

### 1.4.1.Fluorescein

In 1871, the German chemist, Adolf von Bayer first synthesized fluorescein by the reaction of resorcinol and phthalic anhydride via Friedel-Crafts acylation/cyclodehydration in the presence of Lewis acid (Baeyer, 1871)

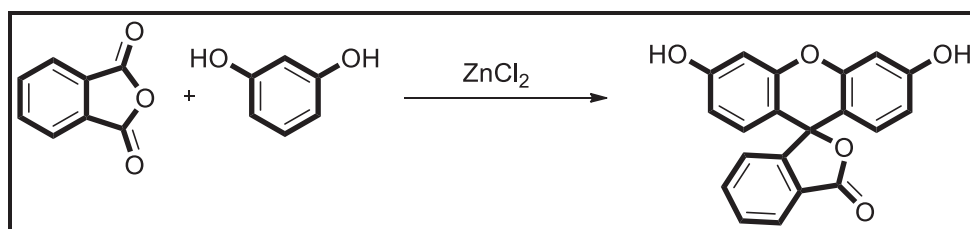


Figure 1.11.Synthesis of fluorescein fluorophore  
(Source: Baeyer, 1871)

In spite of its ancientness, fluorescein is one of the most widely used xanthene based fluorescent dye in modern biochemical, biological and medicinal research. Some

outstanding properties of the fluorescein are good water solubility, visible excitation and emission wavelength, high quantum yields at physiological pH (Gonçalves, 2009). Fluorescein exists in equilibrium between a “closed” lactone form which is non-fluorescent and colorless, and an “open” quinone form which is fluorescent and colorful. Also, in aqueous solution fluorescein can exist in cationic, anionic, neutral and di-anionic forms depending on pH. Under acidic pH (pH 2-4) the fluorescein structure is “closed” non-fluorescent lactone form, at milder acidic pH (pH 5-7) monoanionic form exists with less fluorescent property. When the pH value of fluorescein become 6.4, it exists in dianionic form with a highly hydrophilic and fluorescent feature (Sjöback et al., 1995)

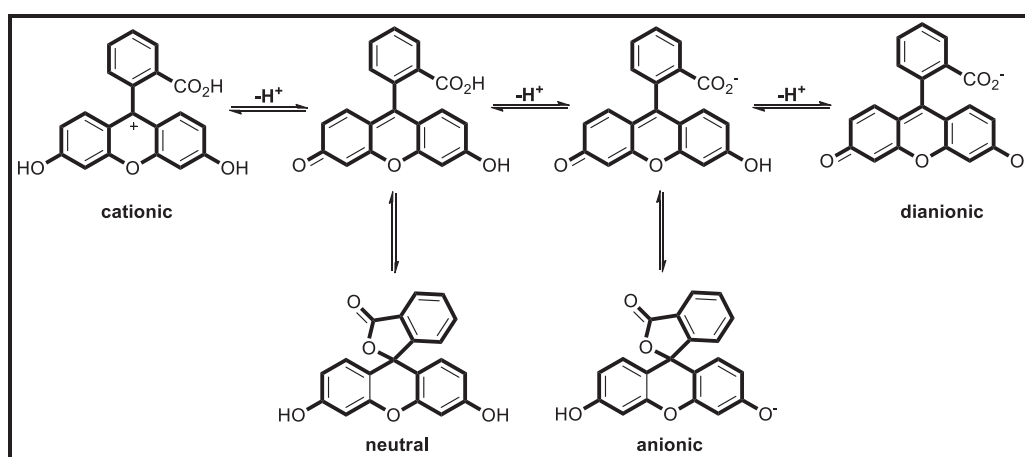


Figure 1.12. pH dependence of fluorescein equilibrium  
(Source: Sjöback et al., 1995)

The fluorescein structure has many reactive sites that can be modified with electrophilic aromatic substitution ( $S_EAr$ ) such as halogenation or sulfonation. 2',4',5',7'-tetrabromofluorescein known as eosin is easily obtained from bromination of the fluorescein moiety. Eosin is counterstain to haematoxylin in the H&E staining which is the most commonly used technique in histology. 2',4',5',7'-tetraiodofluorescein known as erythrosine is another halogenated fluorescein dye used in different field such as food coloring, printing inks, biological staining, dental plaque disclosing agent etc. (R. Martínez-Utrilla et al., 1989).



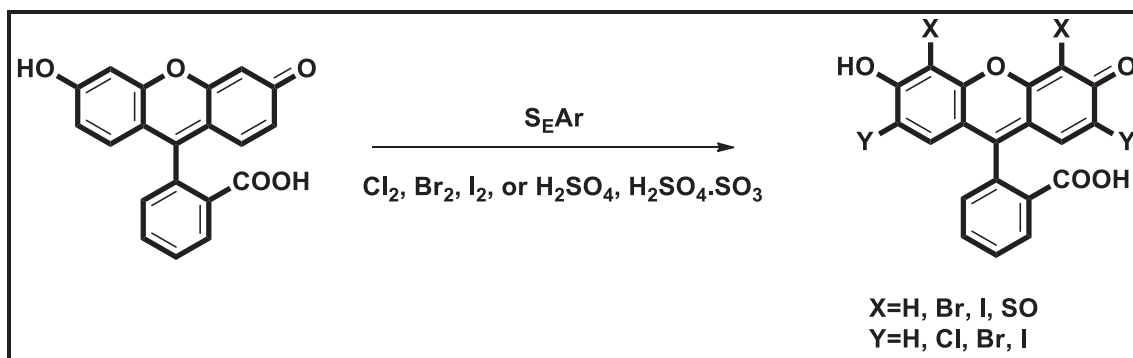


Figure 1.13. Electrophilic aromatic substitution on fluorescein  
(Source: R. Martínez-Utrilla et al., 1989)

Fluorescein and its derivatives are extensively utilized for variety of biological applications in which they are covalently bonded to substances such as peptides, proteins (antibodies), nucleotides, oligonucleotides, drugs, hormones, lipids, and other biomolecules. For example, fluorescein is modified with commercially available reagents through amino or thiol groups of lysine or cysteine residues for labeling of peptides and proteins. Specific labeling of  $\text{NH}_2$  and  $\text{SH}$  is also critical issue that is provided again by succinimidyl and maleimidyl fluorescein derivatives. In addition, fluorescein isothiocyanate (FITC) is the most popular fluorophore used in conjugation with proteins (Gonçalves, 2009).

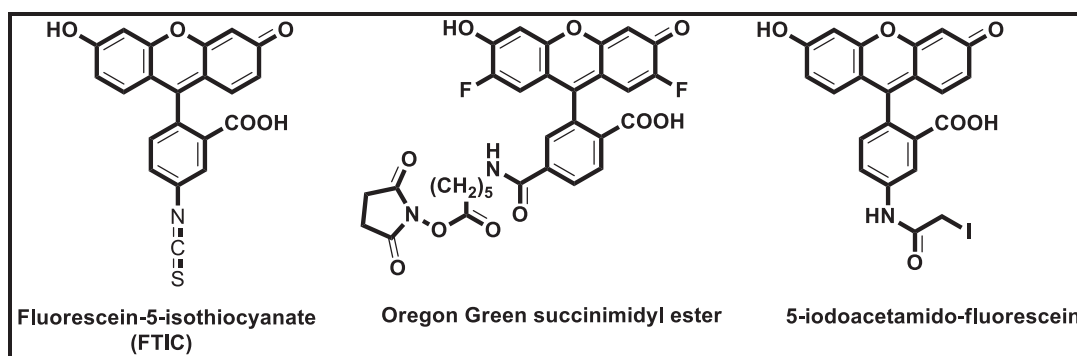


Figure 1.14. Selected fluorescein dyes with different reactive groups

## 1.4.2. Rhodamine

Rhodamine dyes are another class of the xanthene based fluorescent molecules. In 1905, Noelting and Dziewonsky first synthesized rhodamine by the reaction m-aminophenol and phthalic anhydride with a Lewis acid (Noelting and Dziewoński, 1905).

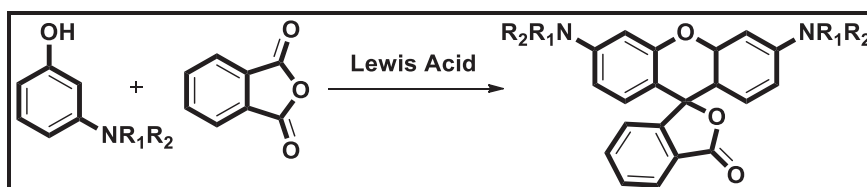


Figure 1.15. Synthesis scheme for rhodamine core  
(Source: Noelting and Dziewoński, 1905)

Recently, rhodamine dyes have attracted significant attention from chemist due to their outstanding photophysical properties such as high photostability, excellent quantum yields, and high extinction/emission coefficients. Rhodamine dyes are widely used in many research area, involving synthetic dyes, laser dyes, fluorescence standards and probes, and fluorescent markers in biological applications (Beija et al., 2009).

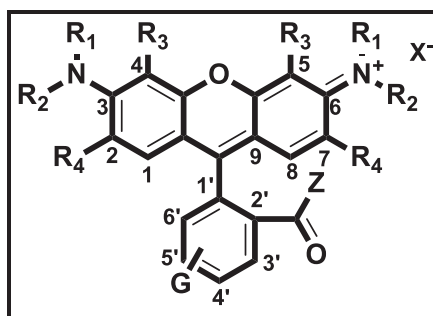


Figure 1.16. General structure of rhodamine dye  
(Source: Beija et al., 2009)

The rhodamine dye shows different photophysical features such as absorption and emission maxima, fluorescence quantum yield ( $\phi$ ) and lifetime ( $\tau$ ) based on the substituents on the phenyl rings (R<sub>1</sub>, R<sub>2</sub>, R<sub>3</sub>, R<sub>4</sub> and G) and even on the counter ion X<sup>-</sup> (usually Cl<sup>-</sup>, Br<sup>-</sup> and ClO<sub>4</sub><sup>-</sup>). Photophysical properties differ from the non-radiative deactivation of the molecule by internal conversion which has both activated and non-activated constituents. The internal conversion of rhodamine dyes competes with the

fluorescence emission of them. Rhodamines with rigid amino groups and bearing none or one alkyl substituent at each nitrogen atoms do not show activated process and their fluorescence efficiency is near to 100% and independent of temperature. However, rhodamines carrying two alkyl substituents at each nitrogen atom present activated internal conversion thus fluorescence efficiency undergoes changing with temperature. Activated internal conversion relates to a non-fluorescent twisted intramolecular charge-transfer (TICT) which is electron transfer process that takes place in molecules that composed of a donor and acceptor part linked by a single bond. In rhodamine dye, electron transfer occurs from amino group to the xanthene ring following a rotation of the bond linking and consequently red-shifted emission is observed. This emission property exhibits interesting behavior depending on the environment such as solvent polarity, pH, and viscosity.

In acidic media, the carboxyl group gains proton and the rhodamine dye turns into its cationic form. However, in a basic media dissociation takes place and rhodamine dye is found as a zwitterion. These two forms have same chromophore indeed, the negative charge causes inductive effect on the central carbon atom of xanthene chromophore inducing a hypochromic shift of both absorption and emission wavelength. When the polarity of organic solvent decreases the zwitterionic form of the dye turns into a colorless lactone form reversibly because of the disruption of  $\pi$ -conjugation of the chromophore. Thus, fluorescence efficiency and life time of the rhodamine dye become very low (Beija et al., 2009)

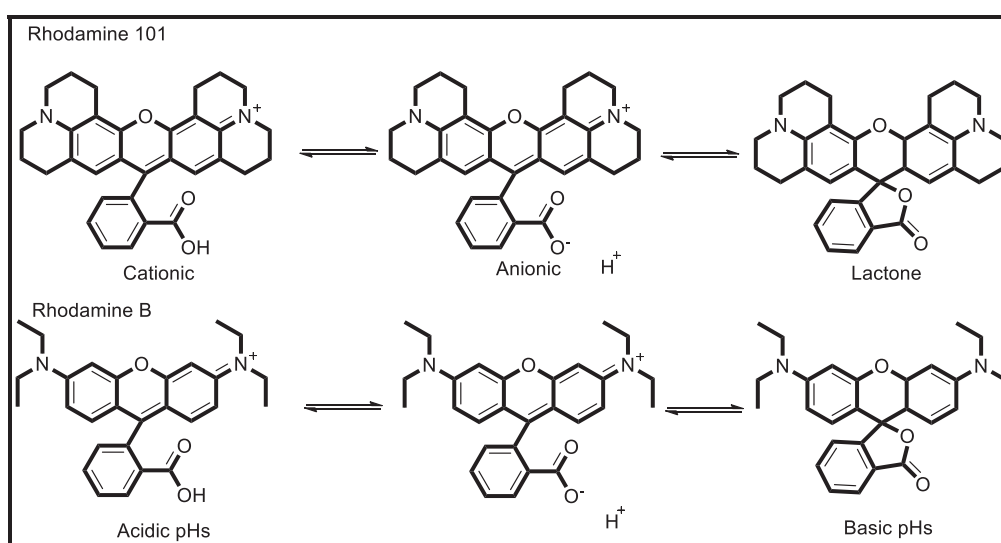


Figure 1.17. Molecular structures of Rhodamine 101 and Rhodamine B in acidic and basic medium (Source: Beija et al., 2009)

Rhodamine and their derivatives are generally obtained from the condensation reaction of m-aminophenol and phthalic anhydride with acid catalyst as mentioned in the beginning of this section. Another method of rhodamine synthesis is direct substitution of 3',6'-dichlorofluoresceins with amines in the presence of  $ZnCl_2$ . This reaction requires elevated temperature and hard work up conditions (Woodroffe et al., 2005)

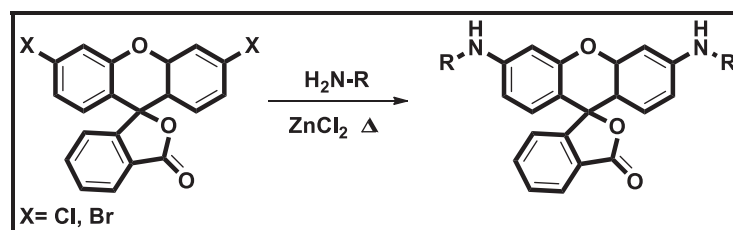
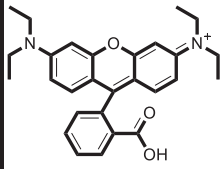
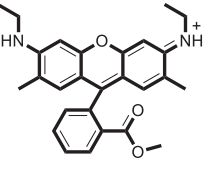
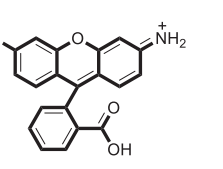
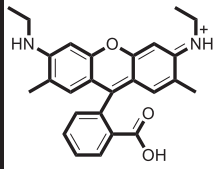
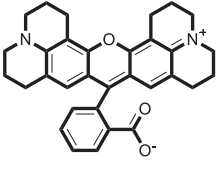
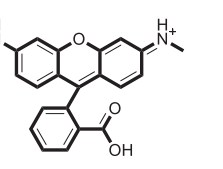


Figure 1.18. Synthesis of rhodamines via direct nucleophilic substitution from halogenated fluorescein (Source: Woodroffe et al., 2005)

Also, some other synthesis strategies are employed to obtain different type of rhodamine derivatives. Generally, commercially available rhodamine dyes are used for this purpose. In figure below, commercially available rhodamine dyes with their price are listed. Rho B and Rho 6G are cheaper dyes of this family and hence they are utilized for further application (Beija et al., 2009).

Structure	€/g <sup>a</sup>	Structure	€/g <sup>a</sup>	Structure	€/g <sup>a</sup>
	0,45		1,60		128
Rho B		Rho 6G		Rho 110	
	156		80		205
Rho 19		Rho 101		Rho 116	

<sup>a</sup>An average price in 2009 for common suppliers: Sigma-Aldrich, Alfa Aesar, Fluka

Figure 1.19. Commercially available rhodamine derivatives (Source: Beija et al., 2009)

## 1.5. Fluorescent Chemosensors

Sensor is a device that detects changes in the environment and responds a corresponding output. The specific input could be light, heat, motion or any other environmental phenomena and the output is a type of a signal that is converted to readable information by humans. Chemosensors are the molecules that detect analyte or molecule being interested and produce detectable response. Chemosensors also called as chromogenic and fluorogenic probes consist of two or three important parts including recognition moiety, signaling moiety and suitable spacer or linker. Signaling moiety acts as signal transducer whose photophysical characteristic change upon reaction with analyte and converts the information into an optical signal. Recognition moiety is responsible for the selective reaction or binding event with analyte depending on the ligand, metal or anion type and solvent characteristic. Spacer or linker holds recognition moiety and signaling moiety close to, but separated from, each other. In the design of chemosensors, there are two main binding strategies, one of them is that the recognition unit is directly attached or integrated into the signaling moiety in which receptor (recognition) unit is a part of the  $\pi$ -electron system of the fluorophore. In other case, there is a spacer or a linker between receptor and signaling subunits that prevents the conjugation (Duke et al., 2010)

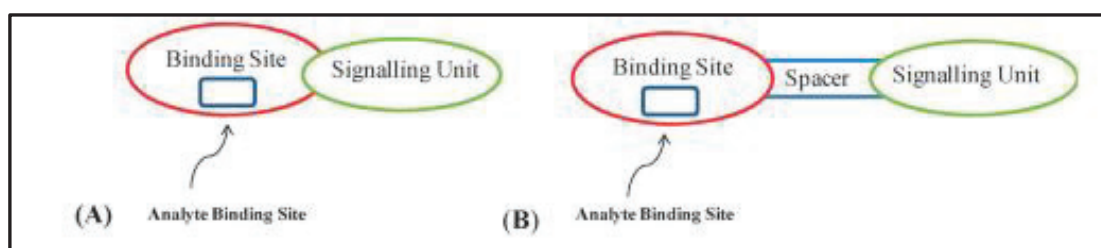


Figure 1.20. Schematic representation of design concept for the construction fluorescent chemosensors (Source: Duke et al., 2010)

The signal of a fluorescent sensor is measured in the changing of absorbance, fluorescence, or fluorescence lifetimes. The changes are observable when the analytes affect photophysical mechanism. There are several types of photophysical mechanism to create fluorescent chemosensors for metal or other analytes such as PET (photoinduced electron transfer), ICT (intermolecular charge transfer), FRET (fluorescence resonance energy transfer), TICT (twisted intramolecular/intermediate charge transfer), and PICT

(planar intramolecular charge transfer). Brief descriptions of the most frequently used mechanisms (PET, ICT, and FRET) are summarized below.

PET generally occurs from donor atoms such as N, O, S, and P having unpaired electrons to the HOMO of the excited fluorophore. Lone pair on the donor atoms interact with the cation and PET process is prevented then “turn-on” fluorescence response is observed. In addition, solvent polarity is very effective for the PET process. When the solvent polarity increases, electron transfer becomes easier and quenching of fluorescence occurs fast. Fluorescence sensors that utilize PET inhibition mechanism, usually does not exhibit spectroscopic shifts of the emission band after binding of analyte to fluorophore (Valeur and Leray, 2000).

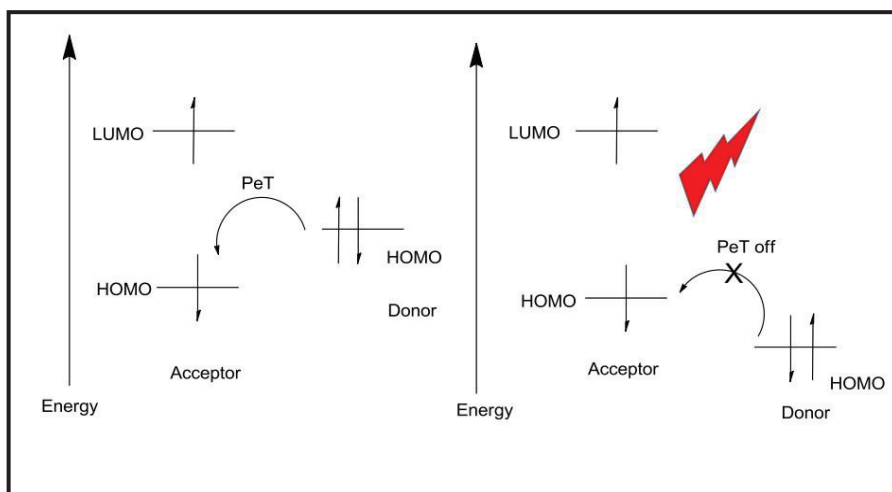


Figure 1.21. Photo induced electron transfer mechanism  
(Source: Valeur and Leray, 2000)

In ICT process, the spacer part between receptor unit and signaling unit is removed and fluorophore is directly bonded to create a  $\pi$ -electron conjugation system in which an electron-rich terminal (donor) and an electron-poor terminal (acceptor) sites. When a receptor moiety bears an electron donating group (such as amino group) conjugated to the signaling unit, the interaction of a cation with a donor unit decreases its electron-donating character which causes a blue shift in absorption spectrum. However, the interaction of a cation with an acceptor unit (such as carbonyl group) improves the electron withdrawing of that group and a red shift is observed in the absorption spectrum (Callan et al., 2005)

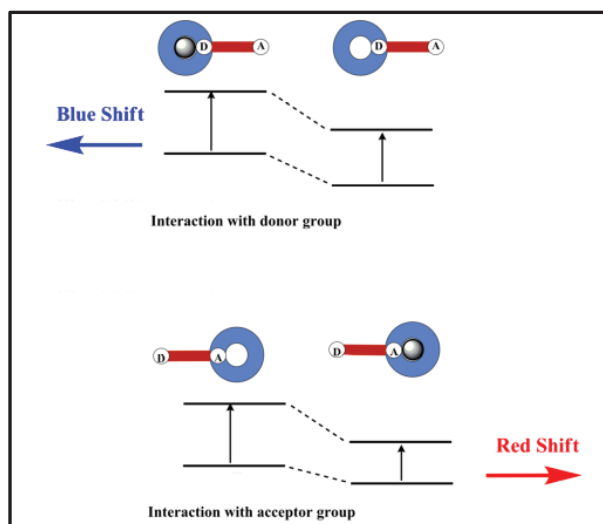


Figure 1.22. Intermolecular charge transfer mechanism (Source: Callan et al., 2005)

In FRET mechanism, two or more fluorophore units are usually connected via non-conjugated linker, the fluorophore having shorter fluorescence emission wavelength provided its energy to another without emission of photons. If FRET occurs upon excitation of a fluorophore, the emission is seen from another fluorophore. To observe FRET process, donor and acceptor units must be in close distance (approximately between 1-10 nm), spectral overlap between donor emission and acceptor absorption must be suitable and relative orientations of their transition dipoles must be nearly parallel (Forster, 1959; Förster, 1948; Serin et al., 2002).

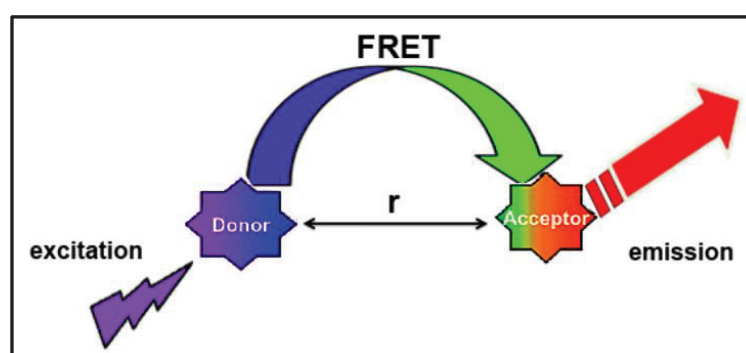


Figure 1.23. Fluorescence resonance energy transfer mechanism (Source: Forster, 1959)

In general, chemical sensors are divided into two main categories depending on sensing event as reversible and irreversible sensors. Irreversible sensors, also known as chemodosimeters, are used to achieve analyte recognition accompanying transduction of

an observable signal by chemical reaction. A specific analyte such as anion, cation or other molecule causes a chemical transformation involving both bond breaking and bond formation. This reaction based approach is also subdivided into two parts (Cheng et al., 2015; Patil et al., 2012).

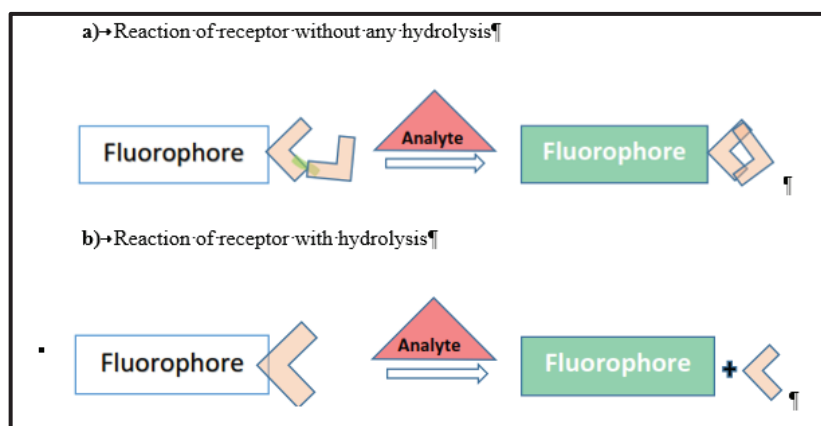


Figure 1.24. Reaction based approaches to construct molecular sensors (Source: Cheng et al., 2015; Patil et al., 2012)

- **Reaction of receptor without any hydrolysis**

In this approach, the fluorescent probe modified with reactive part gives irreversible reaction with targeted analyte without removing any group of the probe. By the aid of this strategy, numerous molecular probes have been designed and developed (X. Li et al., 2014).

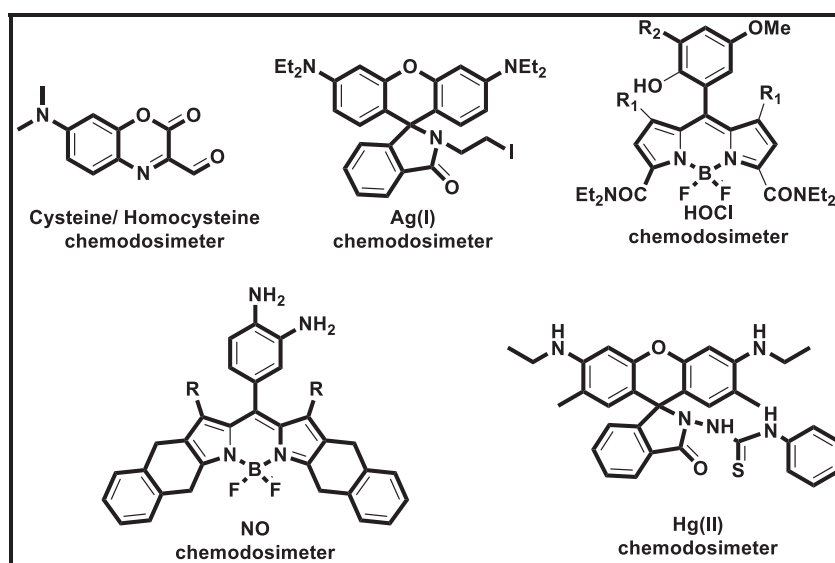


Figure 1.25. Examples of fluorescent molecular sensors classify by reaction based approach (Source: X. Li et al., 2014)



- **Reaction of receptor with hydrolysis**

In this strategy, a fluorophore is bonded to a quencher via cleavable active bond by a certain chemical reaction such as protection-deprotection reaction. The designed probe molecule frequently has no or weak fluorescence before adding targeted analyte. Addition of the analyte provides cleavage of active bond and fluorophore is released, then become fluorescent. Most of these probes exhibit higher selectivity for targeted analytes compare to complexation based chromogenic and fluorogenic probes (Dujols et al., 1997; Karakuş et al., 2016; Lo and Chu, 2003).

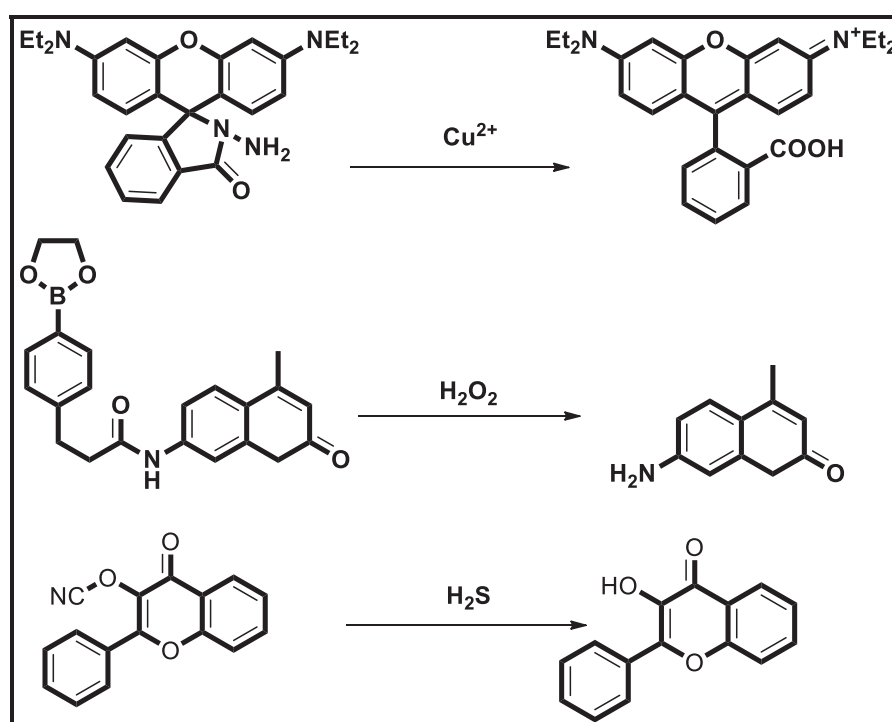


Figure 1.26. Examples of fluorescent molecular sensors classify by hydrolysis reaction based approach (Source: (Dujols et al., 1997; Karakuş et al., 2016; Lo and Chu, 2003))

On the other hand, reversible sensors also known as chemosensors, are used to achieve analyte diagnosis depending on coordination event. The coordination with targeted analyte and coming along signal alteration are reversible which is the major difference between chemosensors and chemodosimeters. The coordination based strategy is also subdivided into two parts.

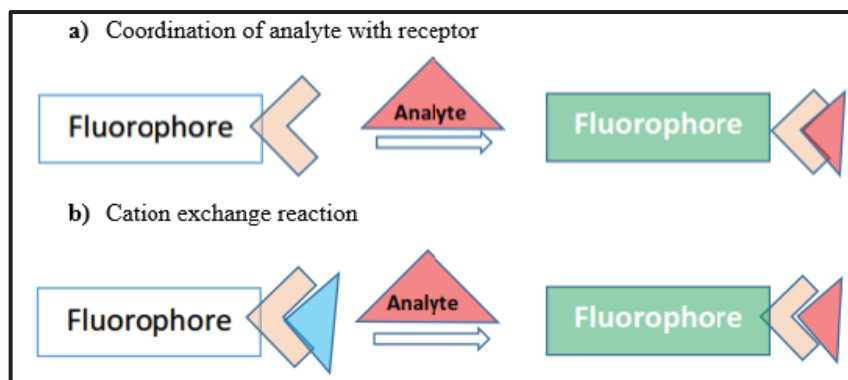


Figure 1.27. Coordination based approaches to construct molecular sensors

- **Coordination of analyte with receptor**

In this approach, the designed probe molecule directly complexes with analyte by noncovalent interactions such as electrostatic interaction, van der Waals interaction and hydrogen-bonding interactions.

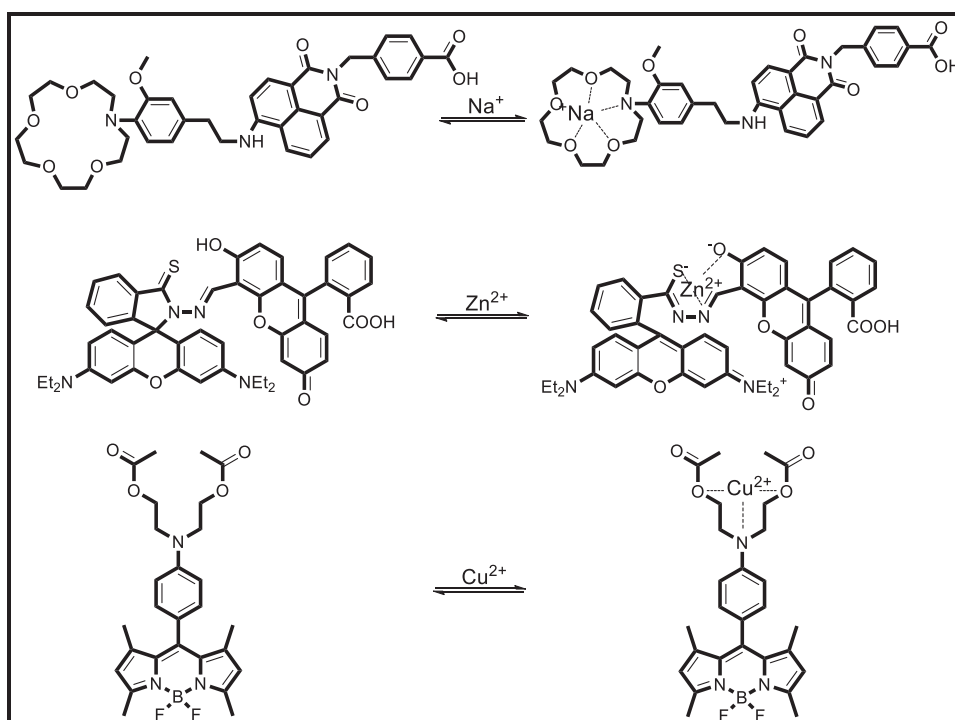


Figure 1.28. Examples of coordination based fluorescent sensors  
(Source: X. Li et al., 2014)

As can be seen in Figure 1.27., the coordination site of the fluorophore attaches the targeted analyte accompanying by changing either in the color or in its fluorescence act. The most essential situation in this strategy is that changing in colorimetric or

fluorometric behavior can be easily reversed with adding specific reagent. Some examples of coordination-based fluorescent sensors are summarized in the figure above (X. Li et al., 2014; Martínez-Máñez and Sancenón, 2003).

- **Cation exchange reaction**

Cation exchange reaction also known as metal displacement or metal exchange reaction in which both fluorophore and receptor units are not covalently bounded but found as molecular ensemble (coordination complex). When a targeted analyte is added into fluorophore-receptor complex, receptor-analyte displacement reaction takes place. If the spectroscopic behavior of the fluorophore in the molecular ensemble is different from its non-coordinated form, observable signal is obtained after analyte exchanging (Martínez-Máñez and Sancenón, 2003).

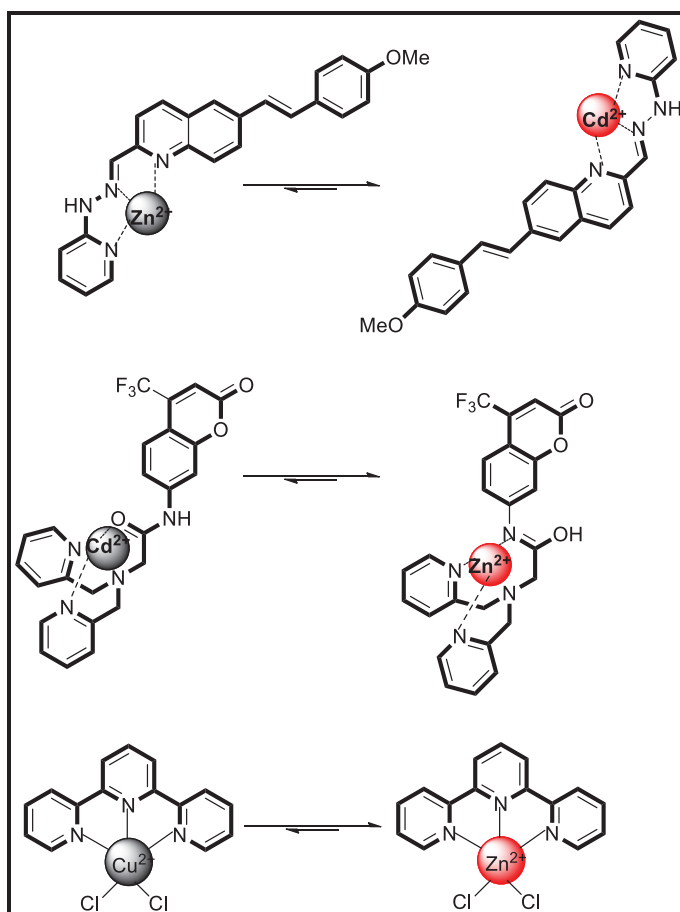


Figure 1.29. Examples of cation exchange reaction based fluorescent sensors (Source: Cheng et al., 2015)

## 1.6. Rhodamine as Molecular Sensor

Rhodamine dyes are well-known fluorophores with remarkable photophysical properties, such as long absorption and emission wavelengths, high fluorescence quantum yields and large absorption coefficients. The unique ring opening equilibrium of their spirocyclic derivatives has been widely utilized in the design of turn-on type fluorescent probes. The rhodamine spirolactam can exist in two isomeric forms which always exhibit completely different fluorescent properties. In its closed form (spirocyclic) is basically colorless and non-fluorescent (turn-off); however, ring-open form displays strong absorption and fluorescence emission (Kim et al., 2008). This unique behavior of rhodamine has been exploited as a signal modulation mechanism in chemosensor and chemodosimeter design.

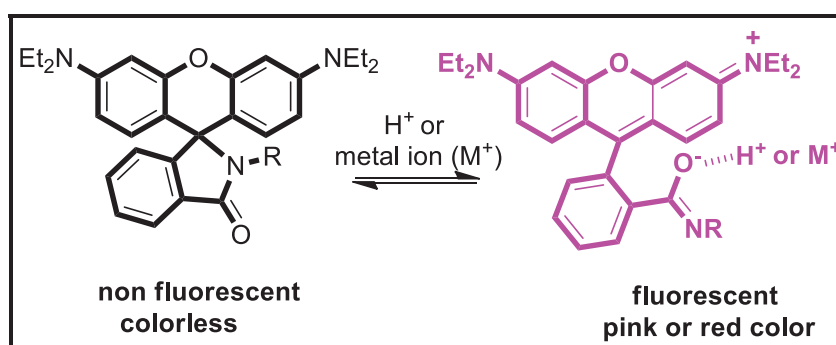


Figure 1.30. Spirolactam ring-opening process of rhodamine derivative  
(Source: Kim et al., 2008)

In 1997, Anthony W. Czarnik pioneered their work by utilizing ring opening process of rhodamine compound. In their study, rhodamine-B hydrazide was used as fluorescent probe for  $Cu^{2+}$  and this derivative can recognize  $Cu^{2+}$  with high selectivity. The  $Cu^{2+}$  promoted hydrolysis can release fluorescent rhodamine-B as a product and the related process is shown in Figure 1.31 (Dujols et al., 1997).

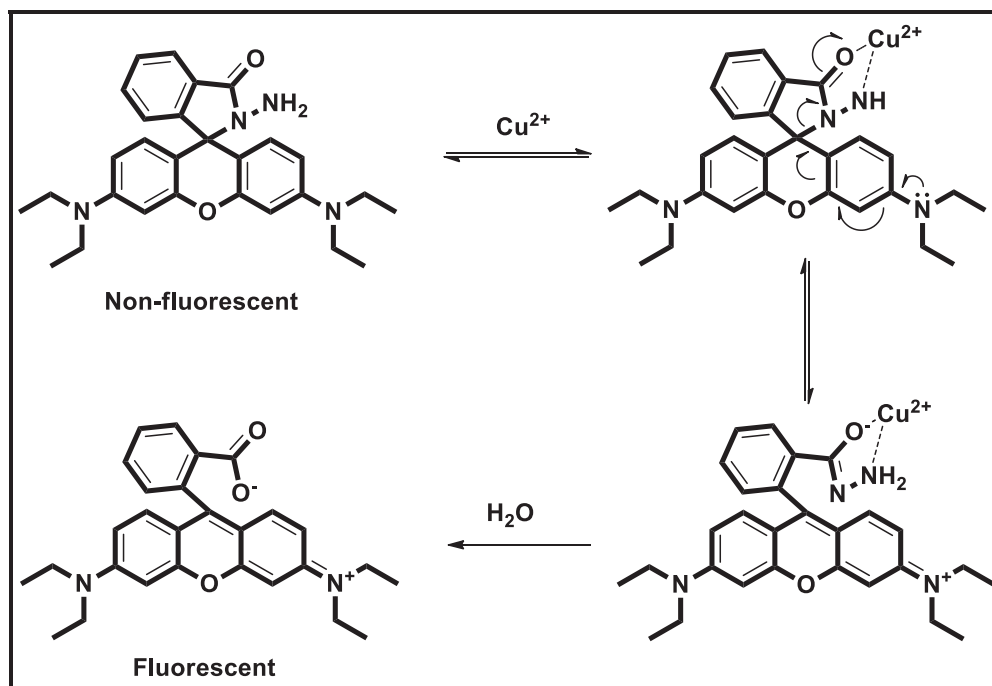


Figure 1.31. Cu<sup>2+</sup>-assisted hydrolysis of Czarnik's rhodamine B hydrazone (Source: Dujols et al., 1997)

After Czarnik's work, many exciting papers involving fluorescent probes depending on ring-opening processes have been reported. Among the species to be detected are different type of metal ions (Cu<sup>2+</sup>, Hg<sup>2+</sup>, Fe<sup>3+</sup>, Zn<sup>2+</sup>, Cr<sup>3+</sup>, Ag<sup>+</sup>, Au<sup>3+</sup>, Pd<sup>2+</sup>, Pb<sup>2+</sup>, Pt<sup>2+</sup> etc.), anions, reactive oxygen species, thiols and involved various pH values, temperature etc.

### 1.6.1. Detection of Metal Ions by Spiroring-Opening of Rhodamine Derivatives

Metals are irreplaceable for human life because they are involved in many important biological processes such as catalysis, osmotic regulation, metabolism and signaling. The significant metals in biological system can be divided into two main categories: Group I and II metals (alkaline and alkaline earth metals such as sodium, potassium, calcium magnesium etc.) and transition metals (e.g. Fe, Zn, Cu, Mn, Co, Ni, Mo, V, and Se). They are often indicated as trace element because they are found as lower level than the group I and II metals. Although some transition metals have vital and beneficial effects in living systems, they are very toxic that causes serious environmental

and health problems. Some of transition metal ions such as  $\text{Fe}^{2+}$ ,  $\text{Zn}^{2+}$ ,  $\text{Cu}^{2+}$ ,  $\text{Co}^{2+}$ ,  $\text{Mn}^{2+}$  and  $\text{Mo}^{6+}$  are crucial for the sustainability of human metabolism. However, when accumulated in the biological system at certain concentrations, they can lead to serious illnesses. Other transition metals such as  $\text{Hg}^{2+}$ ,  $\text{Cd}^{2+}$ ,  $\text{Pb}^{2+}$  and  $\text{As}^{3+}$  are among the most toxic ions known that lack any vital and beneficial effect. Therefore, simple and reliable detection methods for transition metal ions with high selectivity are highly desirable. Trace metal analysis relying on fluorescence technique are very popular. In contrast to the traditional instrumental techniques, fluorescence-based techniques have many preferable advantages such as low cost, simplicity, high sensitivity and reproducibility (Quang and Kim, 2010).

Since the report of Czarnik's rhodamine-B hydrazide, Tae *et al.* presented design, synthesis and spectral properties of a novel rhodamine-6G derivative which operates as a highly selective and sensitive chemodosimeter for  $\text{Hg}^{2+}$  in aqueous solution. The system undergoes an irreversible desulphurization- cyclization reaction to form a oxadiazole derivative (Yang *et al.*, 2005)

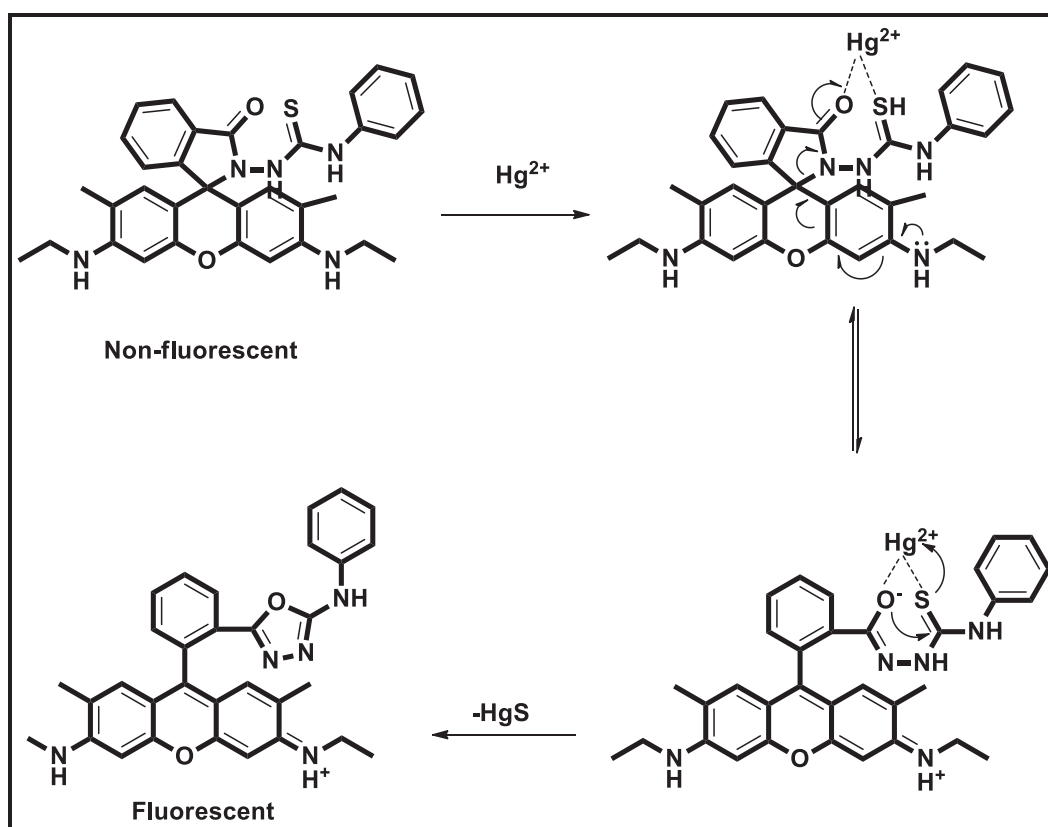


Figure 1.32.  $\text{Hg}^{2+}$  induced ring opening and cyclization of Tae's chemodosimeter (Source: Yang *et al.*, 2005)

Yoon *et al.* also reported another rhodamine-B derivative as a fluorescent chemosensor that allows detection of  $\text{Pb}^{2+}$  ions based on reversible complexation reaction, as shown in Figure 1.33 (Kwon *et al.*, 2005).

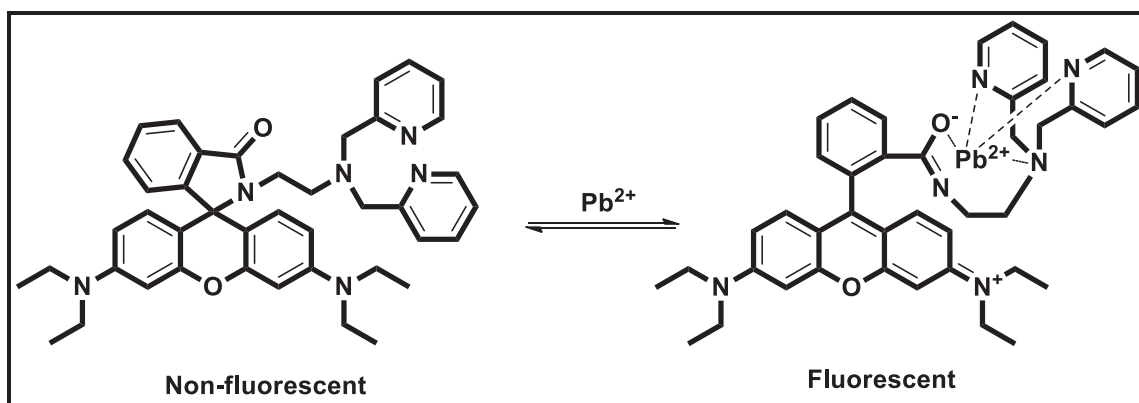


Figure 1.33. Proposed binding mode of Yoon's chemosensors with  $\text{Pb}^{2+}$  (Source: Kwon *et al.*, 2005)

There are many metal ion detection studies in the literature based on developing chemosensor and chemodosimeter by utilizing spiroring-opening reaction of rhodamine derivatives. Outstanding examples of these works are given in Figure 1.34 (Chen *et al.*, 2012).

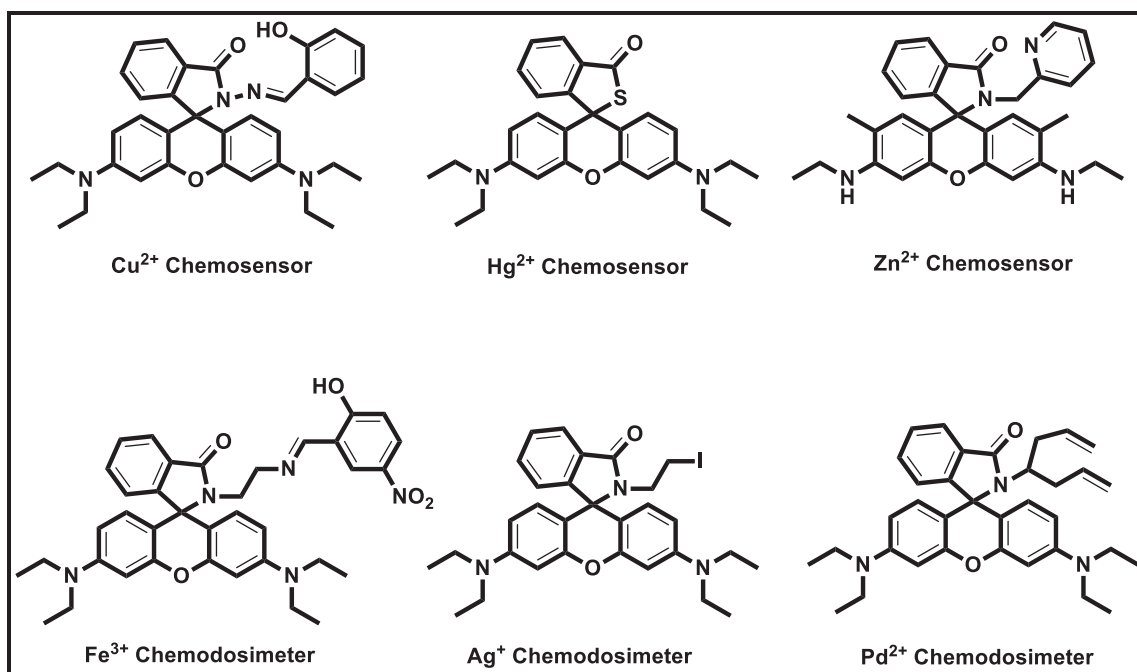


Figure 1.34. Chemosensor and chemodosimeter examples by utilizing spiroring-opening reaction of rhodamine derivatives (Source: Chen *et al.*, 2012)

## 1.6.2. Detection of Anions based on Rhodamine and Related Derivatives

Anions play a key role in a wide range of chemical and biological processes. It is thus important to develop techniques for sensing or quantifying some anions such as potentially toxic anions (e.g. cyanide) or environmentally deleterious anions (e.g. phosphate or nitrate). Until now, there are many examples for the detection of anions utilizing different optical signaling systems, namely (i) the “binding site-signaling subunit” way, (ii) the “displacement” approach and (iii) the “chemodosimeter mode. In the binding site-signaling subunit approach, there are two main parts which are linked through a covalent bond and the interaction of the anion with the binding site alters characteristic of the subunit either in the color or fluorescence behavior. The displacement approach, as in the previous case, contains both signaling and binding subunits but they are not attached covalently. The sensing strategy relies on a displacement; the complexation of a target anion in the binding site result in the release of the signaling subunit accompanying change in its optical behavior (Martínez-Máñez and Sancenón, 2003).

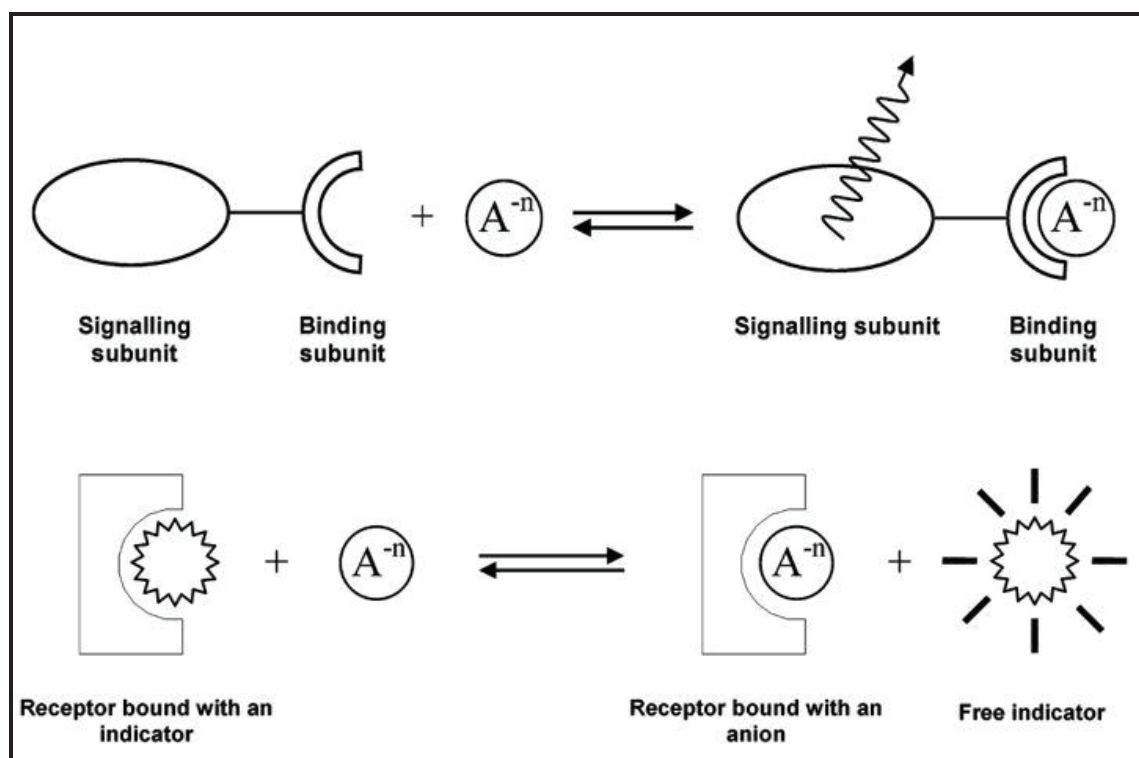


Figure 1.35. Binding site-signaling subunit and displacement approaches for the anion sensing (Source: Martínez-Máñez and Sancenón, 2003)



A third method of the anion sensing is the chemodosimeter approach which involves the targeted anions induce specific chemical reaction (usually irreversible) that results in changing color or emission variations (Martínez-Máñez and Sancenón, 2003).

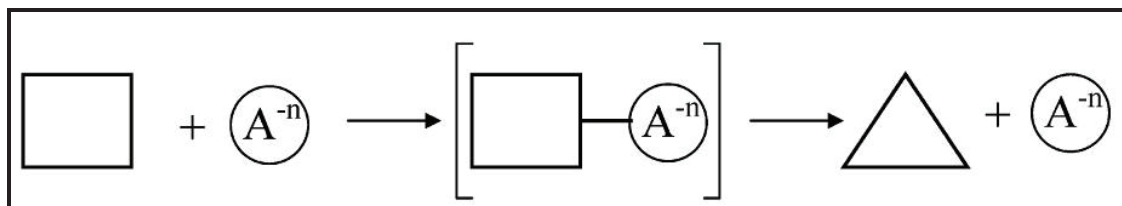


Figure 1.36. Chemodosimeter approach for the anion sensing  
(Source: Martínez-Máñez and Sancenón, 2003)

There are many anion detection works in the literature utilizing spiro ring-opening reaction of rhodamine derivatives. Some examples of these are shown in Figure 1.37.

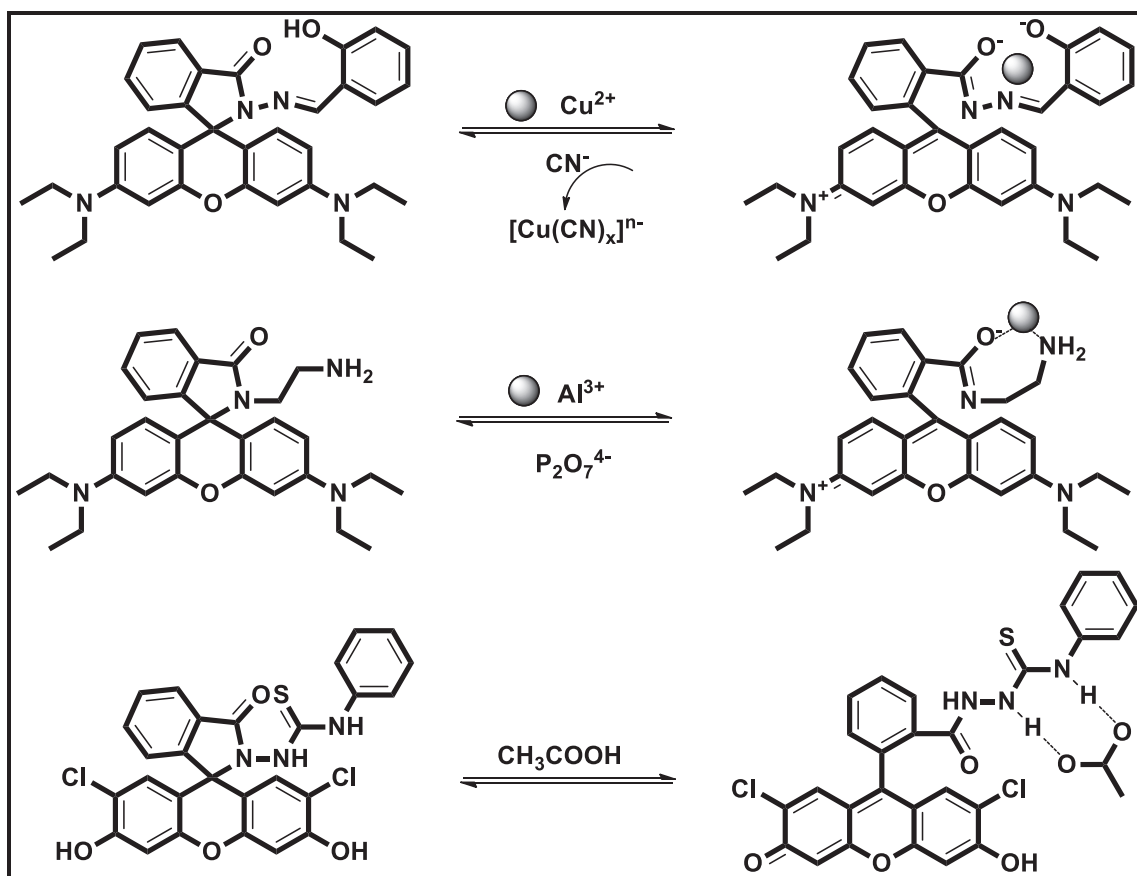


Figure 1.37. Some important anion sensor examples of spirolactam derivatives  
(Source: Chen et al., 2012)

### 1.6.3. Detection of Reactive Oxygen and Nitrogen Species and Thiols based on Rhodamine Derivatives

Reactive oxygen species (ROS) derive from molecular oxygen that is essential for all aerobic organism including human. Hydrogen peroxide ( $\text{H}_2\text{O}_2$ ), hydroxyl radicals ( $\cdot\text{OH}$ ), peroxy radicals ( $\text{ROO}\cdot$ ), singlet oxygen ( $^1\text{O}_2$ ), superoxide anion radicals ( $\text{O}_2\cdot^-$ ) and hypochlorous acid/hypochlorite ions ( $\text{HOCl}/\text{OCl}^-$ ), which are all produced during vital processes in living organisms. Reactive nitrogen species (RNS) such as nitric oxide ( $\cdot\text{NO}$ ), nitrogen dioxide radical ( $\cdot\text{NO}_2$ ), peroxy nitrite anion ( $\text{ONOO}^-$ ) etc. are also continuously generated in small amount during normal cellular processes. ROS and RNS play crucial role in a wide range of physiological and in pathogenic processes. However, when they are overproduced (e.g. due to exogenous stimulation) or when the level of antioxidants become very low these reactive species will be highly harmful, inducing oxidative stress through the oxidation of biomolecules, leading to irreversible cellular damage. Also, pollutants of some ROS and RNS in the environment threaten human health. Due to these adverse effects, sensitive and accurate detection methods are highly demanded to monitor ROS and RNS in living cells, tissues and organisms, as well as in environmental samples. However, reactive species show some behaviors that make them difficult to detect, such as their very short lifetime and the variety of antioxidants existing in vivo, capable of capturing these reactive species. Thus, it is important to develop a strategy to overcome these problems. Fluorescent probes are highly promising for the detection of ROS and RNS as they are highly sensitive, allow the possibility of real-time visual detection of analytes and lack of a requirement for sophisticated instrumentation. These probes also have the advantage of easy visualization of intracellular dynamics and high-resolution localization of biomolecules of interest (Chen et al., 2016).

A variety of rhodamine based fluorescent probes have been developed in the literature to detect ROS/RNS in order to uncover their unique functions in biological systems. Most important examples of these probes are given in Figure 1.38.

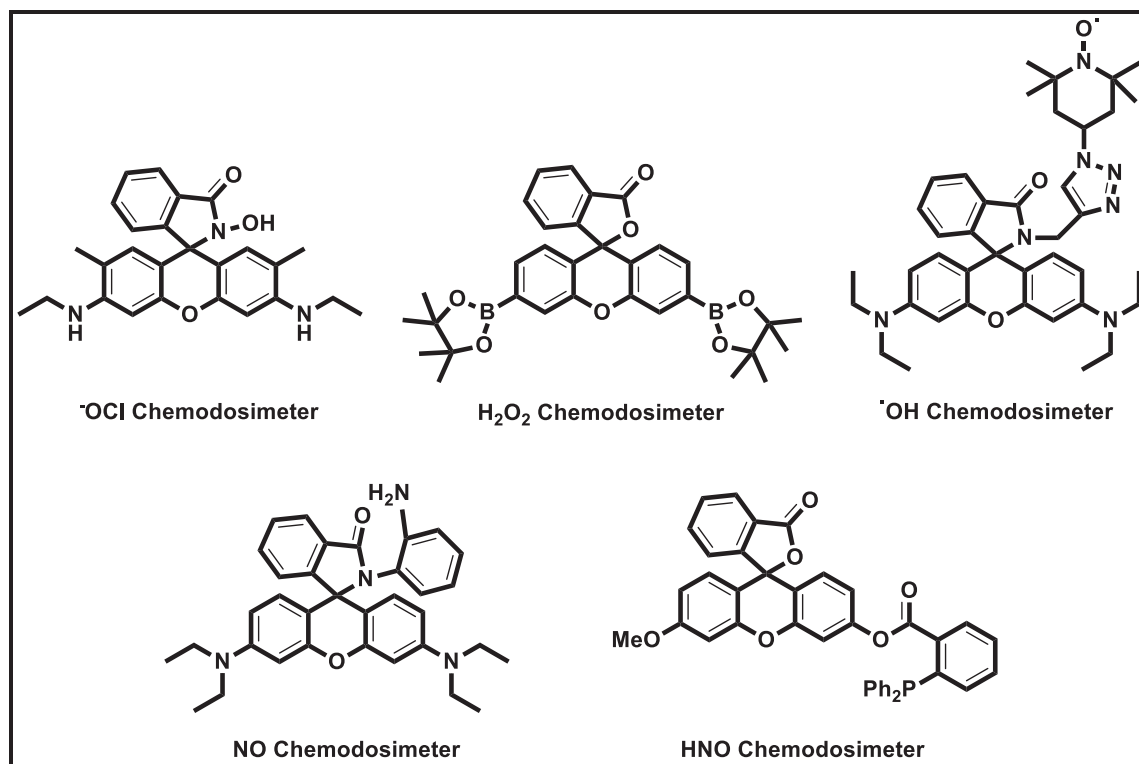


Figure 1.38. Some important ROS/RNS sensor examples of xanthene derivatives  
(Source: Chen et al., 2016)

Biological thiols such as cysteine (Cys), homocysteine (Hcy) and glutathione (GSH) play essential role in living organism and are involved in many biological processes. Generally abnormal level of these thiols is related to number of diseases. For example, Cys deficiency is associated with some syndromes such as slow growth in children, hair depigmentation, edema, lethargy, loss of muscle and fat, liver damage, skin lesions and weakness. Hcy is a risk factor for Alzheimer's disease, folate and cobalamin deficiencies, and cardiovascular diseases. GSH is the most abundant intracellular non-protein thiol, provide many biological processes including maintenance of intracellular redox activities, xenobiotic metabolism and gene regulation. Due to biological importance of thiols, the development of fluorescent and/or colorimetric methods become highly crucial for the detection of these thiols (Jung et al., 2013).

In the literature, there are variety examples of rhodamine based probes for the detection of thiols (Cys, Hcy and GSH) and most important examples are chosen and illustrated in Figure 1.39.

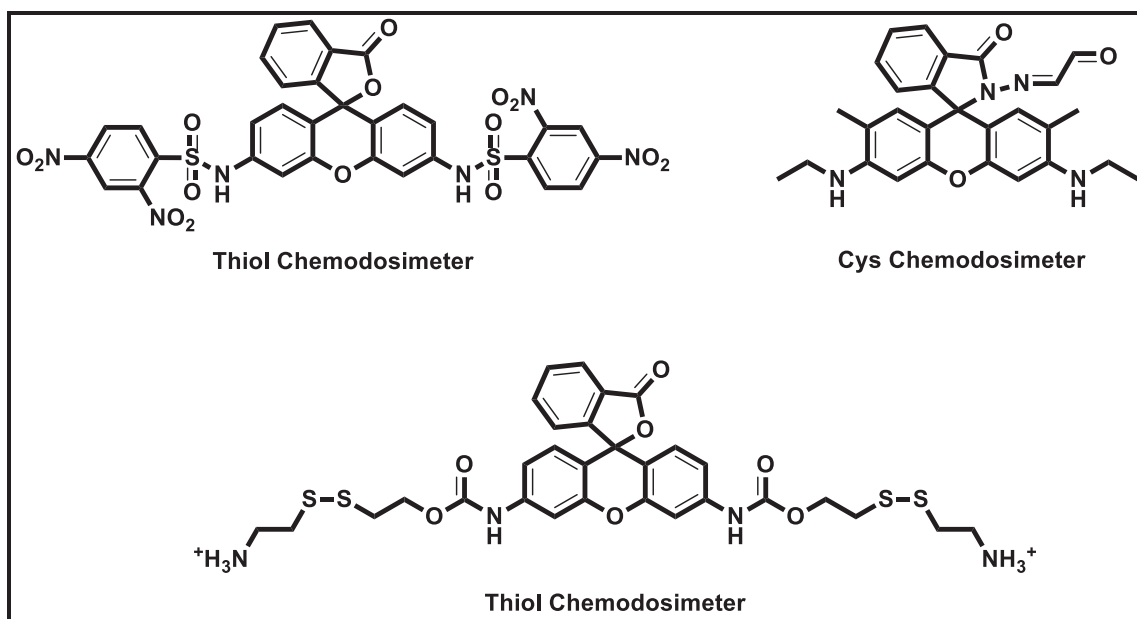


Figure 1.39. Some important thiol probes based on rhodamine derivatives  
(Source: Jung et al., 2013)

## CHAPTER 2

### SPIRO RING OPENING REACTION BASED MOLECULAR SENSORS FOR GOLD ION DETECTION

#### 2.1. Literature Studies

The fluorescent or colorimetric detection of gold ions had not been achieved until 2009 since gold was one of the least reactive chemical elements and due to its quenching property of fluorophore units (heavy atom effect). The first gold ion selective fluorescent chemosensor was published by Tae and co-workers in 2009 (Yang et al., 2009). In this study, they designed a novel rhodamine based chemodosimeter bearing alkyne moiety that did not show any absorption or fluorescence emission in spirocyclic form. The concomitant addition of  $\text{Au}^{3+}$  ions triggered activation of the triple bonds inducing spirocyclic ring opening reaction of rhodamine. The resulting molecule was pink in the solution and gave strong orange fluorescence. Approximately 50 nM of  $\text{Au}^{3+}$  ions could be detected in aqueous media with the developed probe. Another important property of this new sensing strategy was its applicability to living cells. Tea and co-workers also showed bioimaging applications of their molecule in HeLa cells successfully.

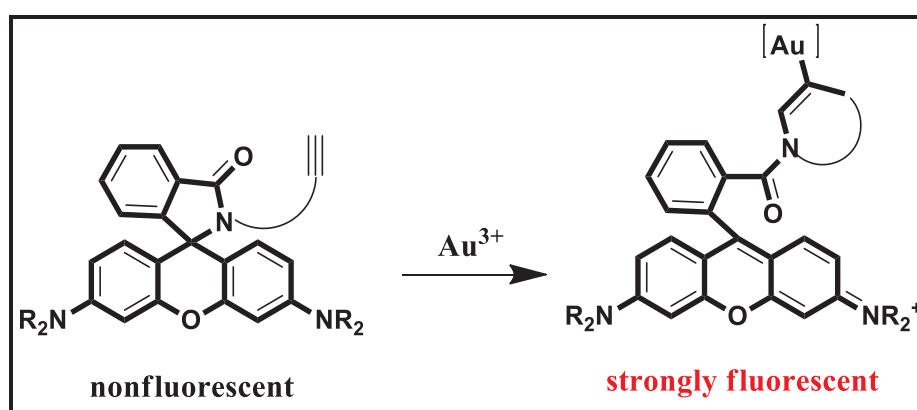


Figure 2.1. First example of gold ion selective and sensitive molecular sensor (Source: Yang et al., 2009)

After Tae's study, two independent groups were reported their work simultaneously (Egorova et al., 2010; Yang et al., 2009). In each study, rhodamine was adopted as a fluorophore and was integrated with an propargyl amine moiety. The fluorescence change was assigned to the ring opening spirolactam followed by intramolecular cyclization reaction forming oxazolecarbaldehyde.

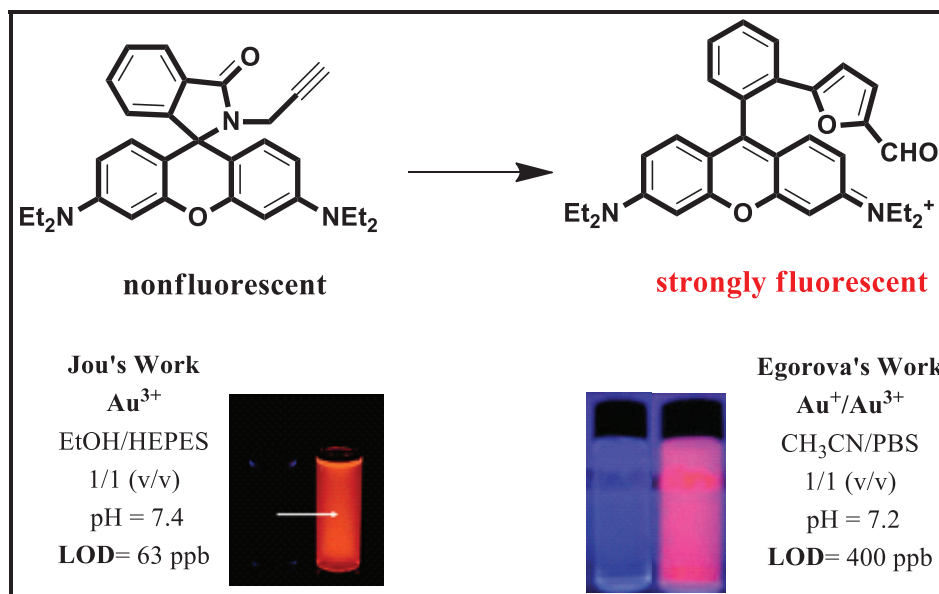


Figure 2.2. Rhodamine-propargylamide based fluorescent sensor for gold ions (Source: Egorova et al., 2010; Yang et al., 2009)

The main difference of these two works was the sensing system media. In Jou's study  $\text{Au}^{3+}$  ions were designated in EtOH/HEPES (1/1 (v/v), pH = 7.4) system; however, the same probe detected both  $\text{Au}^{3+}$  and  $\text{Au}^+$  in  $\text{CH}_3\text{CN}/\text{PBS}$  system (1/1 (v/v), pH = 7.2). These studies obviously showed that the effect of sensing media is very important for analyte selectivity.

In 2011, Yuan *et al.* published a study different from previous works mentioned above in which rhodamine fluorophore bears a recognition unit without alkyne moiety (Yuan et al., 2011). In this work, rhodamine 6G/B hydrazides were integrated with an phenylisocyanate moiety to obtain fast responsive and novel gold ion fluorescent probe. Mechanistic analysis of the probe for the recognition of gold ions was based on unprecedented  $\text{Au}^{3+}$  mediated hydrolysis of acylsemicarbazides to carboxylic acids.

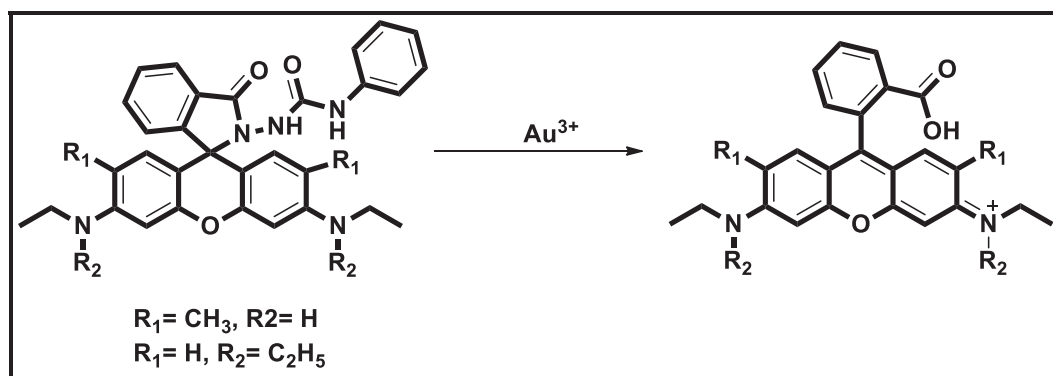


Figure 2.3. Fluorescent molecular sensor works via hydrolysis of acylsemicarbazide (Source: Yuan et al., 2011)

The favorable properties of the unique probe include fast response (<1 min) at room temperature, operating in almost aqueous media, cell membrane permeability, low cytotoxicity, high sensitivity (LOD = 290 nM), and high selectivity. These desirable features made it useful not only for gold ion bioimaging in living cells, but also for detection of residual gold in gold-catalyzed synthetic products for the first time.

Towards the end of 2011, the first example of a reversible  $\text{Au}^{3+}$  probe was reported by Wang *et al.* (Wang et al., 2011). They designed rhodamine based novel fluorescent probe from condensation reaction of rhodamine 6G hydrazide and 8-hydroxyquinoline-2-carbaldehyde followed by the zinc mediated reduction in acetic acid.

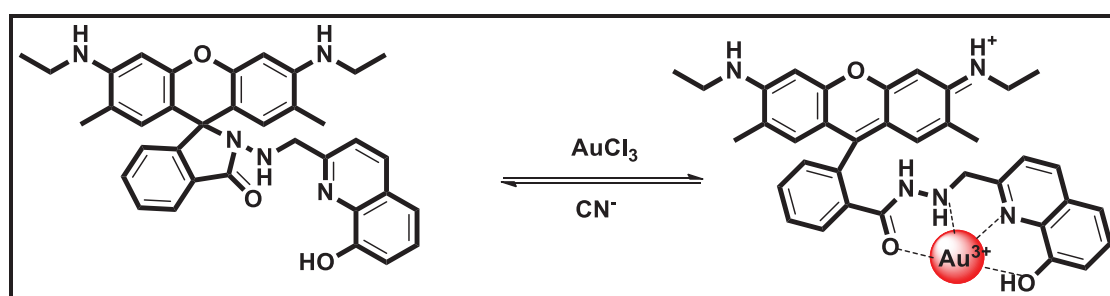


Figure 2.4. The first example of reversible gold (III) ion sensor (Source: Wang et al., 2011)

According to proposed mechanism,  $\text{Au}^{3+}$  made favoring interactions with heteroatoms included in probe molecule. These interactions induced ring opening reaction of spirocyclic rhodamine compound resulting in an enhancement in fluorescence intensity. To investigate whether the process was reversible or not, an excess amount of  $\text{CN}^-$  was added into the medium containing probe molecule and  $\text{Au}^{3+}$  ions. After addition

of  $\text{CN}^-$  the bright fluorescence immediately disappeared. This result proved reversible character of the binding of probe and  $\text{Au}^{3+}$  ions. Also, detection limit of this novel probe was determined as 48 nM and bioimaging application was carried out successfully.

In 2012, Patil and Ahn groups concurrently disclosed an innovative approach, anchoring-unanchoring of a fluorophore, for the detection of gold ions (Patil et al., 2012; Seo et al., 2012). In this approach, fluorescence property of the sensor molecule was quenched with an organic substrate. After interaction of this molecule with gold ions, highly fluorescent part was liberated from the probe with the formation of organic product. (Figure 2.5).

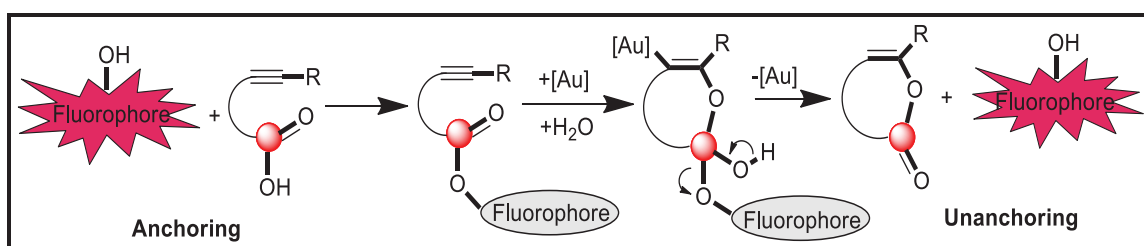


Figure 2.5. Approach involving anchoring-unanchoring of a fluorophore  
(Source: Seo et al., 2012)

In these two works, fluorescein and (2-ethynyl) benzoate were used as a fluorophore and reactive unit respectively. Esterification reaction of 2-iodobenzoic acid and methoxy fluorescein was carried out followed by Sonagashira coupling to synthesize the probe molecule (Figure 2.6).

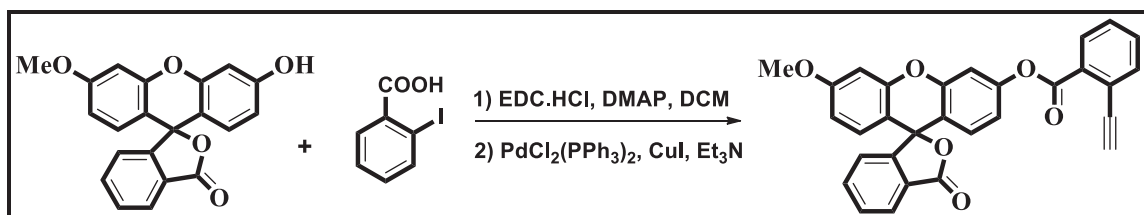


Figure 2.6. Synthesis of fluorescein based gold ion probe  
(Source Seo et al., 2012)

Activation of ethynyl group by  $\text{Au}^{3+}$  would generate oxonium intermediate. Then, this intermediate would subsequently undergo hydrolysis to regenerate the strongly fluorescent fluorescein, along with isochromen-1-one. (Figure 2.7) The favorable features



of the probe were fast responsive, highly sensitive and applicable for bioimaging applications.

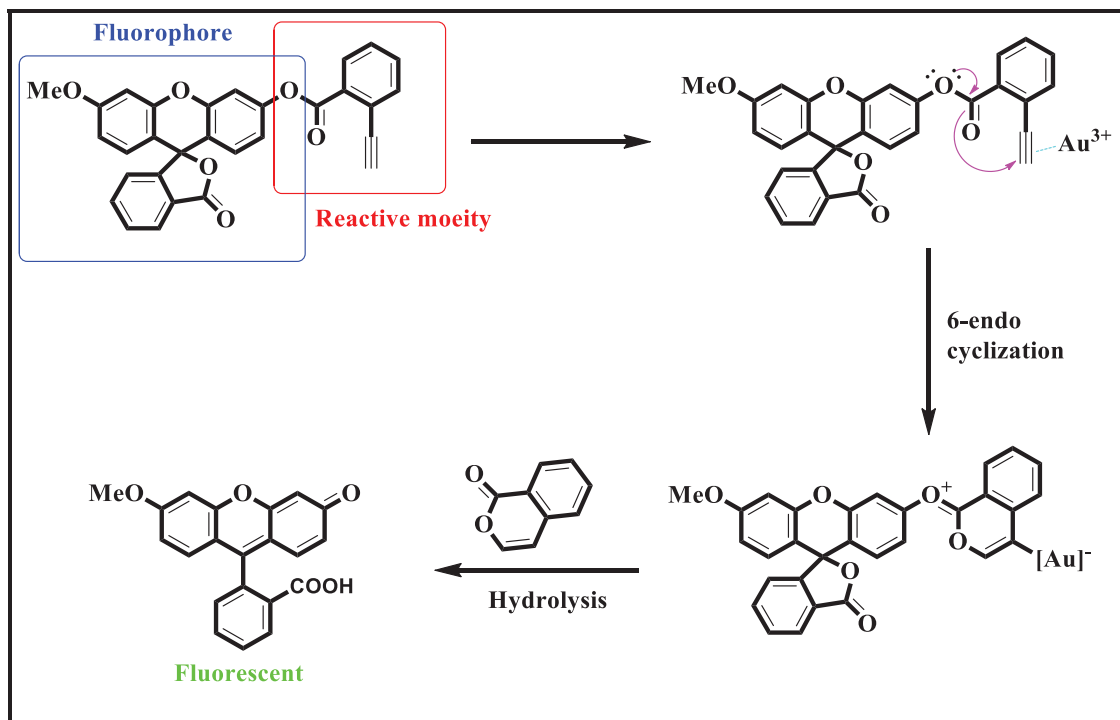


Figure 2.7. Mechanistic pathway of gold ion sensing  
(Source: Patil et al., 2012)

In 2014, Ahn group reported a study to prevent side reactions observed in the reaction based gold ion sensing system based on alkyne activation. By enhancing steric strain around the reaction side, the gold ion triggered ring-opening process was significantly expedited (Seo et al., 2014).

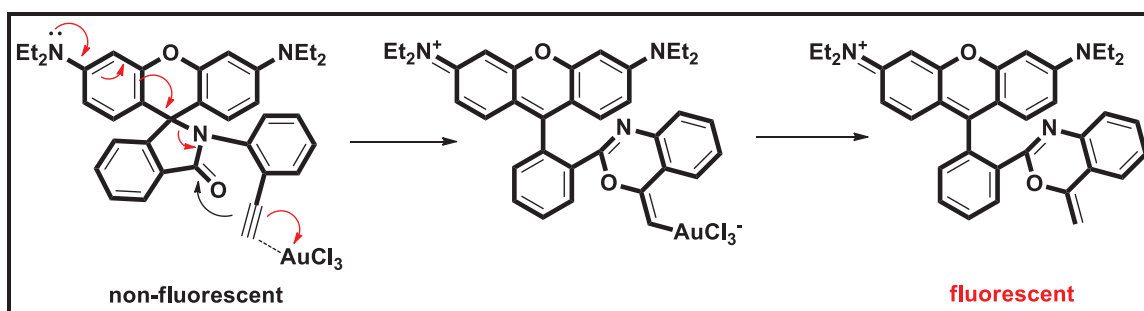


Figure 2.8. Turn-on sensing mechanism of the probe by gold (III) ion  
(Source: Seo et al., 2014)

Probe molecule demonstrated extremely high sensitivity that enabled detection of  $\text{Au}^{3+}$  down to 0.5 ppb level, the lowest detection limit so far obtained. Thus, this probe was useful for the quantification of gold residues in synthetic samples.

At the end of the 2014, Kambam *et al.* developed a novel fluorescein based probe for the detection of  $\text{Au}^{3+}$  ions. The fluorescence enhancement depended on the irreversible  $\text{C}=\text{N}$  bond hydrolysis that resulted from the presence of  $\text{Au}^{3+}$  (Kambam *et al.*, 2015). Detection limit of this novel probe was determined as 70 nM and bioimaging experiment indicated that this probe was cell permeable and could be used to detect  $\text{Au}^{3+}$  within living cells.

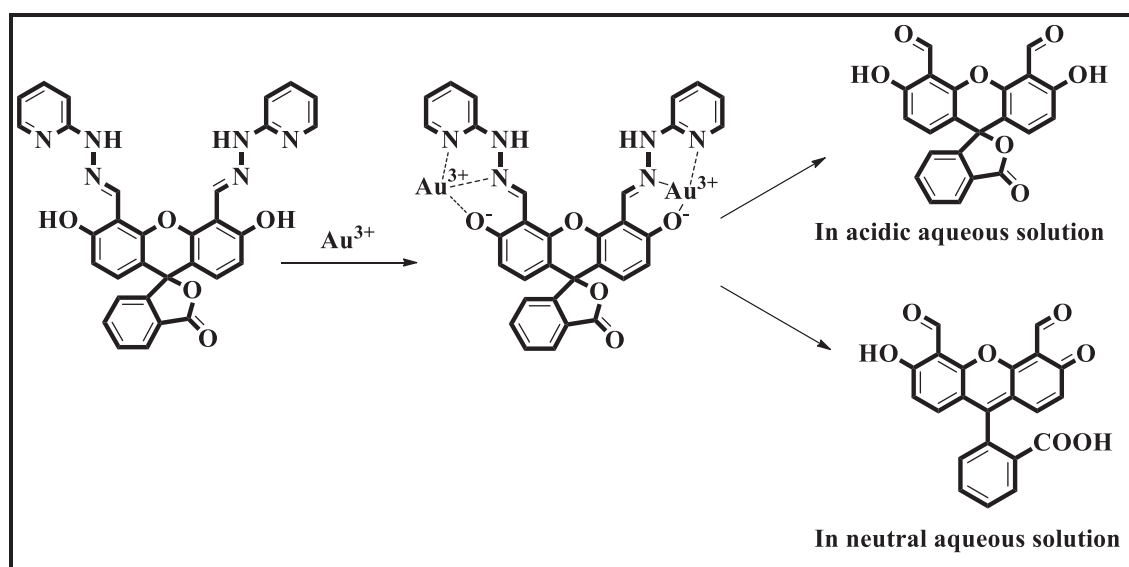


Figure 2.9. Proposed mechanism for the response of probe to gold (III) ion (Source Kambam *et al.*, 2015)

At the beginning of 2016 Wechakorn *et al.* reported a study in which rhodol-based fluorescent probe was used for the detection of  $\text{Au}^{3+}$  ions. In this work, rhodol derivative functionalized with a propargyl moiety which demonstrated excellent selectivity and sensitivity towards  $\text{Au}^{3+}$  in aqueous solution (Wechakorn *et al.*, 2016). Detection limit of this chemodosimeter was determined as 7 ppb and it could be employed to monitor  $\text{Au}^{3+}$  in living cells as well.

In figure 2.10 indicates that  $\text{Au}^{3+}$  ions activated triple bond unit bounded chemically to the rhodol derivative. Furthermore, complex of  $\text{Au}^{3+}$  with probe molecule underwent a 5-endo-dig cyclization reaction to form vinyl-gold intermediate, followed by protonolysis and isomerization to obtain furan product.

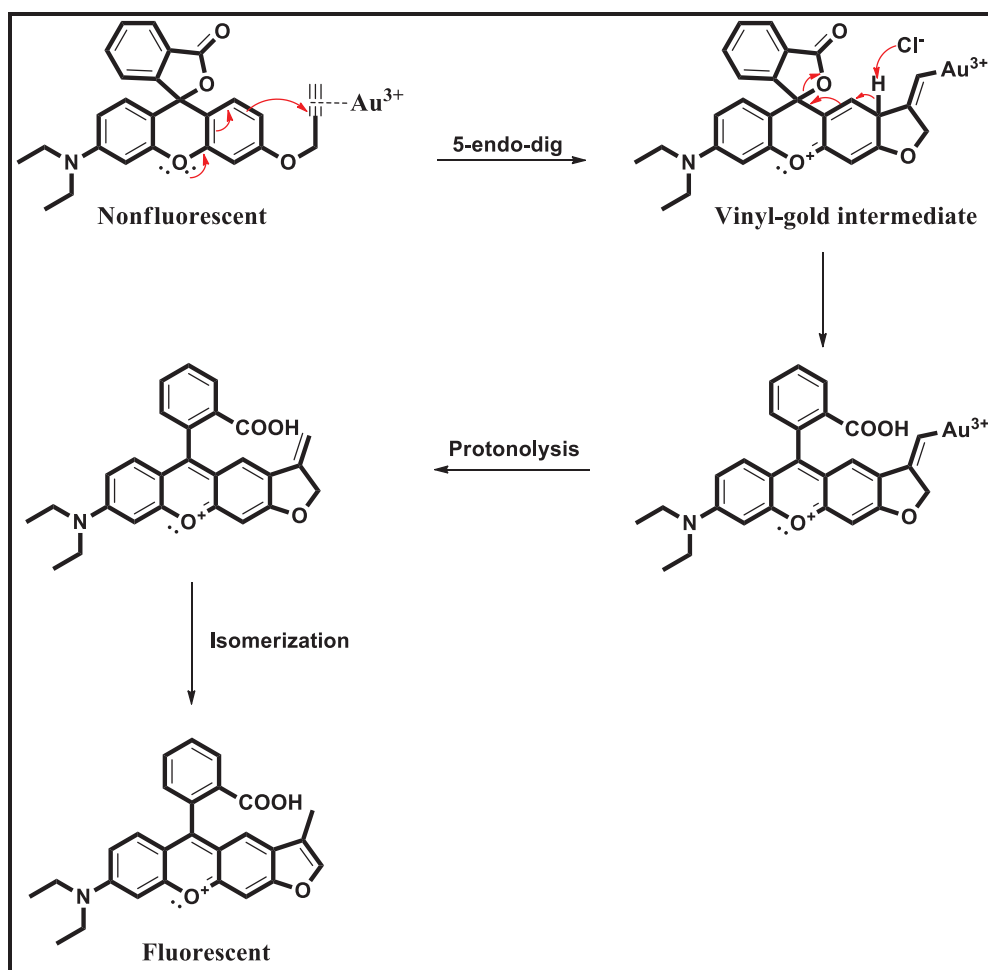


Figure 2.10. A proposed mechanism of the cyclization of the rhodol based probe induced by gold (III) ion (Source: Wechakorn et al., 2016)

Last example of spiro-ring opening reaction based probe for gold ion detection was reported by our research group in 2016. In this work, a water-soluble fluorescein dye was chosen as the signal reporter and modified with an alkyne moiety (Çetintaş et al., 2016) Synthesis of this probe was illustrated in figure 2.11.

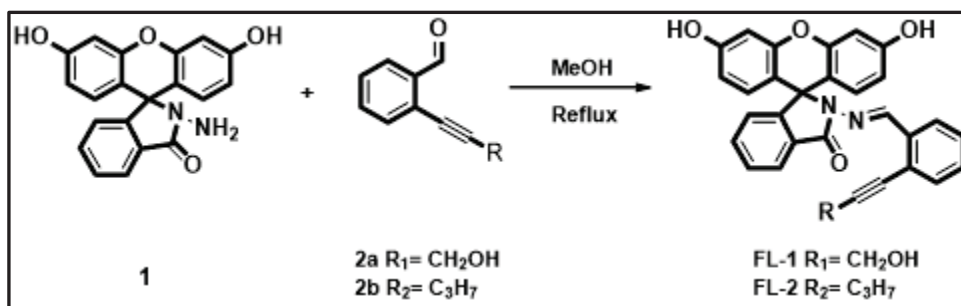


Figure 2.11. Synthesis of fluorescein based gold (III) ion probe  
(Source: Çetintaş et al., 2016)

As expected **FL-1** was non-fluorescent due to spirocyclic ring structure. After addition of  $\text{AuCl}_3$  into sensing media, the color of probe solution immediately changed from colorless to yellow with a green emission. To understand the sensing process, the product of the reaction between **FL-1** and  $\text{Au}^{3+}$  was isolated. TLC and  $^1\text{H}$  NMR results showed that two non-separable major products, endo-dig cyclization product (six-membered ring) and exo-dig cyclization product (five-membered ring), were formed. (Figure 2.12)

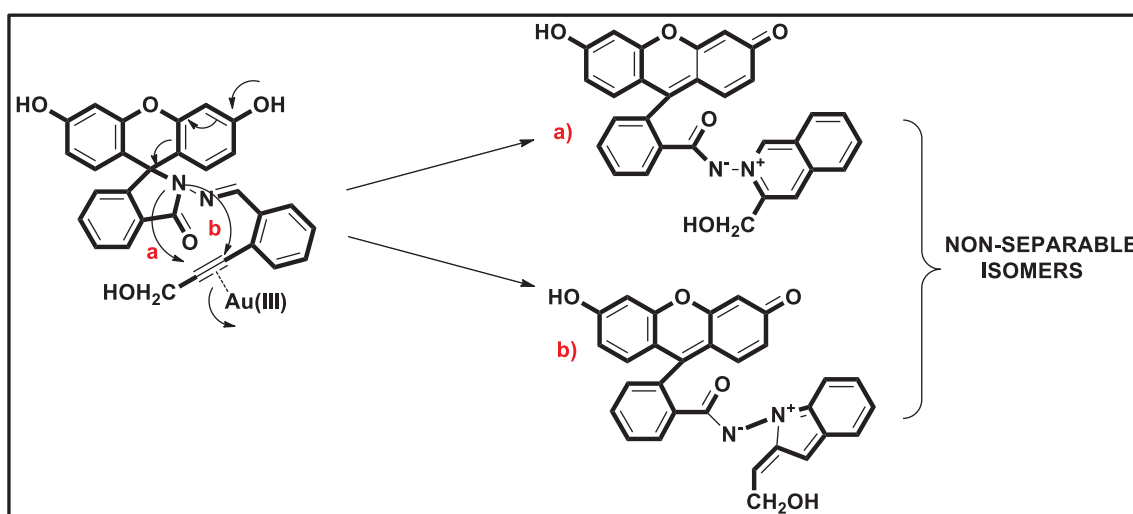


Figure 2.12. Mechanism for the formation of non-separable isomer products of **FL-1**  
(Source: Çetintaş et al., 2016)

To overcome this problem, the alternative probe **FL-2** was designed and it demonstrated highly similar fluorometric features towards  $\text{Au}^{3+}$  ions under identical sensing conditions. Reaction of **FL-2** and  $\text{Au}^{3+}$  gave selectively single product, endo-dig

intramolecular cyclization product, to yield a six-membered ring isoquinoline derivative. (Figure 2.13)

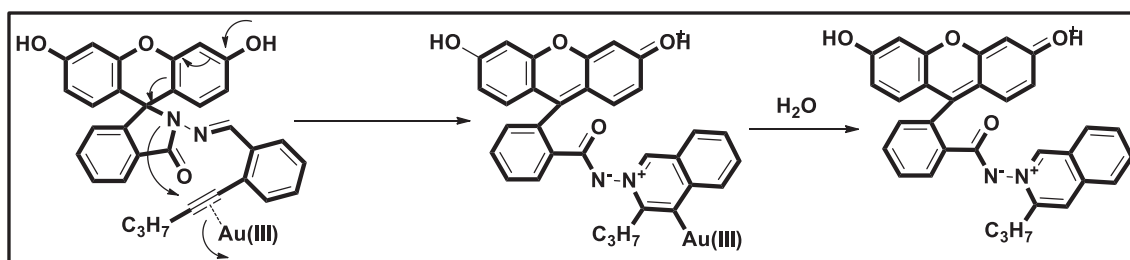


Figure 2.13. Proposed mechanism of FL-2 in the presence of gold (III) ion  
(Source: Çetintaş et al., 2016)

Thus, novel fluorescein based chemodosimeter was developed and synthesized and demonstrated spectroscopic investigations and cell imaging application. The probe illustrated high sensitivity towards  $\text{Au}^{3+}$  (LOD = 11 nM) and it was applicable to quantitative detection of gold residues in synthetic samples.

## 2.2. Rhodamine Based Fluorescent and Colorimetric Sensors for Gold Ions Detection

In this thesis study, three novel fluorescent and colorimetric sensor based on rhodamine structure were designed and synthesized. Their analyte sensitivities and selectivity were carefully investigated. Also, bioimaging applications were performed successfully. (Figure 2.14)

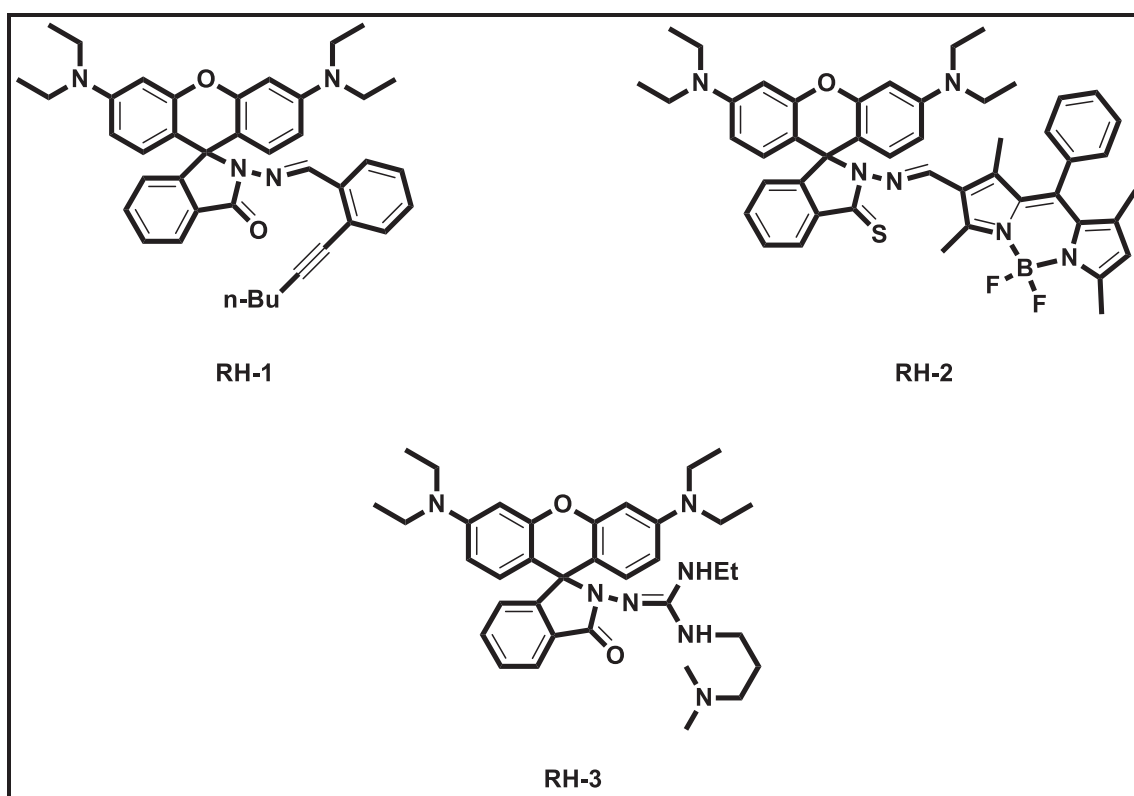


Figure 2.14. Rhodamine based gold ion selective novel probes

### 2.2.1. Gold Ion Sensing Properties of RH-1

The strategy in designing a metal specific fluorescent probe is based on the introduction of a metal binding or reactive unit to a fluorophore that translates the binding event to a fluorescence signal upon interaction with metal species. Alkynes, because of their strong binding affinity to alkynophilic metals, appear as suitable binding platforms for gold ions. Therefore, introducing a reactive alkyne moiety to the fluorophore could provide an efficient route to develop a gold specific fluorescent probe. In this regard, several “turn-on” type fluorescent probes for gold ions based on rhodamine were designed and described as indicated in previous part. Some of these probes have several shortcomings such as cross-sensitivity toward other metal cations, low water solubility, slow response, low fluorescence enhancement and cytotoxicity, which impede the optimum performance of those fluorescent sensing systems.

To overcome these problems, we report the synthesis and application of a novel gold ion selective fluorescent probe (**RH-1**) that operates through a chemical reaction triggered by gold ions. Our goal in this work was to detect and quantify residual gold species in synthetic samples, prepared via gold catalysis, and to monitor the accumulation of gold ions in living cells (Emrullahoglu et al., 2013).

The rhodamine derivative (**RH-1**), which contains a reactive alkyne moiety highly specific for  $\text{Au}^+$  and  $\text{Au}^{3+}$  ions, was synthesized by reacting rhodamine-B hydrazide with 2-alkynylbenzaldehyde in ethanol at reflux temperature in a yield of ca. 70%. (Figure 2.15)

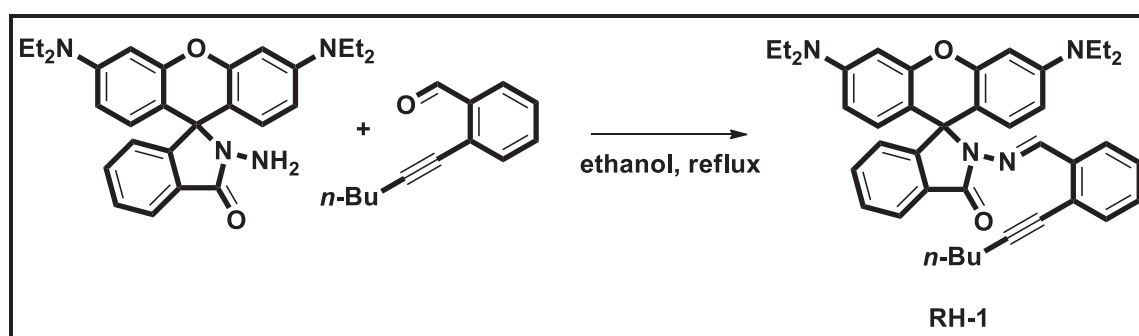


Figure 2.15. Synthesis of probe **RH-1**

We commenced our investigation by first examining the reaction media. Considering that probe **RH-1** is not completely water soluble thus we screened various combinations of solvents including EtOH/H<sub>2</sub>O, CH<sub>3</sub>CN/H<sub>2</sub>O and DMSO/H<sub>2</sub>O. A combination of CH<sub>3</sub>CN/H<sub>2</sub>O (1:1, v/v) proved to be highly efficient for the sensing process. Moreover, we observed that an increase in the ratio of water resulted in a dramatic decrease in the fluorescence intensity which might be due to the deactivation of the catalyst species.

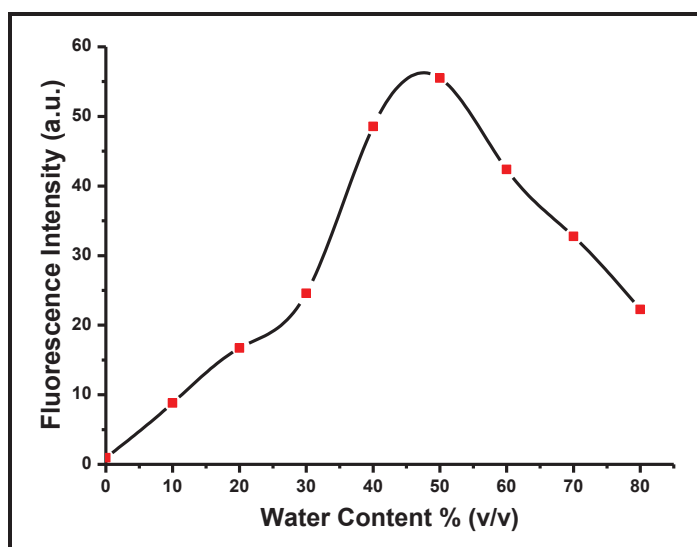


Figure 2.16. Effect of water content on the fluorescence intensity of probe **RH-1** (20  $\mu$ M) in the presence of Au<sup>3+</sup> (20  $\mu$ M) at pH = 7.0

We further investigated the emission responses of probe **RH-1** toward Au<sup>3+</sup> at various pH conditions. Probe **RH-1** showed strong fluorescence intensity changes in the presence of Au<sup>3+</sup> at pH 6–8. However, a gradual decline in the fluorescence intensity was observed at pH > 8 (Figure 2.17). Thus, a reaction medium buffered to pH 7.0 was chosen for physiological application.



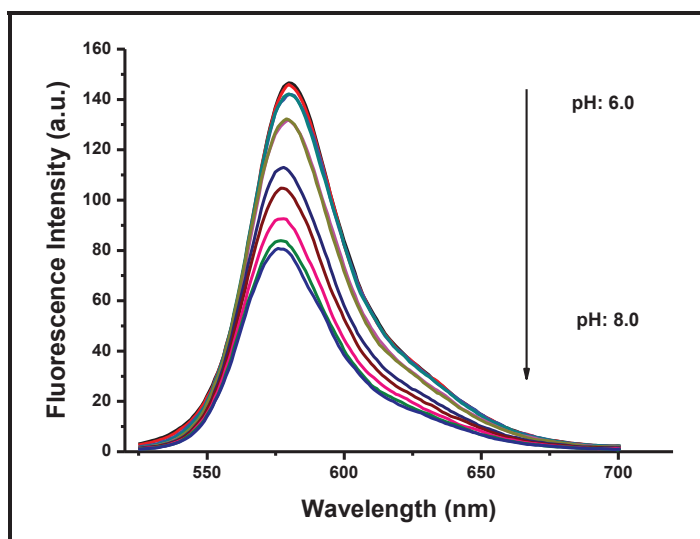
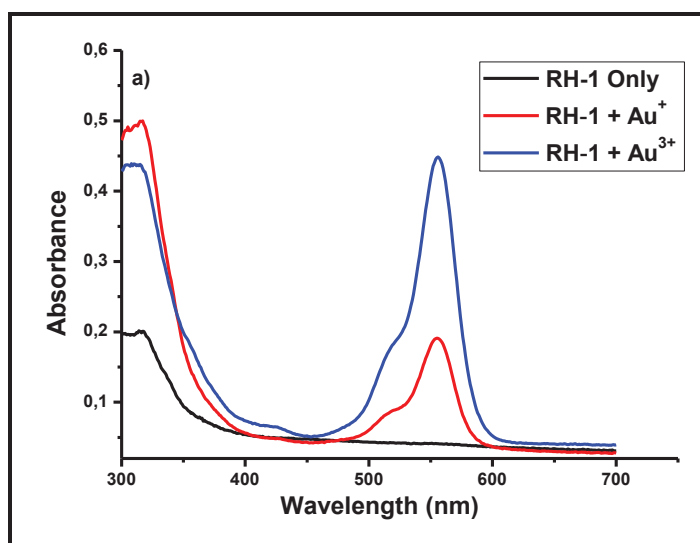


Figure 2.17. Effect of different pH values (pH: 6.0, 6.2, 6.4, 6.6, 6.8, 7.0, 7.2, 7.4, 7.6, 7.8 and 8.0) on the fluorescence intensity of probe **RH-1** (20  $\mu\text{M}$ ) in the presence of  $\text{Au}^{3+}$  (60  $\mu\text{M}$ )

As expected, the resultant compound was colorless in solution (HEPES/ $\text{CH}_3\text{CN}$  (1:1, v/v) (pH=7.0)), showed no absorption in the visible region, and was non-fluorescent, indicating that spirocyclic form of the dye was predominant. However, upon the direct addition of  $\text{AuCl}_3$  (60  $\mu\text{M}$ , 3 equivalents with respect to probe **RH-1**), the colorless and nonfluorescent solution immediately became pink in color and started to fluoresce under UV light (<1 min.). The addition of  $\text{Au}^{3+}$  (3 equiv) lead to the appearance of a new strong absorption band centered at 556 nm and a strong fluorescence band at 580 nm, which was attributed to the delocalized xantheno moiety of rhodamines.



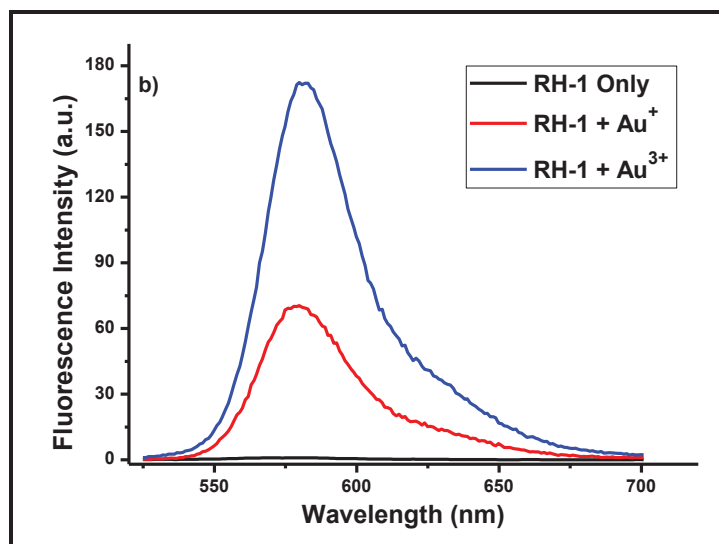


Figure 2.18.(a) Absorption and (b) Emission spectra of probe **RH-1** (20  $\mu\text{M}$ ) and  $\text{Au}^+$  and  $\text{Au}^{3+}$  (60  $\mu\text{M}$ , 3.0 equiv.) in 1:1  $\text{CH}_3\text{CN}/\text{HEPES}$  buffer at  $\text{pH} = 7.0$ ; ( $\lambda_{\text{ex}} = 500 \text{ nm}$ , at  $25 \text{ }^\circ\text{C}$ ).

The titration of  $\text{AuCl}_3$  into probe **RH-1** gave a strong absorbance and fluorescence enhancement with increasing  $\text{Au}^{3+}$  concentrations (Figure 2.19). The fluorescence titration profile of probe **RH-1** with  $\text{Au}^{3+}$  showed a linear relationship for a concentration range of  $1 \mu\text{M}$ - $100 \mu\text{M}$ , indicating the suitability of probe **RH-1** for quantitative analysis. The enhancement of emission intensity ( $> 200$  fold) gets saturated at the addition of 5 equiv of  $\text{Au}^{3+}$ .

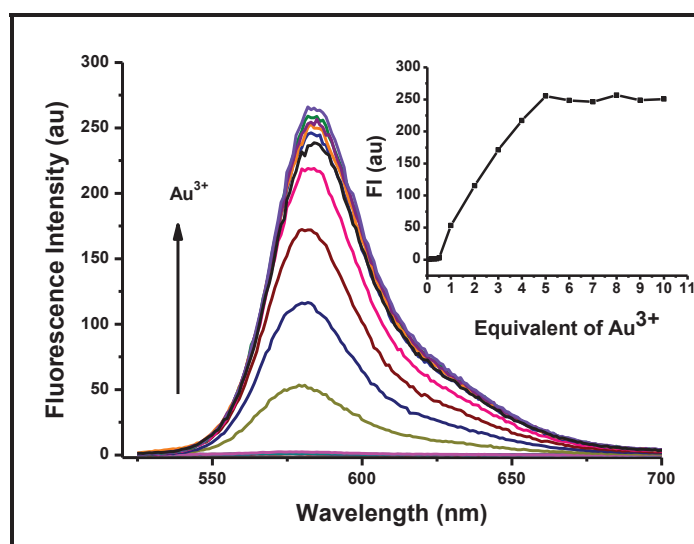


Figure 2.19. Emission titration curve of probe **RH-1** (20  $\mu\text{M}$ ) and  $\text{Au}^{3+}$  (0 to 10 equiv) in 1:1  $\text{CH}_3\text{CN}/\text{HEPES}$  buffer at  $\text{pH} = 7.0$ ; Inset: plot of fluorescence intensity depending on the number of equivalents of  $\text{Au}^{3+}$ .

To evaluate the detection limit of **RH-1** towards  $\text{Au}^{3+}$  a careful titration experiment was performed. The increase in the emission intensity was proportional to the amount of  $\text{Au}^{3+}$  with a good linear correlation and the minimum amount of  $\text{Au}^{3+}$  that can be detected under these conditions was found to be  $2.0 \mu\text{M}$  based on  $S/N = 3$ .

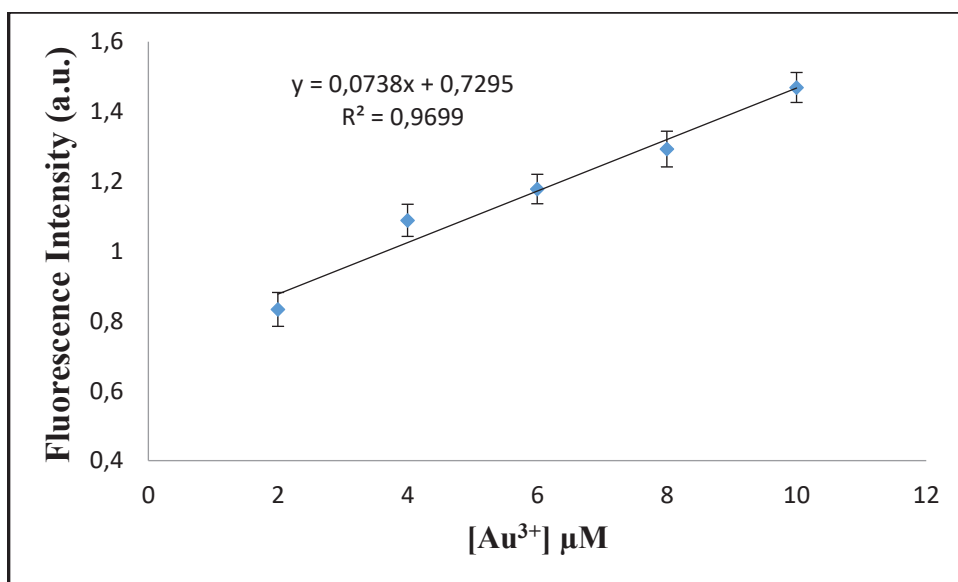


Figure 2.20. Fluorescence intensity changing of probe **RH-1** ( $20 \mu\text{M}$ ) upon addition of  $\text{AuCl}_3$  ( $2.0$  to  $10.0 \mu\text{M}$ ,  $0.1$  to  $0.5$  equiv.) in  $1:1 \text{CH}_3\text{CN}/\text{HEPES}$  buffer at  $\text{pH} = 7.0$ .

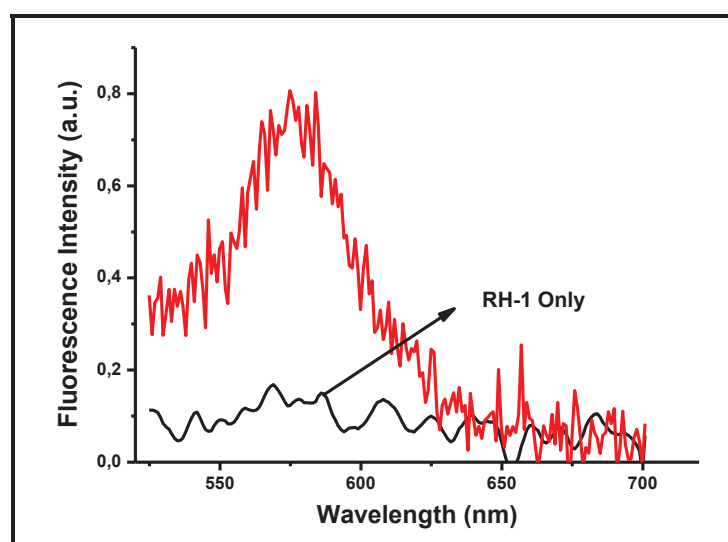


Figure 2.21. Fluorescence spectrum of probe **RH-1** ( $20 \mu\text{M}$ ) upon addition of  $\text{AuCl}_3$  ( $2.0 \mu\text{M}$  /  $0.6 \text{ppm}$ ) in  $1:1 \text{CH}_3\text{CN}/\text{HEPES}$  buffer at  $\text{pH} = 7.0$

The reaction time profile of sensing event was surveyed by the addition of  $\text{Au}^+$  and  $\text{Au}^{3+}$  separately to the sensing media. Even though the spectroscopic response of probe **RH-1** was quite fast ( $< 1$  min), the complete saturation of the signal intensity was observed after 60 min (Figure 2.22).

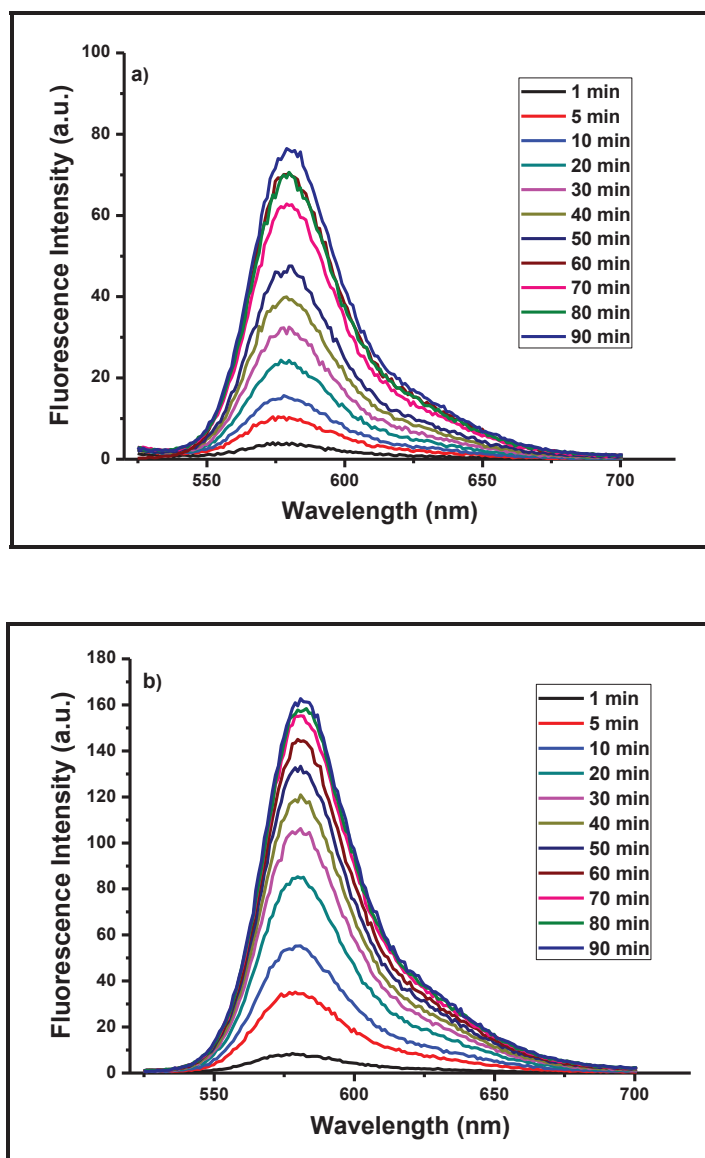


Figure 2.22. Time-dependent fluorescence change of probe **RH-1** ( $20 \mu\text{M}$ ) in the presence of  $60 \mu\text{M}$  of (a)  $\text{AuCl}$  and (b)  $\text{AuCl}_3$  measured in 1:1  $\text{CH}_3\text{CN}/\text{HEPES}$  buffer at  $\text{pH} = 7.0$

It was important to rule out the possible involvement of other alkynophilic metals in the sensing process. Therefore, the titration of probe **RH-1** with various other metal ions was carried under the same sensing conditions. By our delight, related alkynophilic metals such as  $\text{Ag}^+$ ,  $\text{Ni}^{2+}$ ,  $\text{Pd}^{2+}$ ,  $\text{Co}^{2+}$ ,  $\text{Hg}^{2+}$  and other metals including  $\text{Li}^+$ ,  $\text{Na}^+$ ,  $\text{K}^+$ ,  $\text{Ba}^{2+}$ ,  $\text{Ca}^{2+}$ ,  $\text{Cd}^{2+}$ ,  $\text{Mg}^{2+}$ ,  $\text{Mn}^{2+}$ ,  $\text{Zn}^{2+}$ ,  $\text{Pb}^{2+}$ ,  $\text{Cu}^{2+}$  did not trigger any ring opening reaction to give a spectroscopic response. Moreover,  $\text{AuPPh}_3\text{Cl}$  as a gold ion source, was found to be not competing with  $\text{Au}^+$  and  $\text{Au}^{3+}$ . As displayed in figure 2.23, only the addition of  $\text{Au}^{3+}$  and, to a lesser extent the addition of  $\text{Au}^+$  resulted in an enhancement of fluorescence at 580 nm (absorbance at 556 nm), which obviously implied the high selectivity of probe **RH-1** to gold ions. Moreover, no significant color change in probe solution was observed by the addition of other metal ions.

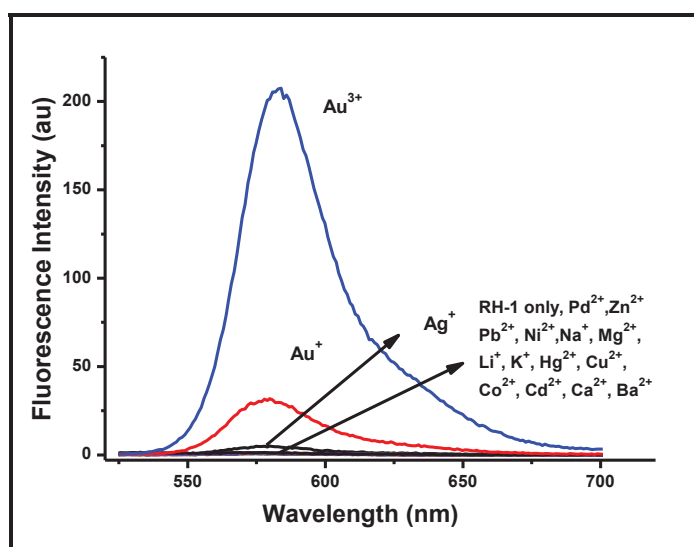


Figure 2.23. Fluorescence intensities of probe **RH-1** (20  $\mu\text{M}$ ) in 1:1  $\text{CH}_3\text{CN}/\text{HEPES}$  buffer at  $\text{pH} = 7.0$  emission at 580 nm ( $\lambda_{\text{ex}} = 500$  nm): in the presence of metal ions (5 equiv). All data were taken after 60 min.

We further explored the fluorescent response of the probe **RH-1** toward  $\text{Au}^{3+}$  (10 equiv) in the presence of the other metal ions (200 equiv) in order to assess possible interferences by metal ions. As shown in figure 2.24 the tested metal ions displayed no interference with the detection of gold ions.

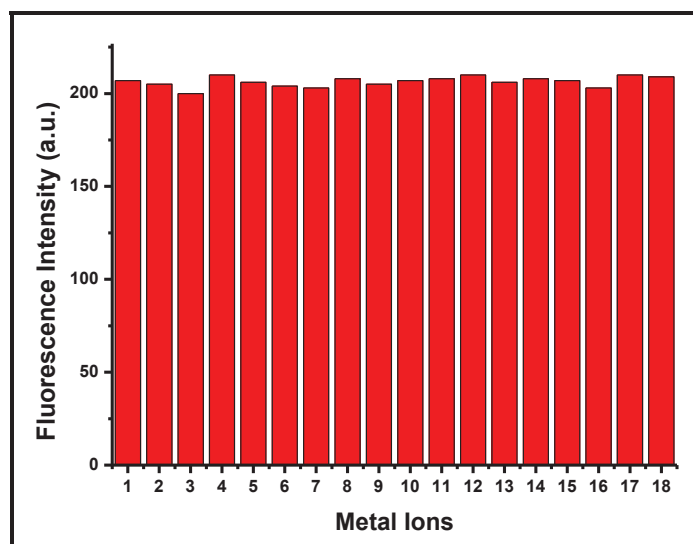


Figure 2.24. Fluorescence intensities of probe **RH-1** (20  $\mu\text{M}$ ) in 1:1  $\text{CH}_3\text{CN}/\text{HEPES}$  buffer at  $\text{pH} = 7.0$  at  $\lambda_{\text{max}}$ : 580 nm in the presence  $\text{Au}^{3+}$  (100  $\mu\text{M}$ , 5.0 equiv.) and 200  $\mu\text{M}$  of the metal ions: 1, none; 2,  $\text{Ag}^+$ ; 3,  $\text{Ba}^{2+}$ ; 4,  $\text{Pd}^{2+}$ ; 5,  $\text{Zn}^{2+}$ ; 6,  $\text{Pb}^{2+}$ ; 7,  $\text{Ni}^{2+}$ ; 8,  $\text{Na}^+$ ; 9,  $\text{Mg}^{2+}$ ; 10,  $\text{Li}^+$ ; 11,  $\text{K}^+$ ; 12,  $\text{Hg}^{2+}$ ; 13,  $\text{Cu}^{2+}$ ; 14,  $\text{Co}^{2+}$ ; 15,  $\text{Cd}^{2+}$ ; 16,  $\text{Ca}^{2+}$ ; 17,  $\text{Cr}^{3+}$ ; 18,  $\text{Fe}^{3+}$

The overall sensing process was suggested to be reaction-based and irreversible. In order to prove this argument, an excess amount of cyanide ion ( $\text{KCN}$ ,  $n\text{-Bu}_4\text{NCN}$  (5 equiv)) was subjected to the colored and fluorescent  $\text{Au}^{3+}$  containing probe **RH-1** solutions. There was no change both in absorbance and fluorescence intensity after the addition of the cyanide source, which indicates that the sensing process is irreversible. Obviously, probe **RH-1** operates through an irreversible chemical reaction and thus can be classified as a chemodosimeter.

Rhodamine derivative (**RH-Ph**), lacking an alkyne moiety, was prepared as a control probe by reacting rhodamine B hydrazide with benzaldehyde according to the literature procedure (Xiang et al., 2006). Under the same sensing conditions, no spectroscopic changes were observed upon the addition of  $\text{Au}^{3+}$  to probe **RH-Ph**. This result clearly indicated that the alkyne moiety available on the probe structure plays a vital role on the signaling process. In other words, the signaling event was directly related to the activation of the alkyne unit by gold ions.

In order to get insight to the sensing mechanism we decided to isolate all possible products formed by treating probe **RH-1** with  $\text{AuCl}_3$ . This reaction afforded quantitatively one product as identified by TLC. The crude product was successfully purified by flash column chromatography and the structure of the product (**RH-1P**) was

confirmed by  $^1\text{H-NMR}$ ,  $^{13}\text{C-NMR}$  and mass spectroscopy analysis (Maldi-TOF-TOF and ESI-TOF). Based on the structure of isolated product, we suggested that the sensing event proceeds through a gold promoted intramolecular cyclization that causes the ring opening reaction to generate the highly fluorescent isoquinoline rhodamine derivative (**RH-1P**) (Figure 2.25). The intramolecular cyclization of  $N'$ -2-(alkynylbenzylidene) hydrazide derivatives to isoquinoline  $N$ -imines was previously investigated by others. Our proposed mechanism for the product formation is consistent with those reported (Ding et al., 2009).

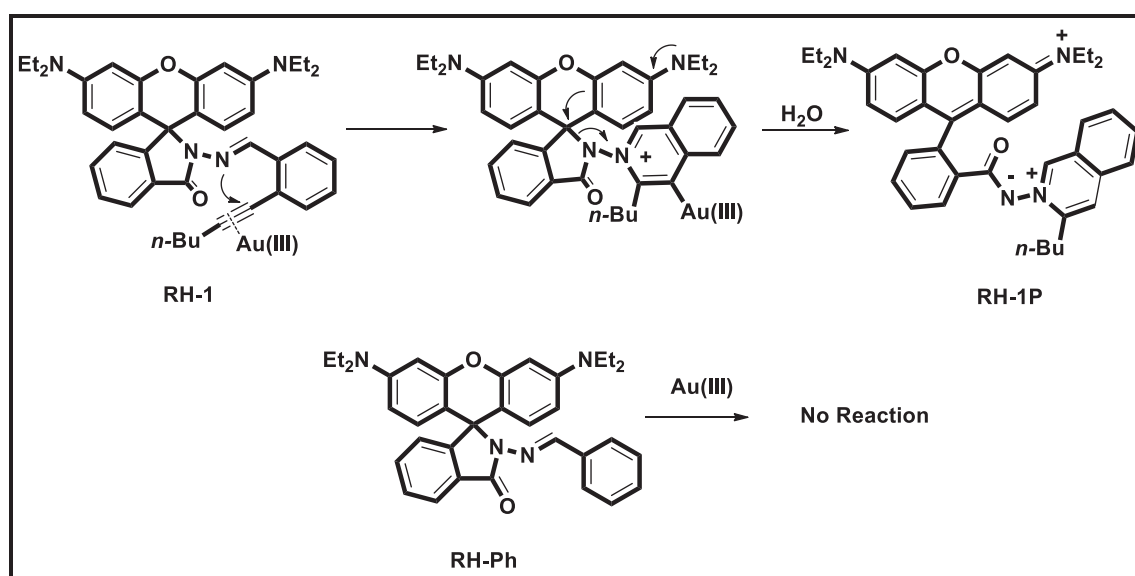


Figure 2.25. Proposed mechanism for the product formation with gold (III) ion

To determine whether probe **RH-1** could be applied for monitoring residual  $\text{Au}^{3+}$  ions in a synthetic end-product, we prepared oxazole **2** by treating propargylic amide **1** with  $\text{AuCl}_3$  (0.05 equiv) following a previously described procedure (Hashmi et al., 2004).

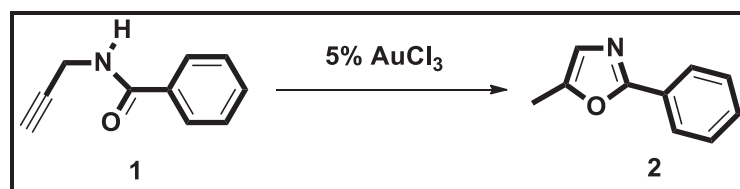


Figure 2.26. Synthesis of oxazole derivative in the presence of gold (III) ion

The resulting crude product was divided into four portions, and each portion was handled in different ways. In order to remove all gold residues from the crude product,

the first portion was extracted with water and diethyl ether, the second portion was purified through a pad of silica gel, the third portion through a pad of celite and the fourth portion through a pad of basic alumina ( $\text{Al}_2\text{O}_3$ ) (eluent: Hexane/EtOAc). Subsequently, each purified sample (2 mg) was sequentially subjected to the solutions of probe **RH-1** ( $20\ \mu\text{M}$  in 1:1  $\text{CH}_3\text{CN}$ /HEPES, at  $\text{pH} = 7.0$ ). We observed a distinct change in color and fluorescence in the sample solution isolated from the first three portions whereas no color and fluorescence change was observed in the sample solution that was purified via  $\text{Al}_2\text{O}_3$  column chromatography. The gold content in the sample, purified through a silica pad, was measured to be  $5.90 \times 10^{-7}\ \text{mol mg}^{-1}$  based on a standard calibration curve. The measured value was in consistence with that obtained by inductively coupled plasma-mass spectrometry (ICP-MS) analysis ( $6.27 \times 10^{-7}\ \text{mol mg}^{-1}$ ). This comparative experiment confirmed not only the viability of probe **RH-1** for quantitative gold analysis, but also the ineffectiveness of silica gel and celite in removing gold residues from crude products. On the other hand, purification through a pad of  $\text{Al}_2\text{O}_3$  (basic) was highly efficient in removing gold impurities from the crude product

Relying on the promising properties of probe **RH-1**, we next questioned whether probe **RH-1** can be used for monitoring the accumulation of gold ions in living cells. Human colon carcinoma cells (HCT-116) were incubated with probe **RH-1** ( $20\ \mu\text{M}$ ) for 30 min., then followed by the addition of  $\text{Au}^{3+}$  and incubation for another 30 min. The fluorescence images were recorded before and after the addition of  $\text{Au}^{3+}$ .

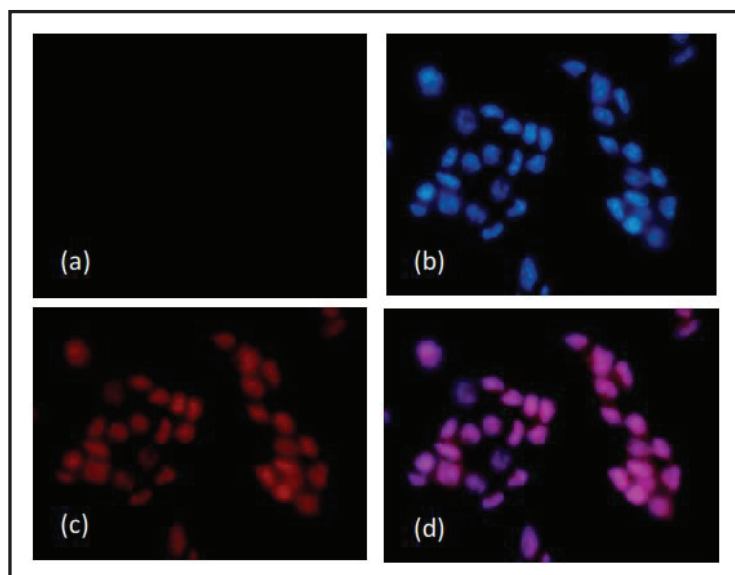


Figure 2.27. Fluorescence images of HCT-116 cells : (a) fluorescence image of HCT-116 cells treated with probe **RH-1** ( $20\ \mu\text{M}$ ) in the absence of  $\text{Au}^{3+}$  (control); (b) fluorescence image of HCT-116 cells treated with Hoechst -34580 ( $2\ \mu\text{M}$ )



(control); (c) fluorescence image of HCT-116 cells treated with Au<sup>3+</sup> (10 μM) and probe **RH-1** (20 μM); (d) merge image of frames b and c.

HCT-116 cells incubated with probe **RH-1** exhibited no fluorescence whereas a bright fluorescence signal was observed in the cells stained with probe **RH-1** and Au<sup>3+</sup>, which suggested that probe **RH-1** is cell membrane permeable and can be efficiently used for in vitro imaging of gold ions in living cells.

Thus, we have developed a highly sensitive “turn-on” type fluorescent probe that allows the naked eye detection of gold ions in various environments. The probe exhibits large fluorescence enhancement, high selectivity and a low detection limit. Furthermore, probe **RH-1** was successfully employed for the quantitative determination of the concentration of Au<sup>3+</sup> residues in synthetic samples. In addition, we have demonstrated the applicability of probe **RH-1** for imaging gold ions in the living cells.

## 2.2.2. Gold Ion Sensing Properties of RH-2

Until now research on the development of molecular sensors for analysing diverse biologically and environmentally important analyte species has increased. While a thumping majority of sensors addressed in such literature are designed to recognize a specific target, less common are sensors capable of differentiating multiple targets. Differential detection of multiple analyte species can be achieved best by recognizing each species through a different signal output (i.e., emission wavelength). Incorporating multiple binding motifs onto a single signal-transducing molecule (chromophore/fluorophore) and, as an alternative, combining different transducing molecules have both appeared as efficient routes for sensors with multiple output modes.

With this goal in mind, it was intended that incorporating both a chemosensor and a chemodosimeter onto a single molecule could provide a suitable sensing platform for the differential detection of metal species. Thus, it was constructed a molecular sensor possessing two different fluorophore units (rhodamine and BODIPY) chemically integrated with each other. Both fluorophore units were elegantly designed to be non-emissive in their initial states and are expected to turn on respectively in response to the metal species of interest (Karakus et al., 2014).

In this part of the thesis study, it was demonstrated the design, synthesis, spectral properties, and cell imaging studies of a novel “turn-on” multi-fluorescent probe **RH-2** that allows the  $\text{Hg}^{2+}$  and  $\text{Au}^{3+}$  species to be differentiated based on distinct fluorescence responses.

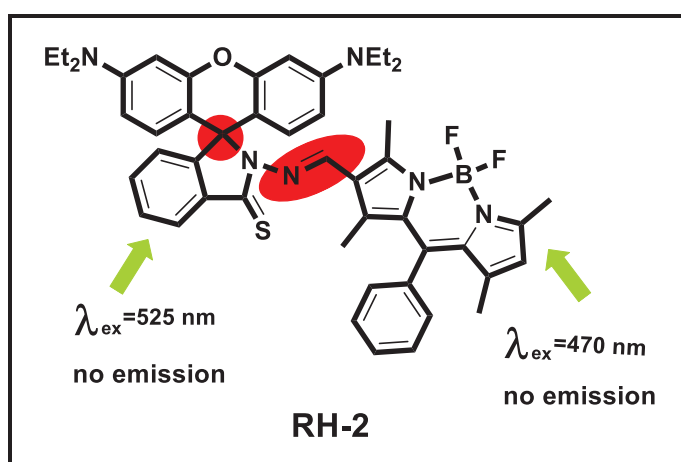


Figure 2.28. Molecular structure of **RH-2**

**RH-2** was prepared by the condensation reaction of BODIPY aldehyde (**BOD-AL**) and rhodamine hydrazide followed by thionation of carbonyl oxygen in a moderate yield. (overall 25%). Synthetic route was demonstrated in the following figure 2.29.

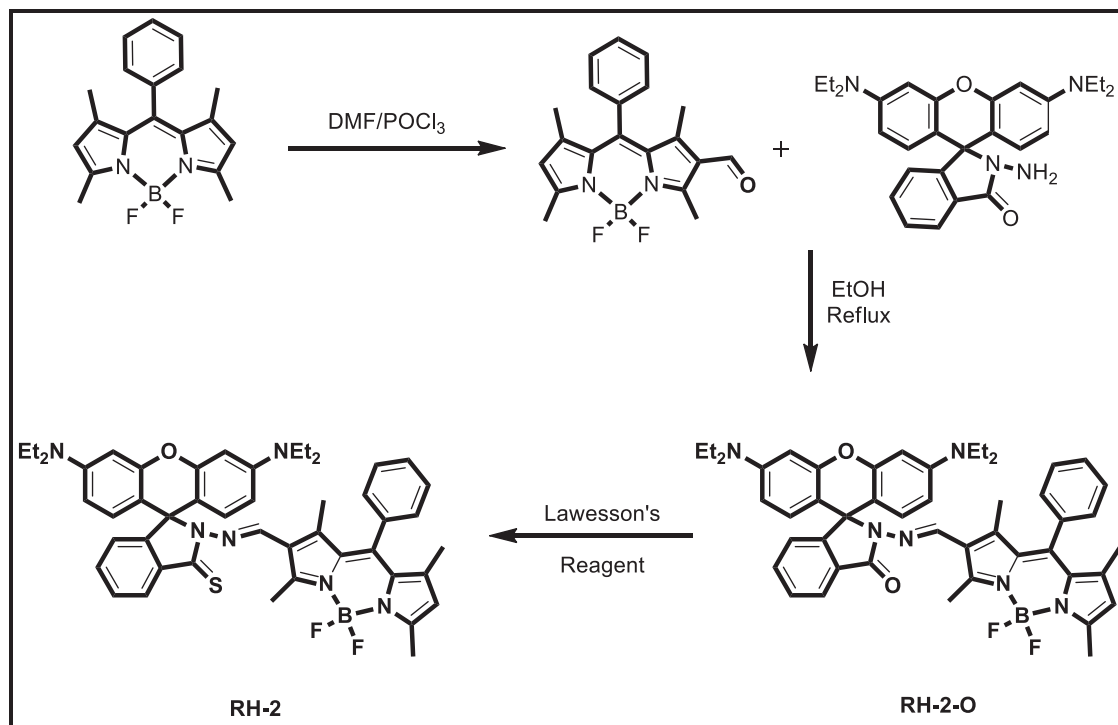


Figure 2.29. Synthetic pathway of **RH-2**

Both fluorophore attached to each other chemically was non-fluorescent before addition of any metal species. After addition of either Au<sup>3+</sup> or Hg<sup>2+</sup> ions, the differential detection of Hg<sup>2+</sup> and Au<sup>3+</sup> could be realized with two distinct fluorescence changes, based on either an Hg<sup>2+</sup>-ligand coordination event or a gold-mediated chemical transformation. Since this thesis study examined rhodamine based fluorescent probes for gold ions, it was focused only rhodamine channel of this hybrid probe for the gold ion detection.

The investigation started with the evolution of the optical behavior of **RH-2** in different sensing conditions (e.g. solvent system, water ratio, pH). Different solvent systems such as EtOH/Phosphate buffer solution (v/v, 1:1, pH = 7.0) and CH<sub>3</sub>CN/HEPES buffer solution (v/v, 1:1, pH = 7.0) were examined for **RH-2** to response Au<sup>3+</sup> ions. The highest increment in fluorescence intensity was observed in CH<sub>3</sub>CN/HEPES buffer solution (v/v, 1:1, pH = 7.0) solvent system. At this point, it was necessary to evaluate the effect of the fraction of water to the spectral behavior of **RH-2**. For the next step,

different ratios of CH<sub>3</sub>CN and 10 mM HEPES buffer solution were examined. And, it was clearly seen that when the molecule is excited at 525 nm, CH<sub>3</sub>CN/HEPES buffer solution (v/v, 1:1, pH = 7.0) system gave the best result for the sensing of Au<sup>3+</sup> ions (Figure 2.30).

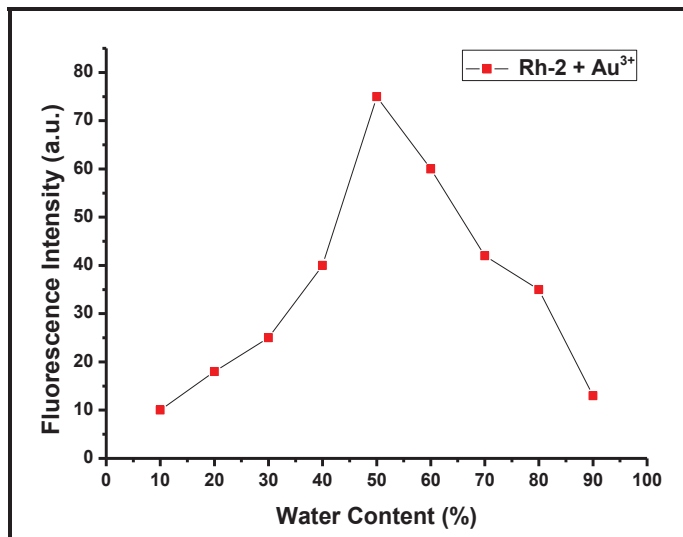


Figure 2.30. Effect of water content on the fluorescence intensity of **RH-2** (5  $\mu$ M) in CH<sub>3</sub>CN/HEPES buffer (pH = 7.0) in the presence Au<sup>3+</sup> (1 equiv.) ( $\lambda_{ex}$  = 590 nm).

The fluorescence intensity at pH 7 was observed to be the highest. It was also most proper pH value for biological application (Figure 2.31).

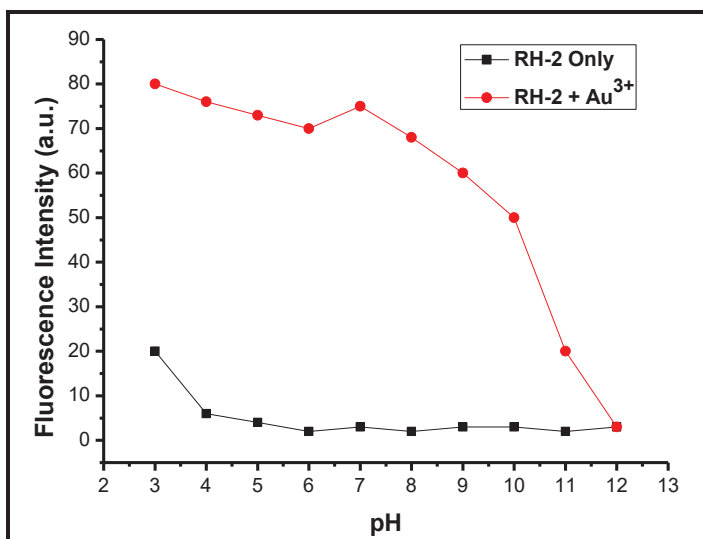


Figure 2.31. Effect of pH on the fluorescence intensity of **RH-2** (5  $\mu$ M) in 10 mM HEPES buffer/CH<sub>3</sub>CN in the absence and presence Au<sup>3+</sup> (1 equiv.) ( $\lambda_{ex}$  = 590 nm).

As figure 2.32 illustrated that the UV/Vis spectrum of free **RH-2** gave a single absorption peak at 527 nm, which belongs to BODIPY core. Due to the ring closed structure of the rhodamine moiety, it did not show any absorption peak in the spectrum.

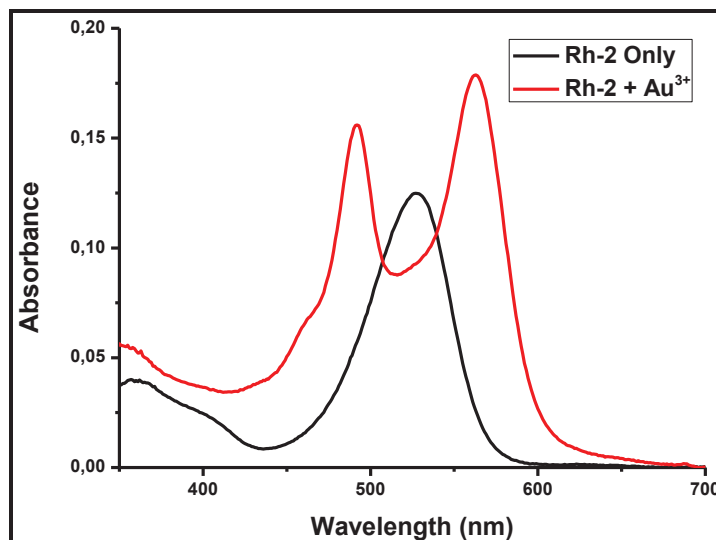


Figure 2.32. Absorption spectra of **RH-2** (5  $\mu$ M) and  $\text{Au}^{3+}$  (1 equiv.) in 1:1  $\text{CH}_3\text{CN}/\text{HEPES}$  buffer at  $\text{pH} = 7.0$

As shown in figure 2.33, the probe solution did not exhibit any emission peak before adding  $\text{Au}^{3+}$ . Nevertheless, soon after  $\text{Au}^{3+}$  was added a new emission band appeared at 585 nm when excited at 525 nm, which was supposed to belong to the ring opened isomer of the rhodamine core.

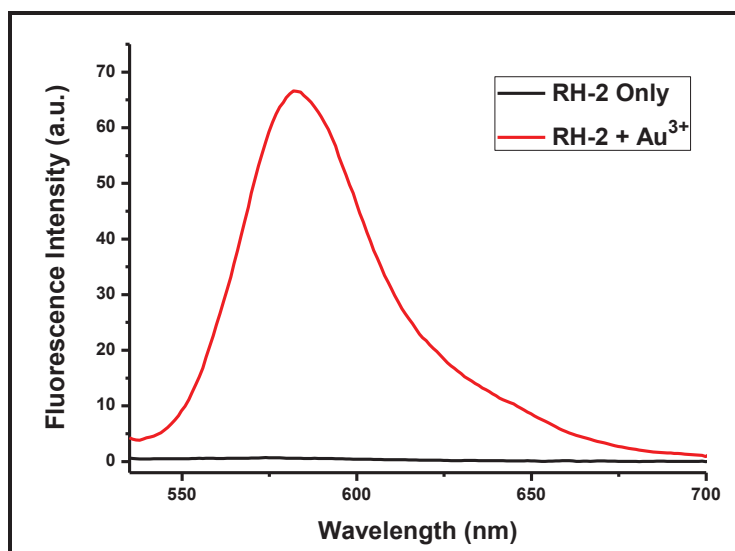


Figure 2.33. Emission spectra of **RH-2** (5  $\mu\text{M}$ ) and  $\text{Au}^{3+}$  (1 equiv.) in 1:1  $\text{CH}_3\text{CN}/\text{HEPES}$  buffer at  $\text{pH} = 7.0$

Fluorescence titration experiments for **RH-2** in terms of the added  $\text{Au}^{3+}$  were carefully scrutinised upon their excitation at 525 nm. The emission band at 585 nm increased linearly in response to  $\text{Au}^{3+}$  over a wide concentration range (5–50  $\mu\text{M}$ ). The saturation point was realised when 2 equiv. of  $\text{Au}^{3+}$  ions were added (Figure 2.34 and 2.35).

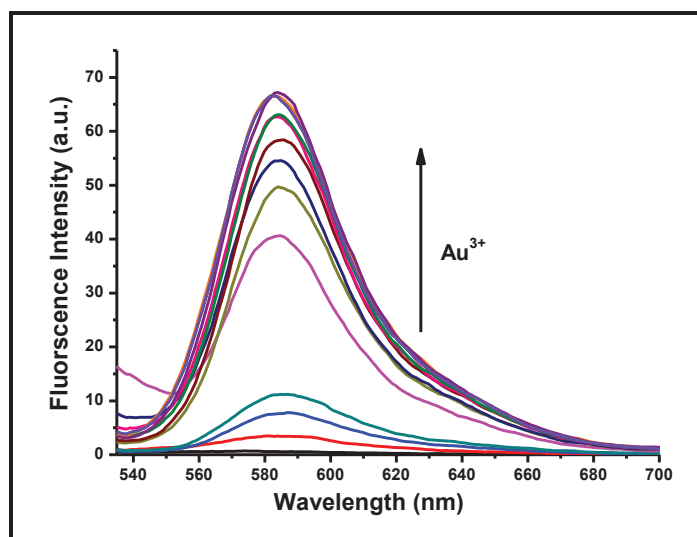


Figure 2.34. Fluorescence titration spectra of **RH-2** (5.0  $\mu\text{M}$ ) in 1:1  $\text{CH}_3\text{CN}/\text{HEPES}$  buffer ( $\text{pH} = 7.0$ ) in the presence of  $\text{Au}^{3+}$  (0-10 equivalent)  $\lambda_{\text{exc}} = 525 \text{ nm}$

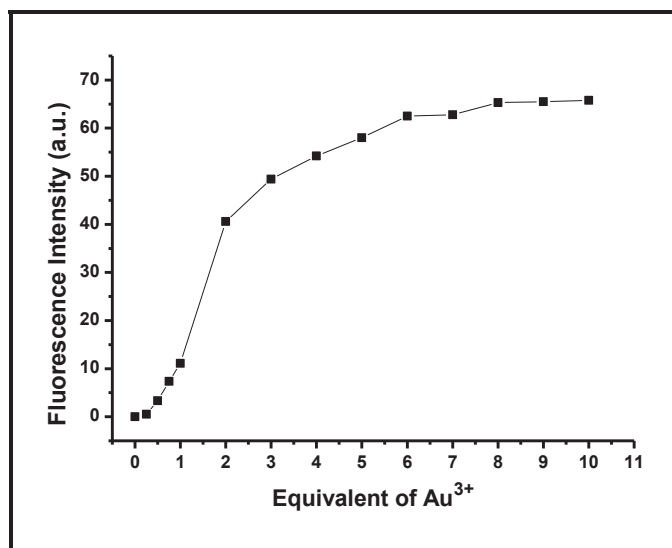
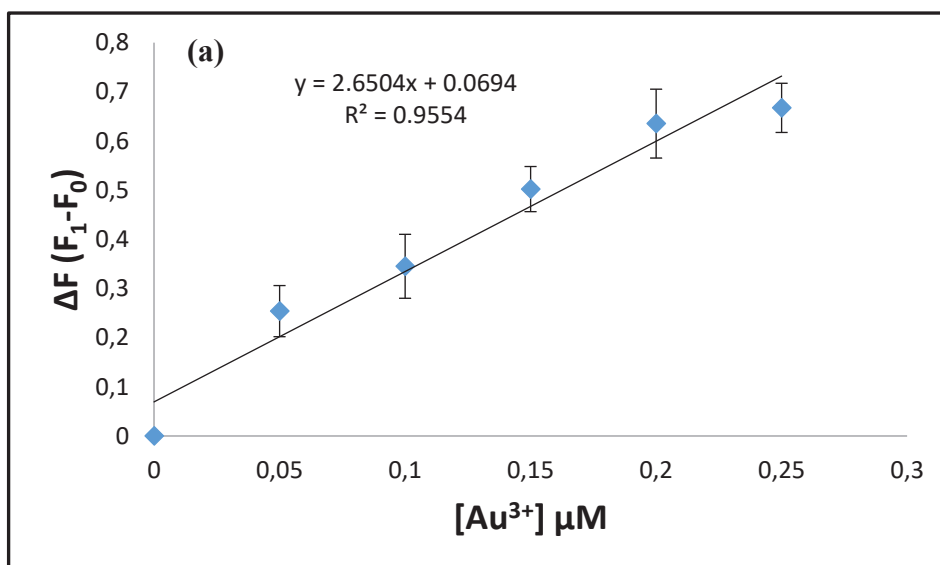


Figure 2.35. Fluorescence intensity changes of **RH-2** vs equivalents of Au<sup>3+</sup>  $\lambda_{ex} = 525$  nm

The detection limit of the probe for Au<sup>3+</sup> was evaluated as 65 nM, based on the signal-to-noise ratio of 3 (Figure 2.36).



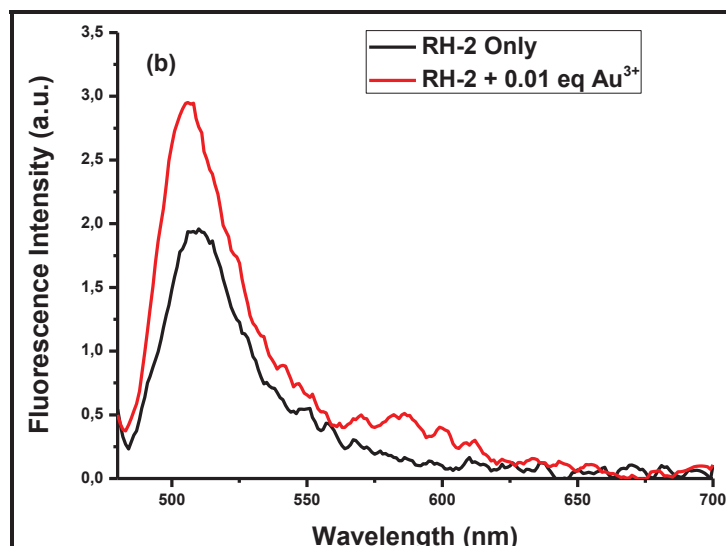


Figure 2.36.(a) Fluorescence changes of **RH-2** (5.0  $\mu\text{M}$ ) upon addition of  $\text{Au}^{3+}$  (0.05 to 0.3  $\mu\text{M}$ , 0.01 to 0.05 equiv.) (b) Fluorescence spectra of **RH-2** (5.0  $\mu\text{M}$ ) in the presence of  $\text{Au}^{3+}$  (0.05  $\mu\text{M}$ , 0.01 equiv.) in 1:1  $\text{CH}_3\text{CN}/\text{HEPES}$  buffer at  $\text{pH} = 7.0$

The selectivity profile of **RH-2** was examined in the presence of various metal cations under optimum sensing conditions. Remarkably, **RH-2** showed no spectral response to metal ions such as  $\text{Au}^+$ ,  $\text{Ag}^+$ ,  $\text{Ni}^{2+}$ ,  $\text{Pd}^{2+}$ ,  $\text{Fe}^{3+}$ ,  $\text{Na}^+$ ,  $\text{K}^+$ ,  $\text{Ba}^{2+}$ ,  $\text{Ca}^{2+}$ ,  $\text{Cd}^{2+}$ ,  $\text{Mg}^{2+}$ ,  $\text{Mn}^{2+}$ ,  $\text{Zn}^{2+}$ ,  $\text{Pb}^{2+}$ ,  $\text{Cu}^{2+}$ , and  $\text{Cr}^{3+}$  except for  $\text{Hg}^{2+}$  and  $\text{Au}^{3+}$ .

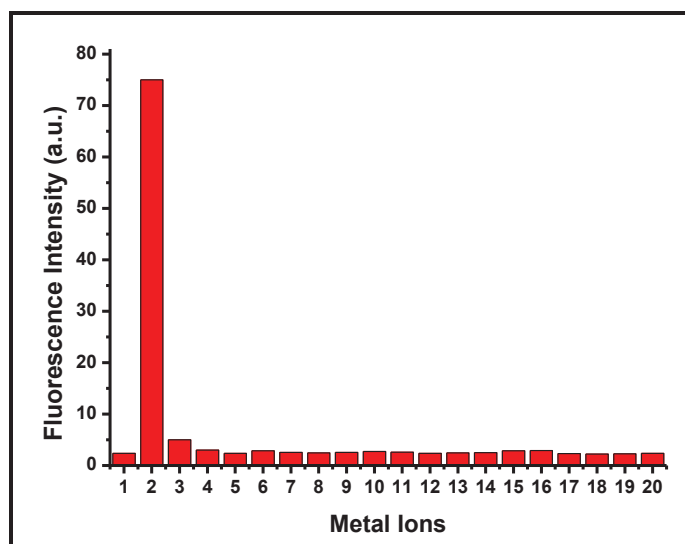


Figure 2.37. Fluorescence intensities of **RH-2** (5  $\mu\text{M}$ ) in 1:1  $\text{CH}_3\text{CN}/\text{HEPES}$  buffer at  $\text{pH} = 7.0$  at  $\lambda_{\text{max}}$ : 590 nm in the presence of 10.0 equivalent of the cations interest. 1, **RH-2** only; 2,  $\text{Au}^{3+}$  (1.0 equiv.); 3,  $\text{Au}^+$ ; 4,  $\text{Cu}^{2+}$ ; 5,  $\text{Zn}^{2+}$ ; 6,  $\text{Pb}^{2+}$ ; 7,  $\text{Ni}^{2+}$ ; 8,  $\text{Na}^+$ ; 9,  $\text{Mg}^{2+}$ ; 10,  $\text{Li}^+$ ; 11,  $\text{K}^+$ ; 12,  $\text{Pd}^{2+}$ ; 13,  $\text{Fe}^{2+}$ ; 14,  $\text{Co}^{2+}$ ; 15,  $\text{Cd}^{2+}$ ; 16,  $\text{Ca}^{2+}$ ; 17,  $\text{Ba}^{2+}$ ; 18,  $\text{Ag}^+$ ; 19,  $\text{Fe}^{3+}$ ; 20,  $\text{Cr}^{3+}$



Surprisingly, while the  $\text{Au}^{3+}$  ion enhances the fluorescence intensity, the  $\text{Au}^+$  ion did not turn on the fluorescence even though 10 equiv. of  $\text{AuCl}$  was added to **RH-2** solution. This is possibly due to a significant interaction between the more highly charged  $\text{Au}^{3+}$  ion and the probe compared to  $\text{Au}^+$  ion. (Figure 2.37)

One of the most significant characteristics of being a good sensor is to have minimum interference with other metal species present in the medium and that no change of signal is observed because of any possible interaction. Having clarified the detection of both metal species, the interference of other metal ions in the detection of  $\text{Au}^{3+}$  was assessed. The spectral response of **RH-2** induced by  $\text{Au}^{3+}$  ions showed no remarkable interference with other metal ions (Figure 2.38).

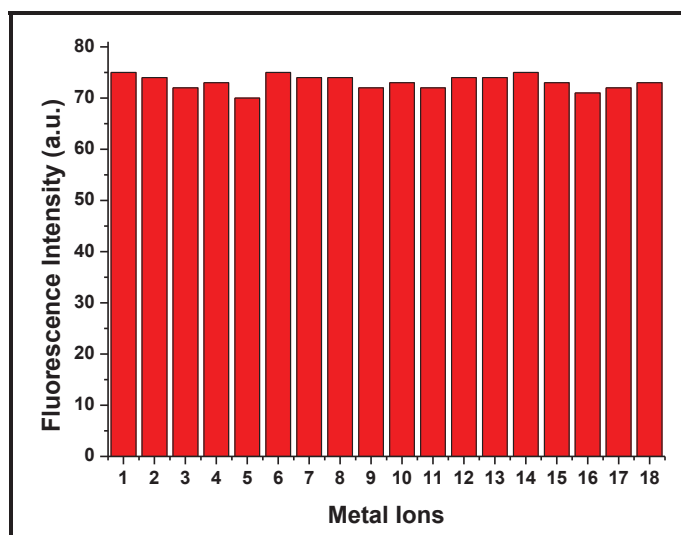


Figure 2.38. Fluorescence intensities of **RH-2** ( $5 \mu\text{M}$ ) in 1:1  $\text{CH}_3\text{CN}/\text{HEPES}$  buffer at  $\text{pH} = 7.0$  at  $\lambda_{\text{max}}$ : 590 nm in the presence  $\text{Au}^{3+}$  (1.0 equiv.) and 10.0 equiv the following metal ions: 1, none; 2,  $\text{Au}^+$ ; 3,  $\text{Cu}^{2+}$ ; 4,  $\text{Zn}^{2+}$ ; 5,  $\text{Pb}^{2+}$ ; 6,  $\text{Ni}^{2+}$ ; 7,  $\text{Na}^+$ ; 8,  $\text{Mg}^{2+}$ ; 9,  $\text{Li}^+$ ; 10,  $\text{K}^+$ ; 11,  $\text{Pd}^{2+}$ ; 12,  $\text{Fe}^{2+}$ ; 13,  $\text{Co}^{2+}$ ; 14,  $\text{Cd}^{2+}$ ; 15,  $\text{Ca}^{2+}$ ; 16,  $\text{Ba}^{2+}$  17,  $\text{Ag}^+$ ; 18,  $\text{Cr}^{3+}$ ; 19,  $\text{Fe}^{3+}$ .

The **RH-2** demonstrated high selectivity towards  $\text{Au}^{3+}$  ions via different emission modes. As discussed above, the addition of  $\text{Au}^{3+}$  to **RH-2** triggers a spiro-ring opening reaction and results in the formation of a highly emissive rhodamine derivative and  $\text{Au}^{3+}$  complex. On the other hand,  $\text{Au}^{3+}$  mediated  $\text{C}=\text{N}$  hydrolysis reaction afforded highly emissive BODIPY aldehyde compound. (Figure 2.39).

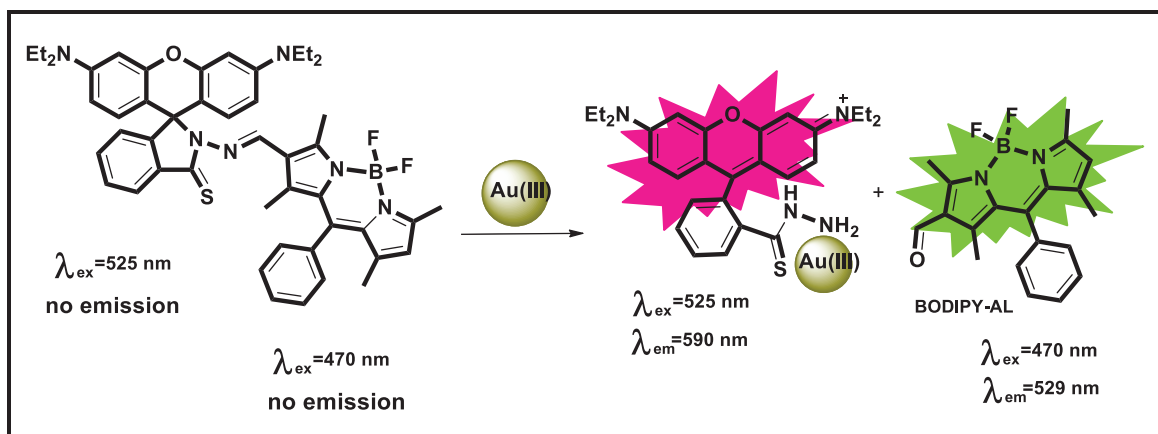


Figure 2.39. Proposed mechanism of **RH-2** towards the addition of  $\text{Au}^{3+}$  ions.

To access to information about rhodamine derivative and  $\text{Au}^{3+}$  complex structure Job's plot experiment was performed. It showed that **RH-2** formed 1:1 complex with  $\text{Au}^{3+}$  ions (Figure 2.40).

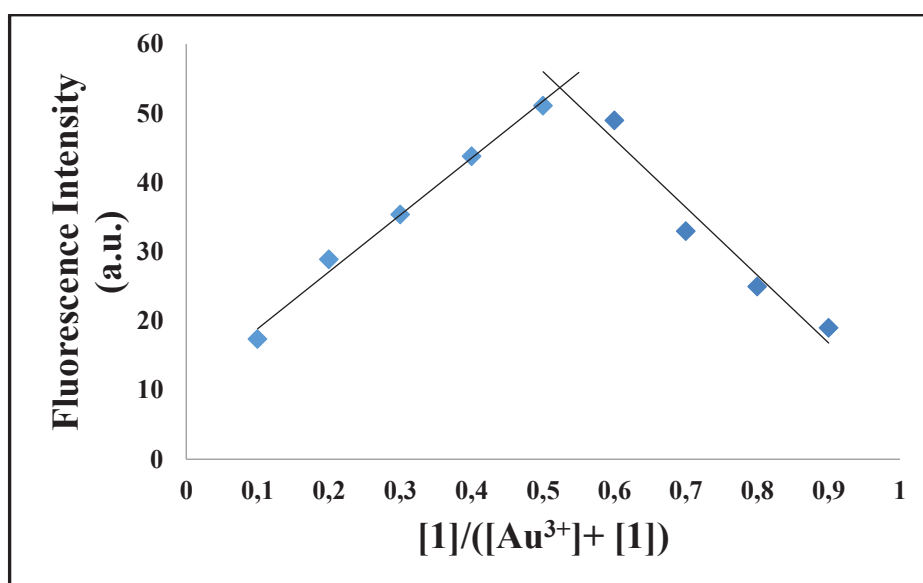


Figure 2.40. Job's plot for the rhodamine derivative and  $\text{Au}^{3+}$  in 1:1  $\text{CH}_3\text{CN}/\text{HEPES}$  buffer at  $\lambda_{\text{ex}}=525 \text{ nm}$ .

**RH-O-BOD**, the oxygen bearing derivative of **RH-2**, was used as the control probe to clarify the nature of the sensing process. Under the same sensing conditions, **RH-O-BOD** displayed no response towards any metal species, indicating the indispensable role of the sulfur functionality in the detection of both metal species (Figure 2.41).

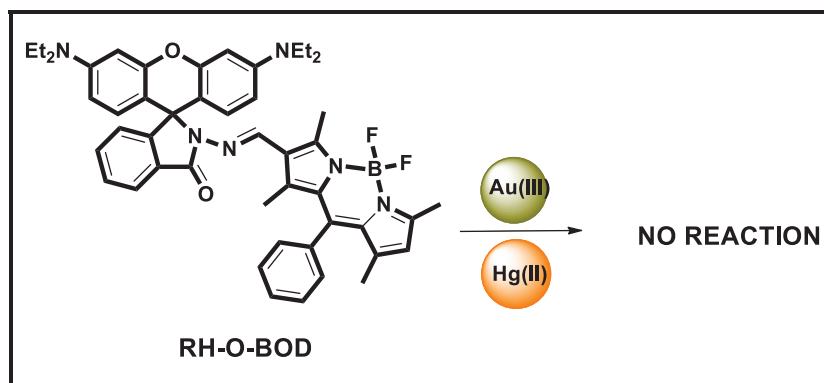


Figure 2.41. Structure of control probe of **RH-2**

As the last part of the study, the capacity of **RH-2** for imaging Au<sup>3+</sup> and Hg<sup>2+</sup> ions in living cells was investigated. To our delight, **RH-2** illustrated the same sensing behavior in living cells. Human A549 lung adenocarcinoma cell lines were incubated with the probe **RH-2** (5 μM) for 40 min. and then followed by the addition of metal species. Au<sup>3+</sup> and Hg<sup>2+</sup> ions were clearly monitored in the cells with the aid of fluorescence microscopy giving differential turn-on response (Figure 2.49).

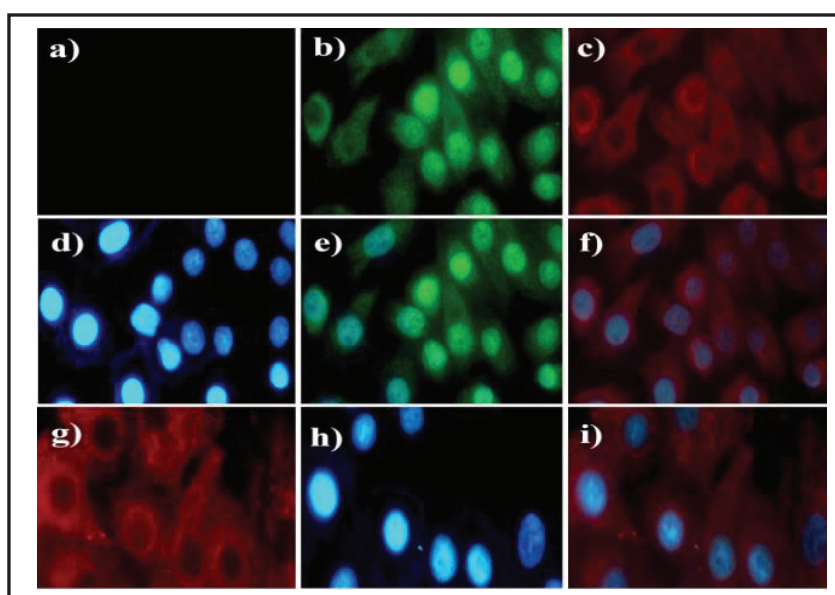


Figure 2.42. a) Fluorescence image of A549 cells treated with only **RH-2** (5 μM); b) Image of cells treated with Au<sup>3+</sup> (5 μM) and probe (5 μM) (λ<sub>ex</sub>=470 nm); c) Cells treated with Au<sup>3+</sup> (5 μM) and probe (5 μM) (λ<sub>ex</sub>=525 nm); d and h) Cells treated with DAPI for 15 min (control); d) Merged image of frame b and d; f) merged image of frame c and d; g) Cells treated with Hg<sup>2+</sup> (5 μM) and probe (5 μM) (λ<sub>ex</sub>=525 nm); i) merged image of frame g and h.

Thus, the synthesis, spectral properties, and biological application of **RH-2**, a new type of fluorescent probe for the differential detection of  $\text{Hg}^{2+}$  and  $\text{Au}^{3+}$  was described. This novel probe features excellent selectivity for  $\text{Hg}^{2+}$  and  $\text{Au}^{3+}$ . Detection of  $\text{Au}^{3+}$  was realized through two distinct fluorescence changes resulting from  $\text{Au}^{3+}$ /ligand coordination or from the hydrolysis of the C=N moiety catalyzed by  $\text{Au}^{3+}$ . Furthermore, probe **RH-2** was successfully employed for the bioimaging applications.

### 2.2.3. Gold Ion Sensing Properties of RH-3

Lately, a series of molecular sensors have been devised that proved highly efficient in monitoring gold ions in chemical and biological environments. Notably, the great majority of those probes use an alkyne motif as a gold ion-recognition site and benefit from the strong alkyne affinity of gold ions to modulate an optical signal. Alternative sensing events such as C=N bond hydrolysis and reversible ion-dipole interactions have also been employed for signal modulation. However, several challenges continue to impede the optimum performance of such sensing systems. For one, other metal ions chronically interfere. Plus, since most sensors are not completely soluble in pure water, they require a mixture of solvent systems that can in turn dramatically limit their usefulness for biological purposes. The prolonged incubation time required to measure any reliable signal change is another problem, as is that only a few can discriminate gold ions of different oxidation states which is nevertheless crucial for studying the redox states of the ions. As such, to overcome general barriers in gold ion sensing, it is essential to propose new types of fluorescent molecules that use alternative recognition strategies and moieties for detecting gold ions (Karakus et al., 2015).

Here, we presented a novel gold ion selective fluorescent probe **RH-3** based on a spirocyclic rhodamine dye with favourable properties, including fast response (<30 s) at room temperature, operability in pure water, cell membrane permeability, and the ability to differentiate Au<sup>3+</sup> from Au<sup>+</sup> (Figure 2.43).

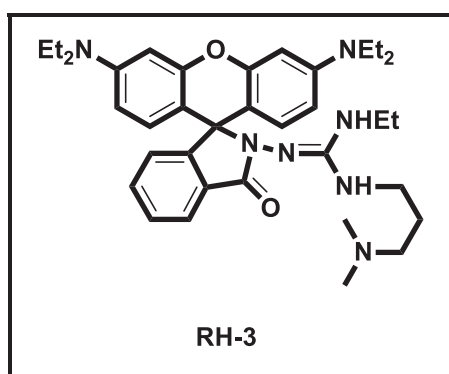


Figure 2.43. Molecular structure of **RH-3**

Our sensor design involved constructing a spirocyclic rhodamine dye modified with a guanidine motif as a gold ion-recognition site. Based on studies that used guanidine derivatives as coordinating ligands for gold ions we envisioned that a guanidine motif on the rhodamine dye would aid the specific recognition of gold ions. Moreover, we speculated that the guanidine motif, capable of forming strong hydrogen bonds with water, would also improve the solubility of the probe in water and eliminate the need of a cosolvent.

The title compound, **RH-3**, was prepared synthetically as outlined in Scheme 1. Rhodamine hydrazide was prepared by reacting rhodamine B with hydrazine hydrate in ethanol at reflux temperature. Rhodamine hydrazide was then treated with EDC [1-ethyl-3-(3-dimethylaminopropyl) carbodiimide] in ethanol in reflux conditions, which produced the title compound (isolated yield 20%). After chromatographic purification, the structure of the probe was clearly confirmed by nuclear magnetic resonance (NMR) and high-resolution mass spectrometry analysis (HRMS)

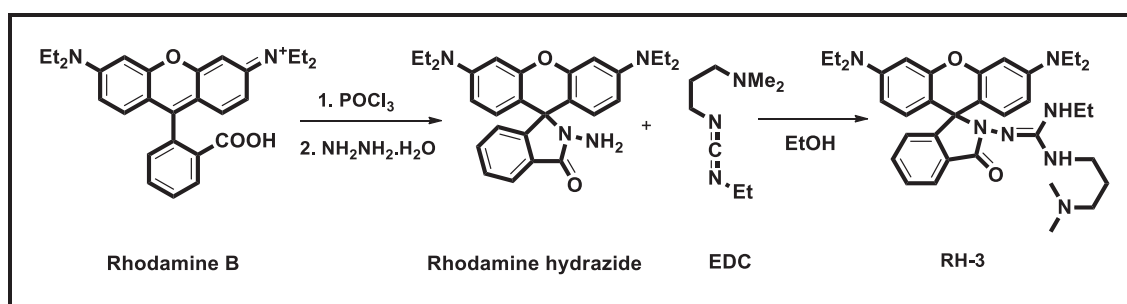


Figure 2.44. Synthetic scheme of **RH-3**

We commenced our investigation by analysing the most efficient environment for the sensing event. In general, spirolactam derivatives of rhodamine, bearing aromatic or aliphatic amide units in their molecular structure, hardly dissolve in water. Typically, a considerable amount of an organic co-solvent is thus required to improve solubility. Notably, **RH-3**, here modified with a guanidine motif, was completely soluble in water, thereby eliminating the need for a co-solvent.

A prominent handicap of rhodamine-based chemosensors is the sensitivity of the rhodamine spirolactam ring to acidity changes. Mostly, the spirolactam-ring of rhodamine is prone to transforming into its open isomeric form upon protonation, which can interfere with the detection of the analyte species. To rule out any discrepancies arising from

acidity changes, we investigated the effect of pH fluctuations on the fluorescence behaviour of the sensing system, and found that **RH-3** was insensitive to pH fluctuations (pH 2.0–12.0). The detection of gold ions by **RH-3** was also not disturbed by changing the pH of the sensing media, indicating that **RH-3** could properly detect  $\text{Au}^{3+}$  across a wide pH range (Figure 2.45). Based on these findings, a reaction medium buffered to pH 7.0 was chosen for physiological applications.

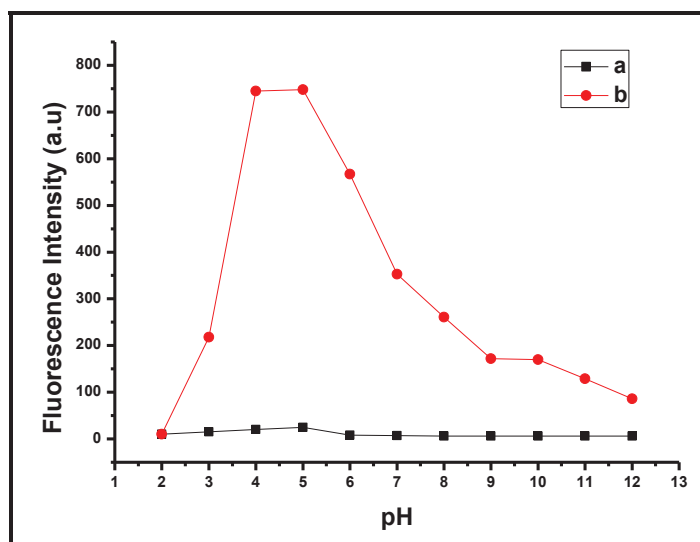


Figure 2.45. Effect of pH on the fluorescence intensity of **RH-3** (10  $\mu\text{M}$ ) in phosphate buffer in the absence (a) and presence (b) of  $\text{Au}^{3+}$  (5.0 equiv.)

With the aid of UV and fluorescence spectroscopy, we systematically studied the probe's spectroscopic behaviour upon reacting to added metal species. Free **RH-3** was colourless in solution, exhibited no visible absorption peak, and was non-fluorescent, indicating that the spirolactam ring was preserved. Upon adding  $\text{Au}^{3+}$  to the **RH-3** solution, a new absorption peak emerged at 554 nm, and the colour of the probe solution became brilliant pink. Meanwhile, a new emission band became centred at 580 nm in the fluorescence spectrum, suggesting that the spirolactam ring of the probe structure was transformed into its open form (Figure 2.46).

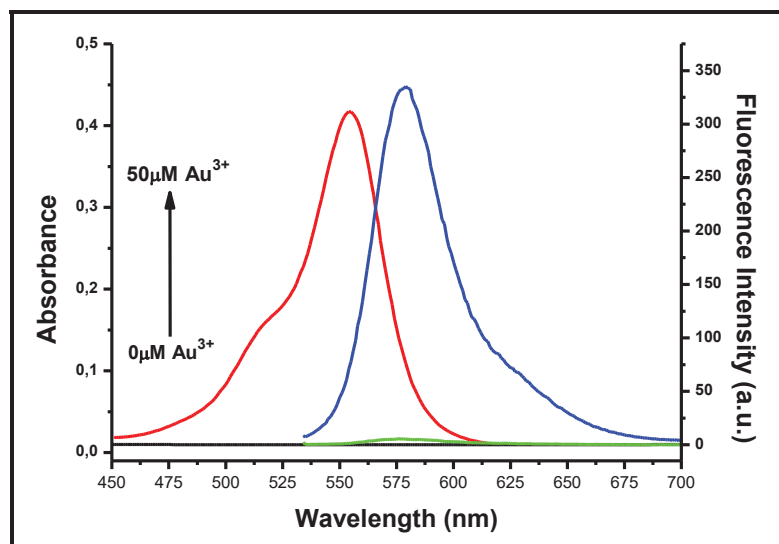


Figure 2.46. Absorbance spectra **RH-3** (10  $\mu\text{M}$ ) in the absence (black line) and presence (red line) of 5 equiv. of  $\text{Au}^{3+}$  and fluorescence spectra of **RH-3** (10  $\mu\text{M}$ ) in the absence (green line) and presence (blue line) of 5 equiv. of  $\text{Au}^{3+}$  in Phosphate buffer (0.1 M).

The intensity of fluorescence emission at 580 nm increased linearly with an increasing concentration of  $\text{Au}^{3+}$  across a wide concentration range.

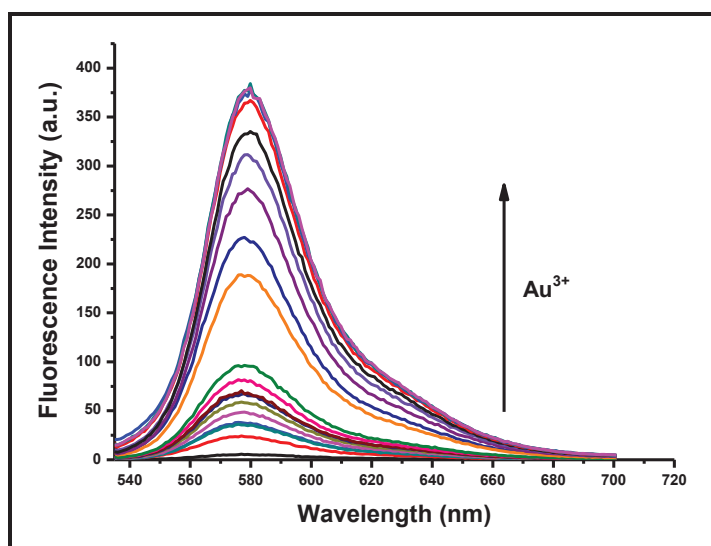


Figure 2.47. Emission titration curve of **RH-3** (10  $\mu\text{M}$ ) and  $\text{Au}^{3+}$  (0 to 10 equiv.) in Phosphate buffer (0.1 M) at pH 7.0 (After 5 min.)



The response of **RH-3** to  $\text{Au}^{3+}$  was extremely fast with the rate constant,  $k_{\text{obs}}=1.37 \times 10^{-2} \text{ sec}^{-1}$  and the enhancement of the emission intensity (>75 fold) became saturated within a couple of minutes when 1 equiv. of  $\text{Au}^{3+}$  was added (Figure 2.48 and 2.49).

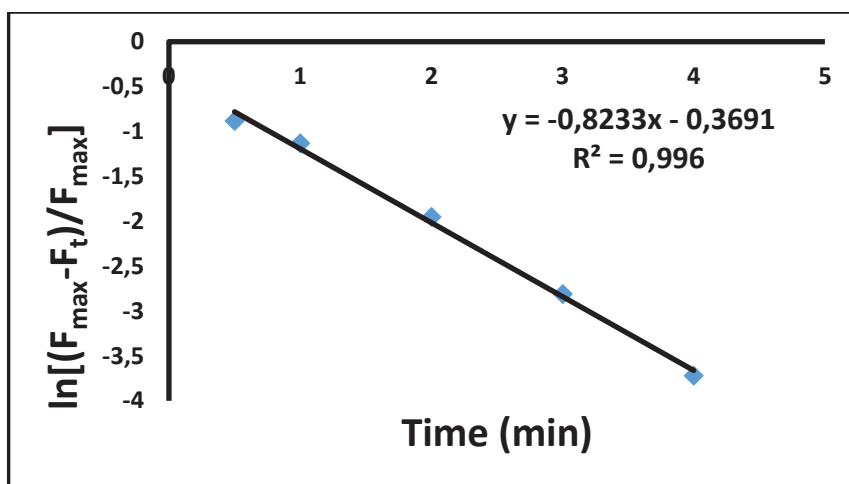


Figure 2.48. A Pseudo-first-order kinetic plot of the reaction between **RH-3** (10  $\mu\text{M}$ ) in the presence of 1.0 equivalent of  $\text{AuCl}_3$  measured in phosphate buffer at pH = 7.0.  $k_{\text{obs}}= 1.37 \times 10^{-2} \text{ sec}^{-1}$

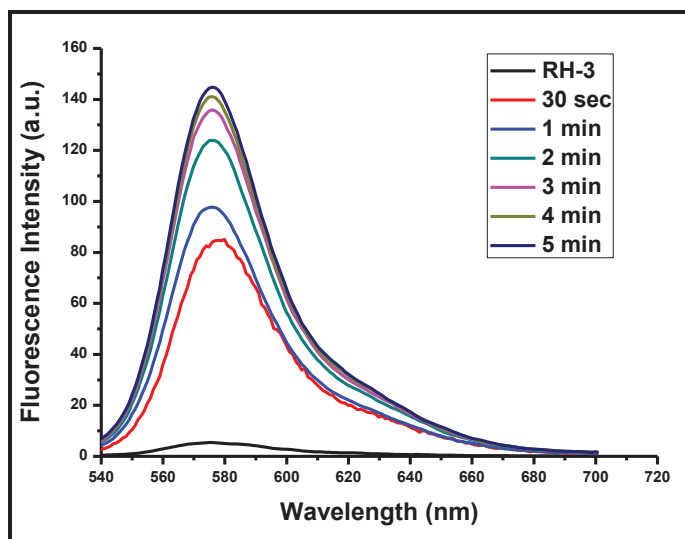


Figure 2.49. Time-dependent fluorescence change of **Rh-3** (10  $\mu\text{M}$ ) in the presence of 1.0 equivalent of  $\text{AuCl}_3$  measured in phosphate buffer at pH = 7.0

At the same time, the detection limit of **RH-3** for detecting  $\text{Au}^{3+}$  was 2.0 nM, based on the signal-to-noise ratio ( $S/N=3$ ) (Figure 2.50).

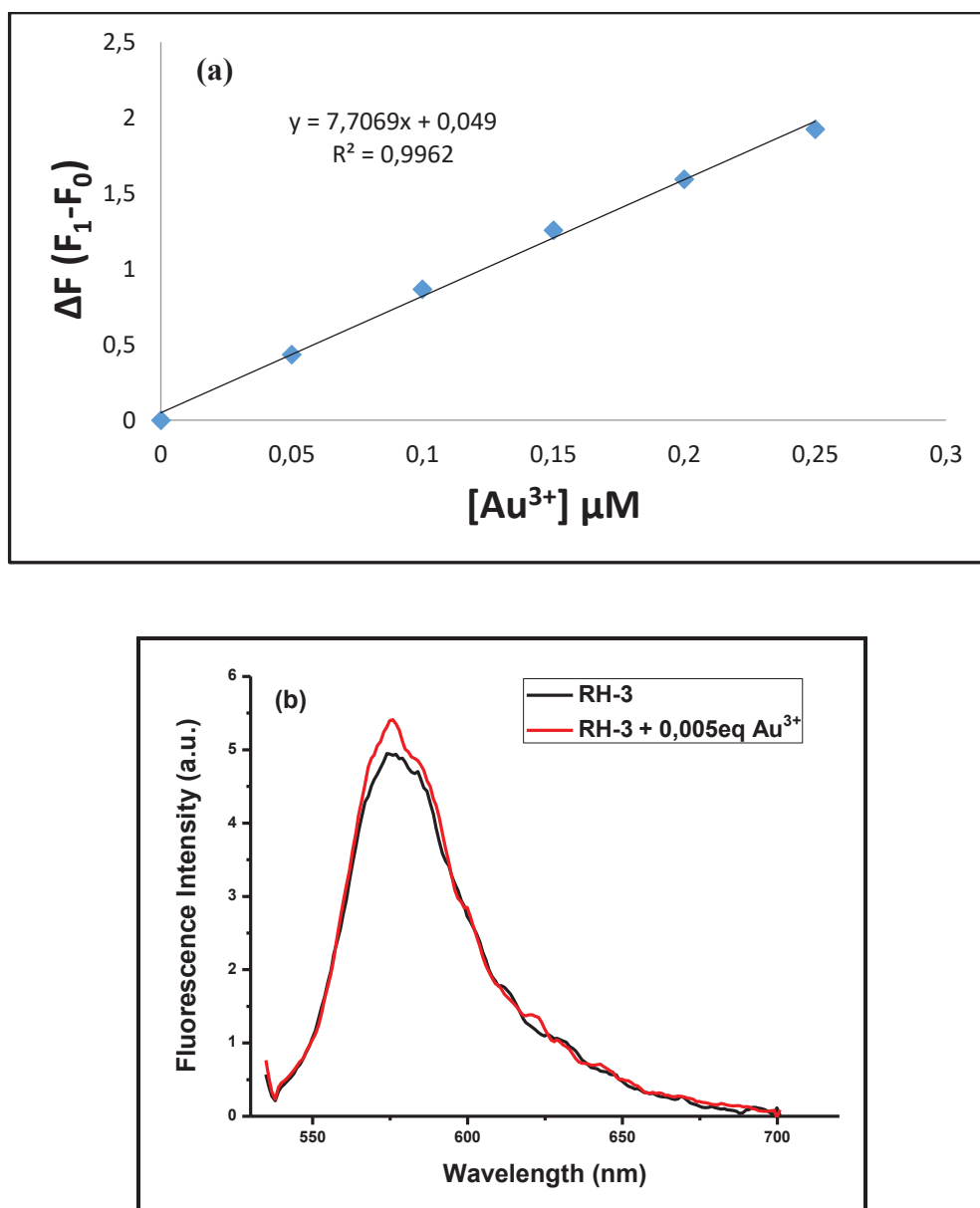


Figure 2.50.(a) Fluorescence changes of **RH-3** (10  $\mu\text{M}$ ) upon addition of  $\text{Au}^{3+}$  (0.05 to 0.3  $\mu\text{M}$ , 0.005 to 0.025 equiv.) (b) Fluorescence spectra of **RH-3** (10  $\mu\text{M}$ ) in the presence of  $\text{Au}^{3+}$  (0.05  $\mu\text{M}$ , 0.005 equiv.) in phosphate buffer at pH = 7.0

The sensitivity of **RH-3** to other possible metal species, including  $\text{Au}^+$ ,  $\text{Pd}^{2+}$ ,  $\text{Hg}^{2+}$ ,  $\text{Cu}^{2+}$ ,  $\text{Zn}^{2+}$ ,  $\text{Ba}^{2+}$ ,  $\text{Pb}^{2+}$ ,  $\text{Ni}^{2+}$ ,  $\text{Na}^+$ ,  $\text{Mg}^{2+}$ ,  $\text{Li}^+$ ,  $\text{K}^+$ ,  $\text{Ag}^+$ ,  $\text{Cd}^{2+}$ ,  $\text{Ca}^{2+}$ ,  $\text{Fe}^{3+}$ , and  $\text{Cr}^{3+}$  was investigated under the same sensing conditions. For all other metal species tested, no obvious spectral changes were observed. Fortunately,  $\text{Ag}^+$ ,  $\text{Hg}^{2+}$ , and  $\text{Pd}^{2+}$ , the three most competitive metal species in detecting gold species, did not cause any spectral change. Furthermore, no change was detected in the spectrum when  $\text{Au}^+$  ions were present, showing that **RH-3** allows the successful discrimination of  $\text{Au}^{3+}$  from  $\text{Au}^+$  (Figure 2.51)

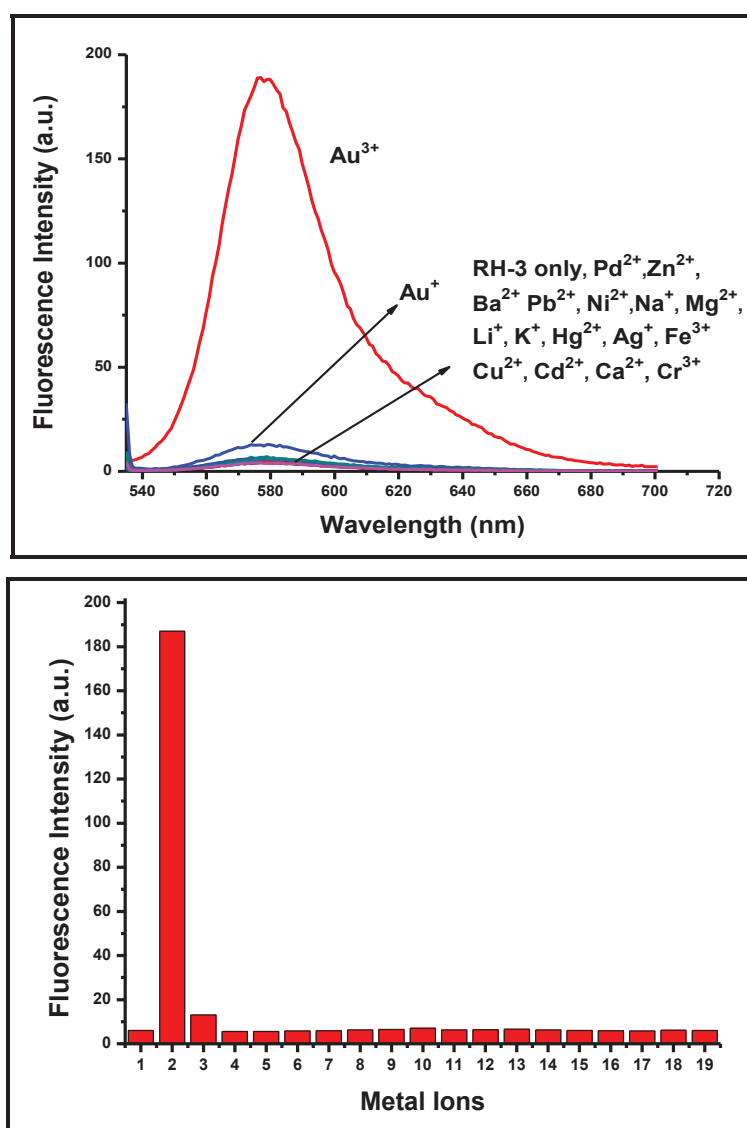


Figure 2.51. Fluorescence intensities of **RH-3** (10  $\mu\text{M}$ ) in phosphate buffer at pH = 7.0 at  $\lambda_{\text{max}}$ : 580 nm in the presence of 10.0 equivalent of the cations interest: 1, **RH-3** only; 2,  $\text{Au}^{3+}$  (1.0 equiv.); 3,  $\text{Au}^+$ ; 4,  $\text{Ag}^+$ ; 5,  $\text{Ba}^{2+}$ ; 6,  $\text{Ca}^{2+}$ ; 7,  $\text{Cd}^{2+}$ ; 8,  $\text{Cr}^{3+}$ ; 9,  $\text{Cu}^{2+}$ ; 10,  $\text{Fe}^{3+}$ ; 11,  $\text{Hg}^{2+}$ ; 12,  $\text{K}^+$ ; 13,  $\text{Li}^+$ ; 14,  $\text{Mg}^{2+}$ ; 15,  $\text{Na}^+$ ; 16,  $\text{Ni}^{2+}$ ; 17,  $\text{Pb}^{2+}$ ; 18,  $\text{Pd}^{2+}$ ; 19,  $\text{Zn}^{2+}$ .

$\text{Au}^{3+}$  species are prone to react with thiol species to form thiol complexes of gold ions. This kind of a transformation could make it highly challenging to realize gold species in the biological system. It was thus highly essential to investigate the spectral response of the probe toward  $\text{Au}^{3+}$  in the presence of reactive biothiol species, such as cysteine, the most nucleophilic and chemically reactive of the common amino acids. Meanwhile, we have also examined the interference of other metal ions in the selectivity of **RH-3**. The results from the competition experiments showed that **RH-3** could smoothly detect  $\text{Au}^{3+}$  ions in the mixtures of other related species (Figure 2.52).

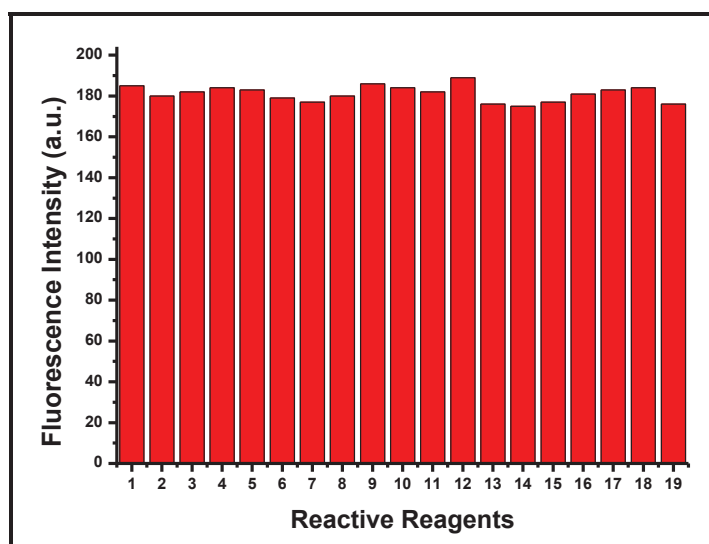


Figure 2.52. Fluorescence intensities of **RH-3** (10  $\mu\text{M}$ ) in phosphate buffer at pH = 7.0 at  $\lambda_{\text{max}}$ : 580 nm in the presence  $\text{Au}^{3+}$  (1.0 equiv.) and 10.0 equivalent of the cations interest: 1, **RH-3** only; 2,  $\text{Au}^+$ ; 3,  $\text{Ag}^+$ ; 4,  $\text{Ba}^{2+}$ ; 5,  $\text{Ca}^{2+}$ ; 6,  $\text{Cd}^{2+}$ ; 7,  $\text{Cr}^{3+}$ ; 8,  $\text{Cu}^{2+}$ ; 9,  $\text{Fe}^{3+}$ ; 10,  $\text{Hg}^{2+}$ ; 11,  $\text{K}^+$ ; 12,  $\text{Li}^+$ ; 13,  $\text{Mg}^{2+}$ ; 14,  $\text{Na}^+$ ; 15,  $\text{Ni}^{2+}$ ; 16,  $\text{Pb}^{2+}$ ; 17,  $\text{Pd}^{2+}$ ; 18,  $\text{Zn}^{2+}$ ; 19, Cysteine.

To clarify the nature of the sensing process, we first questioned whether it is reversible. To this end,  $\text{CN}^-$  ions were introduced into the solution of **RH-3** pre-treated with  $\text{Au}^{3+}$ . Interestingly, even after the addition of an excessive amount of cyanide ions, the solution preserved its colour and emission, suggesting that the sensing process might be based on an irreversible chemical reaction mediated by gold ions.

The outcome of the sensing process could be easily observed with thin-layer chromatography (TLC). The appearance of an orange emissive compound on the TLC plate strongly suggested the formation of a new rhodamine derivative. With the aid of

NMR spectroscopy, the structure of this new compound was confirmed to be rhodamine B, the hydrolysis product of **RH-3**. HRMS analysis of the probe solution (probe + Au<sup>3+</sup>) elucidated the sensing mechanism in showing two molecular ion peaks at m/z 443.23 and 457.26, attributed respectively to rhodamine-B and rhodamine hydrazide (Figure 2.53).

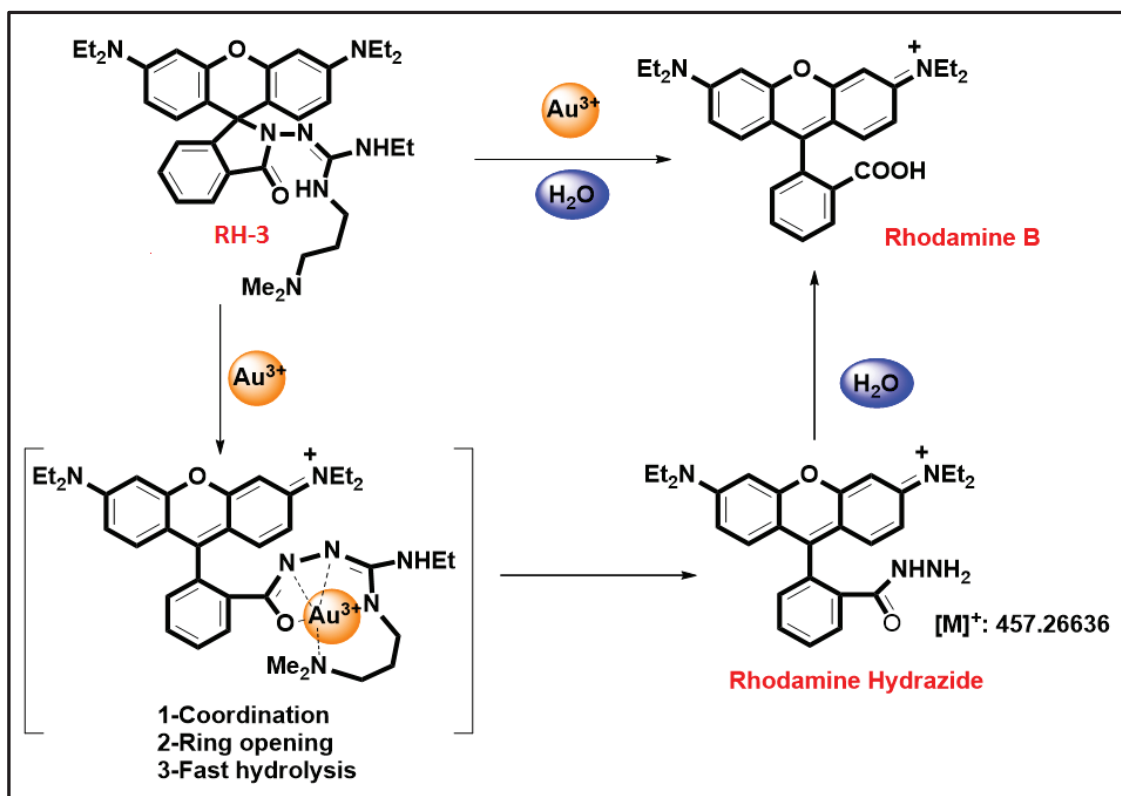


Figure 2.53. Proposed mechanism for the detection of Au<sup>3+</sup> ions

As illustrated in figure 2.53, the sensing mechanism is thought to proceed from the simultaneous coordination of Au<sup>3+</sup> with the ligand and dye, which promotes the opening of the spiro-amide ring. Specifically, rapid hydrolysis of the C=N bond via the attack of water results first in the formation of rhodamine hydrazide, which further hydrolyses to rhodamine B, thereby producing the distinct colour and emission of the solution.

Since **RH-3** displayed nearly all desirable features necessary for recognizing gold ions in the living milieu, we assessed the capacity of **RH-3** to track gold species in living cells. To this end, human colon carcinoma cells (A-549) were first incubated with **RH-3** (10 μM), to which was added Au<sup>3+</sup> (10 μM) and incubated for another 30 min. The cells were stained with a nucleus staining dye (DAPI) for another 10 min, and fluorescence images were taken with and without Au<sup>3+</sup> (10 μM). As figure 2.54 shows, the human lung

adenocarcinoma (A549) cells incubated with **RH-3** did not display any fluorescence in the absence of  $\text{Au}^{3+}$  species. Based on the nucleus counter stain and the red fluorescence emitting from the cells, we thus conclude that the probe passes through the cell membrane and detects  $\text{Au}^{3+}$  from within the cell, particularly in the cytosol.

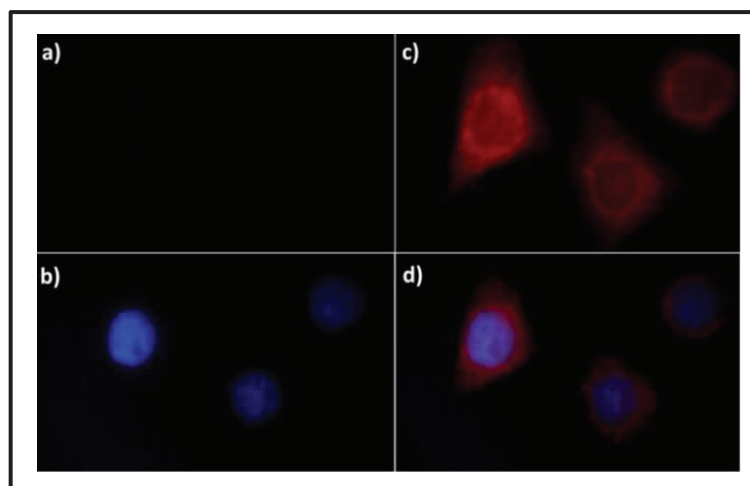


Figure 2.54. Images of A-549 cells: (a) Cells treated with **RH-3** (10  $\mu\text{M}$ ) in the absence of  $\text{Au}^{3+}$  (control) did not have any fluorescent signal (b) Cells were detected with DAPI nuclear counter-stain (c) Cells treated with **RH-3** (10  $\mu\text{M}$ ) and  $\text{Au}^{3+}$  (10  $\mu\text{M}$ ) displayed strong red fluorescence (d) The fluorescent signal appeared in and around of the nucleus judged by the DAPI counterstain in the merged image; **DAPI** blue, **RH-3** red.

Encouraged by the success of the cell imaging study, we next questioned the potential of the probe to detect  $\text{Au}^{3+}$  ions in living organisms. Though *in vivo* fluorescence sensing of certain metal species such as  $\text{Hg}^{2+}$ ,  $\text{Cu}^{2+}$ ,  $\text{Pd}^{2+}$ , and  $\text{Zn}^{2+}$  has previously been reported, tracking gold ions in the living organism, particularly in zebrafish, with fluorescent probes has not been investigated before. In fact, to the best of our knowledge, this is the first report to describe a fluorescence-based method for monitoring gold ions *in vivo*.

The species of zebrafish was chosen as a vertebrate animal model chiefly due to its small size and optical transparency. For the imaging study, zebrafish embryos 2dpf (days post fertilization) were pre-incubated with **RH-3** (10  $\mu\text{M}$ ) for 20 min, unbound **RH-3** was washed out and embryos were incubated with 20  $\mu\text{M}$   $\text{Au}^{3+}$  for another 20 min. As figure 2.55 shows, no signs of fluorescence emission emerged in the specimen in the absence of external gold ions. However, upon adding gold ions, strong fluorescence intensity was observed throughout the body and yolk of the embryo, indicating that the

probe and  $\text{Au}^{3+}$  species interacted within the organism to form a highly fluorescent product, consistent with the results obtained in the solution. This preliminary study with living organisms and their cells established that the probe can smoothly enter living cells and zebrafish and, once inside, track gold species in the living milieu.

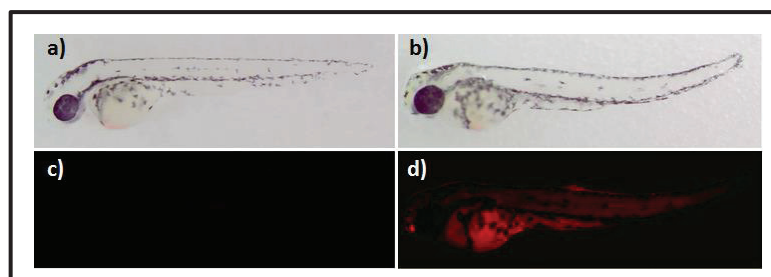


Figure 2.55. Brightfield microscopic images of zebrafish embryos treated with (a) **RH-3** (10  $\mu\text{M}$ ) in the absence of  $\text{Au}^{3+}$ , (b) **RH-3** (10  $\mu\text{M}$ ) and  $\text{Au}^{3+}$  (20  $\mu\text{M}$ ). Fluorescence images of zebrafish embryos treated with (c) **RH-3** (10  $\mu\text{M}$ ) (control) (d) **RH-3** (10  $\mu\text{M}$ ) and  $\text{Au}^{3+}$  (20  $\mu\text{M}$ ) showing that **RH-3** fluoresces in the embryo only in presence of  $\text{Au}^{3+}$

In sum, we have developed a rhodamine-based, off-on type fluorescent probe showing a remarkable fluorescence change in response to  $\text{Au}^{3+}$  ions with high sensitivity and selectivity over other metal ions. Remarkably, this probe is soluble in pure water, insensitive to pH fluctuations, and efficiently operable in physiological conditions, which is of crucial importance for biological imaging studies. Moreover, it displays high specificity for  $\text{Au}^{3+}$  ions with an extremely low detection limit—by far the lowest detection limit reported in gold ion sensing. Apart from the rapid and specific response to  $\text{Au}^{3+}$  in the solution, this probe proved highly successful in imaging gold species in both living cells and living organisms.

## CHAPTER 3

### EXPERIMENTAL STUDY

#### 3.1. General Methods

All reagents were obtained from commercial suppliers (Sigma-Aldrich and Merck) and used without any purification unless otherwise stated.  $^1\text{H}$  NMR and  $^{13}\text{C}$  NMR were measured on a Varian VNMRJ 400 Nuclear Magnetic Resonance Spectrometer. Agilent Technologies 6530 Accurate-Mass Q-TOF LC/MS was used for mass spectrometry analysis. Agilent 7500ce Octopole Reaction System (ORS) was used for inductively coupled plasma mass spectroscopy (ICP-MS) measurement UV absorption spectra were obtained on Shimadzu UV-2550 Spectrophotometer. Fluorescence measurements were performed by using Varian Cary Eclipse Fluorescence spectrophotometer. Cell imaging was performed with Zeiss Axio fluorescence microscope. Samples were contained in quartz cuvettes with a path length of 10.0 mm (2.0 mL volume). The slit width was 5 nm for both excitation and emission. pH was recorded by HI-8014 instrument (HANNA). All measurements were conducted at least in triplicate.

#### 3.2. Determination of Detection Limit

The detection limit was determined depending on fluorescence intensity changes. (Wu et al., 2011). To calculate the detection limit, the emission intensity of probe molecules without metal ions was measured ten times and the standard deviation of blank measurements was determined. Under this condition, a good linear relationship between the fluorescence intensity and metal ion concentration could be obtained in a definite concentration range. The detection limit is calculated by the equation: detection limit =  $3\sigma_{bi}/m$ , where  $\sigma_{bi}$  is the standard deviation of blank measurements;  $m$  is the slope between fluorescence intensity versus sample concentration.



### 3.3. Detection of Residual Au<sup>3+</sup> Content using Inductively-Coupled Plasma Mass Spectroscopy (ICP-MS)

A sample of compound (5.0 mg) prepared in 2.0 mL aqua regia (HNO<sub>3</sub>: HCl, 1:3 v/v) and incubated 30 min. Then, degradation process was applied with Cem Mars X microwave instrument. The solution was completed to 50.0 mL with deionized water. The resulting solution was subjected to ICP-MS analysis. A standard calibration curve was acquired with the known concentration of Au<sup>3+</sup> solutions. The measurement was conducted in triplicate

### 3.4. Kinetic Study

The reaction of **RH-3** (10 μM) with AuCl<sub>3</sub> (1 equiv) in phosphate buffer was monitored by the fluorescence intensity at 580 nm at 25 °C. The pseudo-first-order rate constant for the reaction was determined by the following equation:

$$\ln [(F_{\max}-F_t)/F_{\max}] = -k' t$$

where  $F_t$  and  $F_{\max}$  are the fluorescence intensities at 580 nm at time  $t$  and the maximum value obtained after the reaction was complete, respectively, and  $k'$  is the pseudo-first-order rate constant. The negative slope of the line represents the pseudo-first-order rate constant.

### 3.5. Cell Imaging

A549 Human Lung Adenocarcinoma cell lines were grown in DMEM supplemented with 10% FBS (fetal bovine serum) in an atmosphere of 5 % CO<sub>2</sub> at 37 °C. The cells were plated on 12mm cover glasses in 6-well plate and allowed to grow for 24h. Before the experiments, the cells were washed with PBS buffer, and then the cells were incubated with probe molecule (5 or 10 μM) for 20 min at 37 °C then washed with PBS three times. After incubating with Au<sup>3+</sup> (10 or 20 μM) for 20 min at 37 °C, cells were rinsed with PBS three times, and DAPI for 10 min at 37 °C then washed with PBS three times. Then, the fluorescence images were acquired.

### 3.6. Synthesis of Probe Molecules

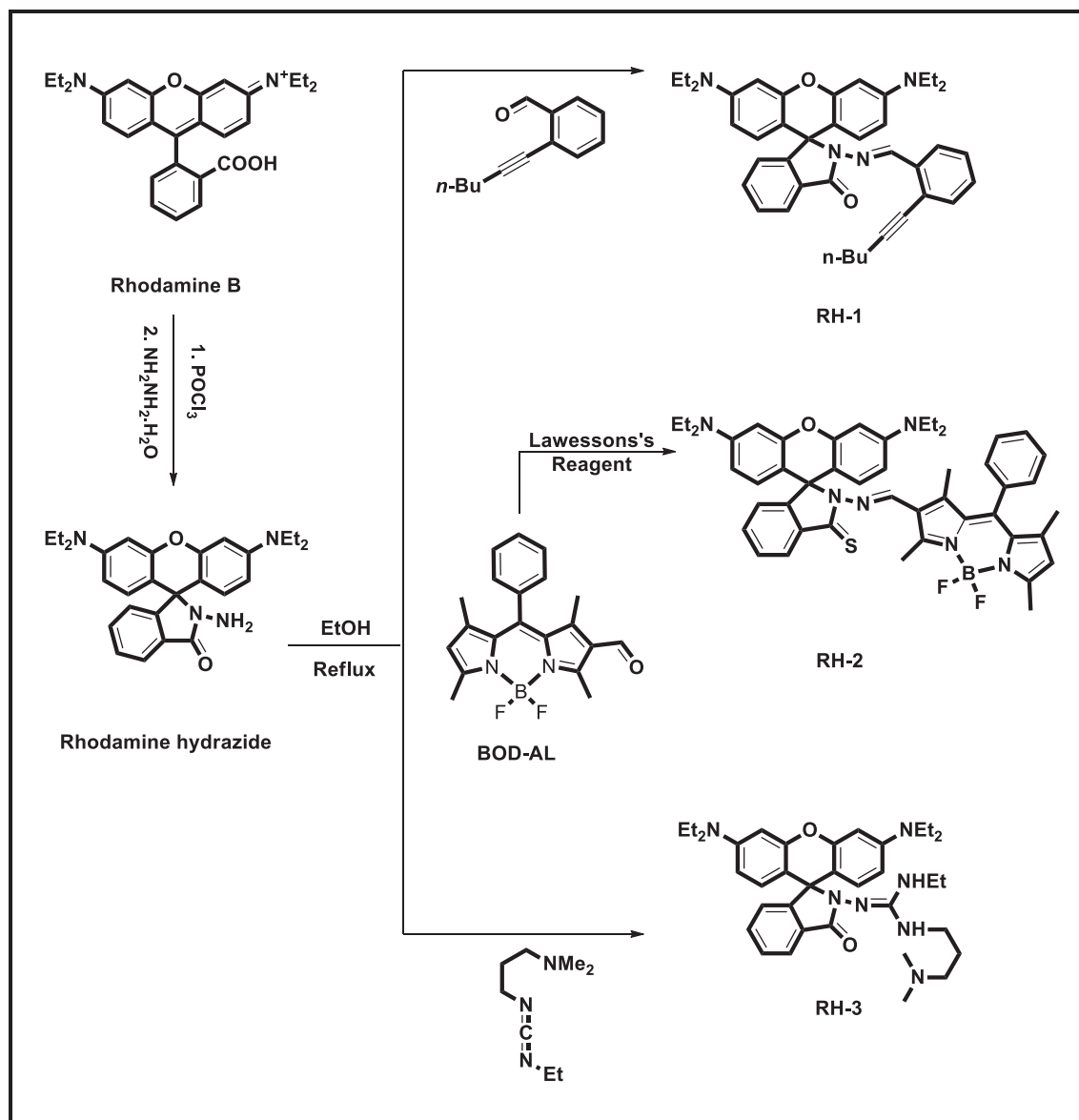
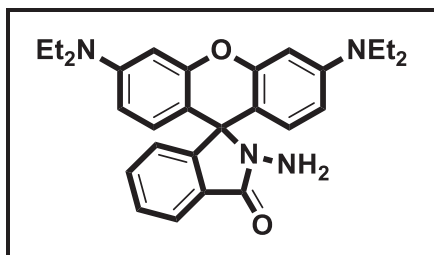


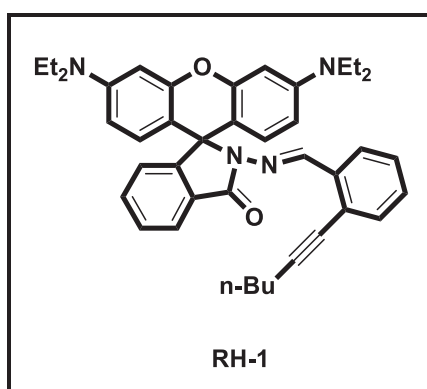
Figure 3.1. Synthetic routes of probe molecules

### 3.6.1. Synthesis of Rhodamine Hydrazide



Rhodamine B (2.40 g, 5 mmol) was stirred in 25 mL of ethanol and excess hydrazine (10 ml, hydrazine content > 50) was added dropwise. Then the reaction mixture was heated to reflux for 5h with stirring and monitoring with TLC, during which time the pink color disappeared gradually. After cooling to room temperature, the solvent was removed on a rotary evaporator. The residue was dissolved in HCl (1M) and adjusted the solution to pH 7 by 0.5 M NaOH. The resulting precipitate was filtered and washed many times with water and further recrystallized with petroleum ether to get 1.97 g of rhodamine hydrazide as lavender crystals in 80% percent yield. <sup>1</sup>H NMR (400 MHz, CDCl<sub>3</sub>) d: 7.95–7.93(1H, m), 7.46–7.44 (2H, m), 7.12–7.10 (1H, m), 6.47–6.42 (4H, dd), 6.31–6.28 (2H, s), 3.61(2H, s), 3.37–3.31(8H, q), 1.18–1.14 (12H, t). <sup>13</sup>C NMR (100 MHz, CDCl<sub>3</sub>) d:166.16, 153.86, 151.57, 148.89, 132.53, 130.03, 128.11, 128.12, 123.84,123, 108.04, 104.54, 97.96, 65.93, 44.38, 12.62 ppm.

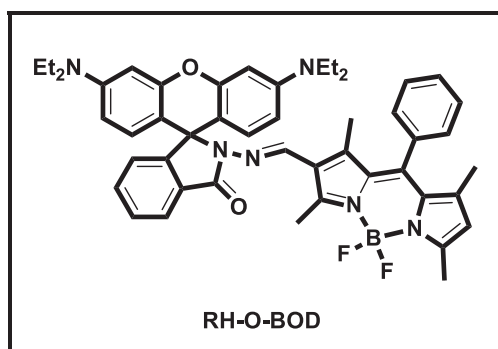
### 3.6.2. Synthesis of RH-1



To a solution of rhodamine B hydrazide (150mg, 0.33 mmol) in absolute ethanol (10 ml) was added 2-(hex-1-yn-1-yl) benzaldehyde (123mg, 0.66 mmol). This compound was synthesized according to known procedure (Dai and Larock, 2001). The solution

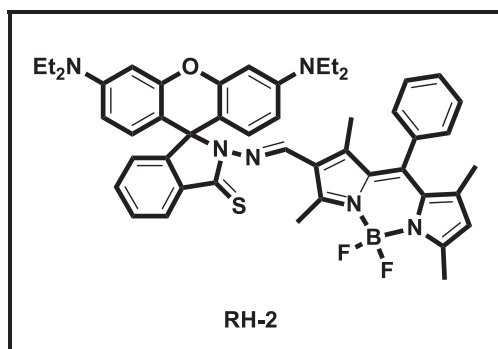
was stirred overnight at room temperature. The reaction mixture was extracted with dichloromethane (3 x 10 mL). Then the collected organic layers were dried over anhydrous MgSO<sub>4</sub>, concentrated under vacuum, and purified by column chromatography (hexane/EtOAc = 8/1) to give 140 mg of compound **1** (68%) as a pink solid. <sup>1</sup>H-NMR (400 MHz, CDCl<sub>3</sub>) δ: 8.87 (s, 1H), 8.02 (dd, J=18.6 Hz, 7.2 Hz, 2H), 7.45 (quint, J=6.4 Hz, H), 7.26-7.08 (m, H), 6.57 (d, J= 8.0 Hz, 2H), 6.42 (s, H), 6.24 (dd, J=9.2 Hz, 2.4 Hz, 2H), 3.36-3.26 (m, 8H), 2.49 (t, J=7.2 Hz, 2H), 1.63 (quint, J=7.2 Hz, 2H), 1.51 (sextet, J=7.2 Hz, 2H), 1.15 (t, J=6.8 Hz, 12H), 0.99 (t, J=7.6 Hz, H). <sup>13</sup>C NMR (100 MHz, CDCl<sub>3</sub>) δ: 165.30, 152.78, 152.51, 148.86, 144.89, 136.17, 133.37, 132.19, 128.97, 127.62, 127.42, 125.12, 123.56, 123.45, 108.09, 105.85, 97.96, 95.79, 65.66, 44.29, 30.87, 22.23, 19.31, 13.77, 12.63. MS (MALDI-TOF): m/z: Calcd. for C<sub>41</sub>H<sub>44</sub>N<sub>4</sub>O<sub>2</sub>: 625.3464 [M+H]<sup>+</sup>, Found: 625.291[M+H]<sup>+</sup>. MS (ESI-TOF): m/z: Calcd. for C<sub>41</sub>H<sub>44</sub>N<sub>4</sub>O<sub>2</sub>: 625.3464 [M+H]<sup>+</sup>, Found: 625.3544[M+H]<sup>+</sup>.

### 3.6.3. Synthesis of RH-O-BOD and RH-2



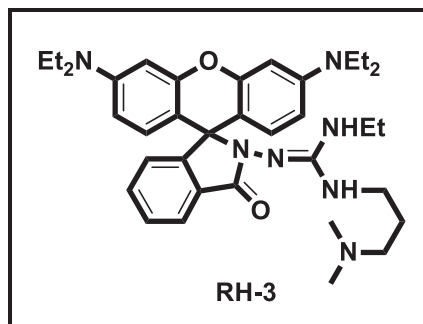
To a solution of rhodamine B hydrazide (150mg, 0.33 mmol) in absolute ethanol (10 ml) was added **BODIPY-AL** (116mg, 0.33mmol). **BODIPY-AL** was synthesized by using literature procedure (Isik et al., 2013). The solution was stirred overnight at reflux temperature. The reaction mixture was extracted with dichloromethane (3 x 10 mL). Then the collected organic layers were dried over anhydrous MgSO<sub>4</sub>, concentrated under vacuum, and purified by column chromatography (hexane/EtOAc = 8/1) to give 156 mg of **RH-O-BOD** (60%) as a pink oily. <sup>1</sup>H-NMR (400 MHz, CDCl<sub>3</sub>) δ: 9.12 (s, 1H), 7.94-7.92 (m, 1H), 7.49-7.45 (m, 4H), 7.20-7.12 (m, 3H), 6.98 (t, J=7.2 Hz, 1H), 6.47-6.26 (m, 6H), 5.99 (s, 1H), 3.32 (br. s, 8H), 2.47 (s, 3H), 2.31 (s, 3H), 1.33 (s, 6H), 1.15 (br. s, 12H). <sup>13</sup>C NMR (100 MHz, CDCl<sub>3</sub>) δ: 164.13, 156.58, 153.37, 150.80, 148.80, 143.88,

142.01, 140.88, 137.76, 134.76, 132.06, 131.99, 130.92, 130.61, 129.88, 129.18, 128.28, 127.89, 126.00, 124.04, 123.06, 121.89, 107.88, 106.28, 97.75, 66.23, 44.36, 14.68, 14.47, 14.16, 12.58, 11.99. MS (MALDI-TOF): m/z: Calcd. for C<sub>48</sub>H<sub>49</sub>BF<sub>2</sub>N<sub>6</sub>O<sub>2</sub>: 791.479 [M+H]<sup>+</sup>, Found: 791.471 [M+H]<sup>+</sup>.



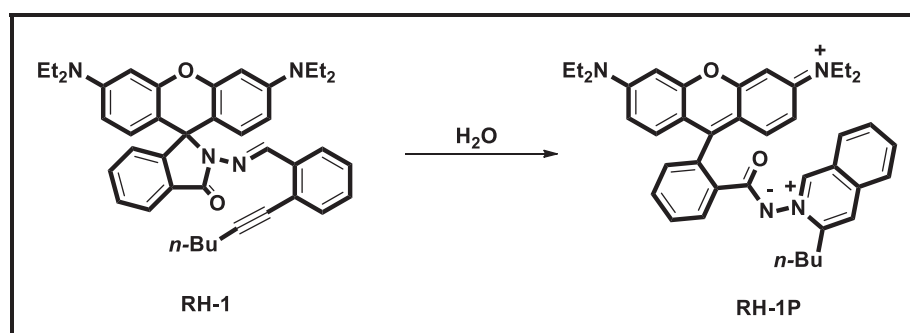
The **RH-O-BOD** (100 mg, 0.13mmol) and Lawesson's reagent (53mg, 0.13mmol) were dissolved in dry toluene, and reaction mixture was refluxed for 2 h under N<sub>2</sub> atmosphere. After removal of toluene, the residue was purified by column chromatography (hexane/EtOAc = 10/1) to give 42 mg of **RH-2** (40%) as a purple solid. <sup>1</sup>H-NMR (400 MHz, CDCl<sub>3</sub>) δ: 8.63 (s, 1H), 8.07 (dd, J=6.0 Hz, 3.2 Hz, 1H), 7.48-7.47 (m, 3H), 7.39 (dd, J=6.0 Hz, 3.2 Hz, 2H), 7.27-7.26 (m, 2H), 7.10 (dd, J=6.0 Hz, 3.2 Hz, 1H), 6.76 (d, J=8.4 Hz, 2H), 6.30-6.27 (m, 4H), 6.04 (s, 1H), 3.32 (q, J=7.2 Hz, 8H), 2.81 (s, 3H), 2.58 (s, 3H), 1.59 (s, 3H), 1.38 (s, 3H), 1.15 (t, J=7.2 Hz, 12H). <sup>13</sup>C NMR (100 MHz, CDCl<sub>3</sub>) δ: 170.92, 157.99, 156.58, 155.55, 152.94, 151.74, 148.14, 144.95, 142.49, 141.94, 135.05, 134.71, 131.96, 130.36, 129.24, 129.16, 127.92, 127.70, 127.12, 123.93, 122.48, 122.09, 110.58, 108.17, 97.38, 62.68, 44.34, 14.81, 14.64, 14.09, 12.88, 12.64. MS (MALDI-TOF): m/z: Calcd. for C<sub>48</sub>H<sub>49</sub>BF<sub>2</sub>N<sub>6</sub>OS: 807.375 [M+H]<sup>+</sup>, Found: 807.451 [M+H]<sup>+</sup>.

### 3.6.4. Synthesis of RH-3



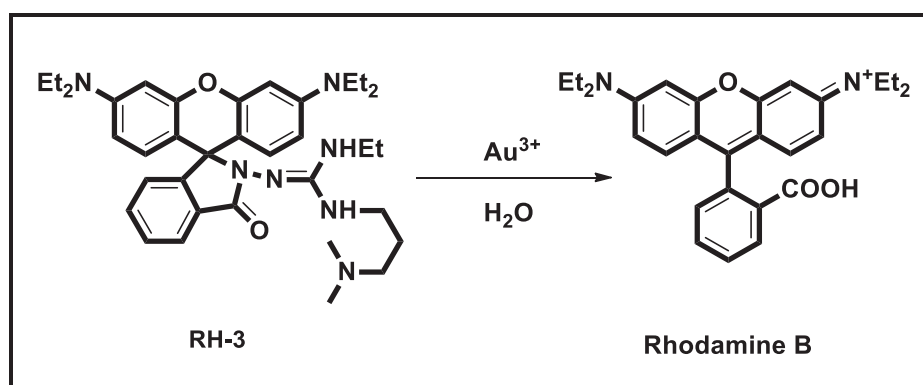
To a solution of rhodamine B hydrazide (100mg, 0,22 mmol) in absolute ethanol (5 mL) was added 1-Ethyl-3-(3-dimethylamino-propyl) carbodiimide (68mg, 0,44 mmol). The solution was stirred overnight at reflux temperature. The reaction mixture was extracted with dichloromethane (3 x 10 mL). Then the collected organic layers were dried over anhydrous MgSO<sub>4</sub>, concentrated under vacuum, and purified by column chromatography (DCM/Methanol= 10/1) to give 28mg of **RH-3** (20%) as a pink solid. <sup>1</sup>H-NMR (400 MHz, CDCl<sub>3</sub>) δ: 9.20 (br. s, 1H), 7.96 (s, 1H), 7.68-7.60 (m, 2H), 7.29 (d, *J*=7.6 Hz, 1H), 6.40-6.37 (m, 4H), 6.30- 6.28 (m, 2H), 4.66 (br. s, 1H), 3.39-3.20 (m, 14H), 2.37 (br. s, 2H), 1.88 (br. s, 6H), 1.15 (t, *J*=6.8 Hz, 12H), 0.87 (t, *J*=6.0 Hz, 3H). <sup>13</sup>C NMR (100 MHz, CDCl<sub>3</sub>) δ: 165.6, 157.3, 154.7, 149.2, 148.9, 133.9, 130.1, 129.1, 127.7, 124.7, 123.6, 107.8, 104.9, 97.9, 67.2, 52.9, 44.4, 42.5, 38.6, 37.6, 29.9, 26.0, 14.0, 12.5. HRMS: *m/z*: Calcd. for C<sub>36</sub>H<sub>49</sub>N<sub>7</sub>O<sub>2</sub>: 612.40271 [M+H]<sup>+</sup>, found: [M+H]<sup>+</sup> 612.40205.

### 3.6.5. Synthesis of RH-1P



Compound **RH-1** (38 mg, 0.06 mmol) was dissolved in CH<sub>3</sub>CN/HEPES (1.6: 0.4 mL) and then AuCl<sub>3</sub> (18 mg, 0.06 mmol) was added. Subsequently, the reaction mixture was stirred at room temperature for 90 min. The reaction mixture was evaporated under reduced pressure, and was filtered through celite. Then column chromatography was applied for the purification (CH<sub>2</sub>Cl<sub>2</sub>/MeOH 100:5) to obtain 15 mg of reddish solid. <sup>1</sup>H-NMR (400 MHz, CDCl<sub>3</sub>) δ: 8.72 (d, *J*= 8.4 Hz, 1H), 8.24 (d, *J*=7.2 Hz, 1H), 7.91 (t, *J*=7.4 Hz, 1H), 7.79 (quint, *J*=7.6 Hz, 1H), 7.70 (s, 1H), 7.51-7.47 (m, 2H), 7.31-7.26 (m, 1H), 6.86 (d, *J*=8.8 Hz, 2H), 6.56 (dd, *J*=9.2 Hz, 2.4 Hz, 2H), 6.25 (s, 2H), 3.40-3.34 (m, H), 2.84 (t, *J*=8.0 Hz, 2H), 1.32-1.13 (m, H), 0.82 (t, *J*=7.2 Hz, 3H). <sup>13</sup>C NMR (100 MHz, CDCl<sub>3</sub>) δ: 166.02, 155.80, 151.67, 149.02, 147.58, 141.09, 135.62, 133.21, 132.68, 130.61, 130.17, 129.16, 127.96, 126.68, 126.44, 125.79, 109.82, 106.62, 97.89, 45.03, 33.67, 29.68, 29.56, 22.88, 13.58, 12.45. MS (MALDI-TOF): *m/z*: Calcd. for C<sub>41</sub>H<sub>45</sub>N<sub>4</sub>O<sub>2</sub>: 625.3543 [M<sup>+</sup>], Found: 625.304 [M<sup>+</sup>]. MS (ESI-TOF): *m/z*: Calcd. for C<sub>41</sub>H<sub>45</sub>N<sub>4</sub>O<sub>2</sub> 625.3543 [M<sup>+</sup>], Found: 625.3557 [M<sup>+</sup>].

### 3.6.6. Synthesis of Rhodamine B from RH-3



**RH-3** (30 mg, 0.046 mmol) was dissolved in EtOH/Phosphate buffer (1:1 mL) and then AuCl<sub>3</sub> (13 mg, 0.046 mmol) was added. Subsequently, the reaction mixture was stirred at room temperature for 5 min. The reaction mixture was evaporated under reduced pressure, and was filtered through celite and MgSO<sub>4</sub>. Rhodamine B was obtained as 20 mg without applying further purification method. <sup>1</sup>H-NMR (400 MHz, D<sub>2</sub>O) δ: 8.07-8.05 (m, 1H), 7.62 (t, *J*=3.6 Hz, 2H), 7.11-7.09 (m, 1H), 6.81 (d, *J*=9.6 Hz, 2H), 6.58 (d, *J*=9.6 Hz, 2H), 6.41 (s, 2H), 3.33-3.30 (m, 8H), 1.00 (t, *J*=7.2 Hz, 12H). <sup>13</sup>C NMR (100 MHz,

D<sub>2</sub>O)  $\delta$ : 168.9, 159.0, 155.0, 132.8, 132.6, 131.0, 130.7, 130.4, 130.0, 113.9, 112.5, 95.8, 45.6, 11.9.



## CHAPTER 4

### CONCLUSION

In conclusion, three novel molecular probes were designed and synthesized for the selective and sensitive detection of gold ions in various environments (Figure 4.1).

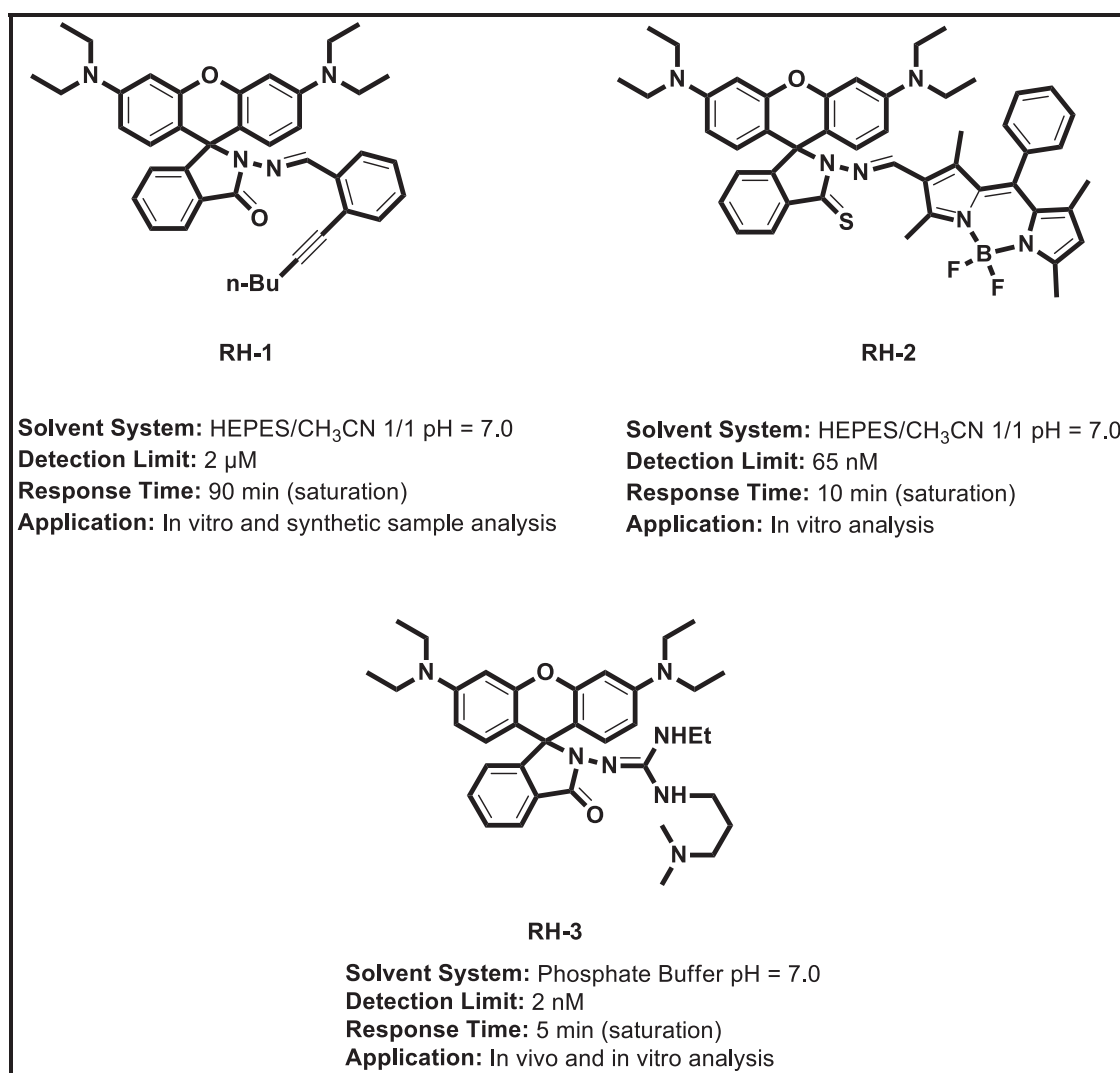


Figure 4.1. Summary of synthesized probe molecules

We suggested novel and interesting approaches in the design of each fluorescent sensors. Alkynes, because of their strong binding affinity to alkynophilic metals, appear as suitable binding platforms for gold ions. Therefore, introducing a reactive alkyne moiety to the fluorophore could provide an efficient route to develop a gold specific fluorescent probe. **RH-1** probe functionalized with an alkyne moiety, demonstrated highly selective recognition towards both Au(I) and Au(III) ions over other metal ions. Furthermore, we quantified residual gold species in synthetic samples, prepared via gold catalysis, and monitored the accumulation of gold ions in living cells by **RH-1** probe. **RH-2** probe was constructed by exploiting C=N functionality between rhodamine and BODIPY cores to detect and differentiate both Hg(II) and Au(III) species. The C=N receptor unit was used for the first time which worked via gold ion mediated hydrolysis mechanism. Thioamide functionality on the rhodamine ring also displayed indispensable role in the detection of both metal species. Moreover, cell imaging application was successfully demonstrated. **RH-3** probe design involved constructing rhodamine dye modified with a guanidine motif as a gold ion recognition site. Moreover, it was speculated that the guanidine motif, capable of forming strong hydrogen bonds with water, would also improve the solubility of the probe in water and eliminate the need of a co-solvent. Thus, **RH-3** probe exhibited excellent selectivity and sensitivity towards Au (III) ions and easily differentiated Au (III) ions from Au(I) ions in 100% aqueous media. Remarkably, this probe was also insensitive to pH fluctuations and efficiently operable in physiological conditions, which is of crucial importance for biological imaging studies. Moreover, it displayed high specificity for Au (III) ions with an extremely low detection limit—by far the lowest detection limit reported in gold ion sensing. Apart from the rapid and specific response to Au (III) ions in the solution, this probe proved highly successful in imaging gold species in living cells and living organisms (zebrafish). In fact, to the best of our knowledge, this was the first report to describe a fluorescence-based method for monitoring gold ions *in vivo*.

## REFERENCES

- Arcadi, A. Alternative Synthetic Methods through New Developments in Catalysis by Gold. *Chemical Reviews*, 108 (2008), 3266-3325.
- Aulsebrook, M. L.; Graham, B.; Grace, M. R.; Tuck, K. L. Coumarin-based fluorescent sensors for zinc(II) and hypochlorite. *Supramolecular Chemistry*, 27 (2015), 798-806.
- Baeyer, A. On A New Class of Dyes. *Berichte der Deutschen chemischen Gesellschaft zu Berlin*, 4 (1871), 555-558.
- Bates, M.; Huang, B.; Dempsey, G. T.; Zhuang, X. Multicolor Super-Resolution Imaging with Photo-Switchable Fluorescent Probes. *Science*, 317 (2007), 1749-1753.
- Beija, M.; Afonso, C. A. M.; Martinho, J. M. G. Synthesis and applications of Rhodamine derivatives as fluorescent probes. *Chemical Society Reviews*, 38 (2009), 2410-2433.
- Boens, N.; Leen, V.; Dehaen, W. Fluorescent indicators based on BODIPY. *Chemical Society Reviews*, 41 (2012), 1130-1172.
- Boens, N.; Verbelen, B.; Dehaen, W. Postfunctionalization of the BODIPY Core: Synthesis and Spectroscopy. *European Journal of Organic Chemistry*, 2015 (2015), 6577-6595.
- Callan, J. F.; de Silva, A. P.; Magri, D. C. Luminescent sensors and switches in the early 21st century. *Tetrahedron*, 61 (2005), 8551-8588.
- Cao, X.; Lin, W.; Ding, Y. Ratio-Au: A FRET-based Fluorescent Probe for Ratiometric Determination of Gold Ions and Nanoparticles. *Chemistry – A European Journal*, 17 (2011), 9066-9069.
- Chakraborty, I.; Tang, W. C.; Bame, D. P.; Tang, T. K. MEMS micro-valve for space applications. *Sensors and Actuators A: Physical*, 83 (2000), 188-193.
- Chen, X.; Pradhan, T.; Wang, F.; Kim, J. S.; Yoon, J. Fluorescent Chemosensors Based on Spiroring-Opening of Xanthenes and Related Derivatives. *Chemical Reviews*, 112 (2012), 1910-1956.
- Chen, X.; Wang, F.; Hyun, J. Y.; Wei, T.; Qiang, J.; Ren, X., . . . Yoon, J. Recent progress in the development of fluorescent, luminescent and colorimetric probes for detection of reactive oxygen and nitrogen species. *Chemical Society Reviews*, 45 (2016), 2976-3016.

- Cheng, J.; Zhou, X.; Xiang, H. Fluorescent metal ion chemosensors via cation exchange reactions of complexes, quantum dots, and metal-organic frameworks. *Analyst*, 140 (2015), 7082-7115.
- Corti, C. W.; Holliday, R. J.; Thompson, D. T. Developing new industrial applications for gold: Gold nanotechnology. *Gold Bulletin*, 35 (2002), 111-117.
- Corti, C. W.; Holliday, R. J.; Thompson, D. T. Progress towards the commercial application of gold catalysts. *Topics in Catalysis*, 44 (2007), 331-343.
- Çetintaş, C.; Karakuş, E.; Üçüncü, M.; Emrulloğlu, M. A fluorescein-based chemodosimeter for selective gold(III) ion monitoring in aqueous media and living systems. *Sensors and Actuators B: Chemical*, 234 (2016), 109-114.
- Dai, G.; Larock, R. C. Synthesis of 3,4-Disubstituted Isoquinolines via Palladium-Catalyzed Cross-Coupling of o-(1-Alkynyl)benzaldimines and Organic Halides. *Organic Letters*, 3 (2001), 4035-4038.
- Ding, Q.; Chen, Z.; Yu, X.; Peng, Y.; Wu, J. Highly efficient electrophilic cyclization of N'-(2-alkynylbenzylidene)hydrazides. *Tetrahedron Letters*, 50 (2009), 340-342.
- Dujols, V.; Ford, F.; Czarnik, A. W. A Long-Wavelength Fluorescent Chemodosimeter Selective for Cu(II) Ion in Water. *Journal of the American Chemical Society*, 119 (1997), 7386-7387.
- Duke, R. M.; Veale, E. B.; Pfeffer, F. M.; Kruger, P. E.; Gunnlaugsson, T. Colorimetric and fluorescent anion sensors: an overview of recent developments in the use of 1,8-naphthalimide-based chemosensors. *Chemical Society Reviews*, 39 (2010), 3936-3953.
- Duncan, B.; Kim, C.; Rotello, V. M. Gold nanoparticle platforms as drug and biomacromolecule delivery systems. *Journal of Controlled Release*, 148 (2010), 122-127.
- Egorova, O. A.; Seo, H.; Chatterjee, A.; Ahn, K. H. Reaction-Based Fluorescent Sensing of Au(I)/Au(III) Species: Mechanistic Implications on Vinylgold Intermediates. *Organic Letters*, 12 (2010), 401-403.
- Emrulloğlu, M.; Karakuş, E.; Ucuncu, M. A rhodamine based "turn-on" chemodosimeter for monitoring gold ions in synthetic samples and living cells. *Analyst*, 138 (2013), 3638-3641.
- Eun Jun, M.; Roy, B.; Han Ahn, K. "Turn-on" fluorescent sensing with "reactive" probes. *Chemical Communications*, 47 (2011), 7583-7601.
- Forster, T. 10th Spiers Memorial Lecture. Transfer mechanisms of electronic excitation. *Discussions of the Faraday Society*, 27 (1959), 7-17.

- Förster, T. Zwischenmolekulare Energiewanderung und Fluoreszenz. *Annalen der Physik*, 437 (1948), 55-75.
- Gabbiani, C.; Casini, A.; Messori, L. Gold(III) compounds as anticancer drugs. *Gold Bulletin*, 40 (2007), 73-81.
- Gonçalves, M. S. T. Fluorescent Labeling of Biomolecules with Organic Probes. *Chemical Reviews*, 109 (2009), 190-212.
- Goodman, C. M.; McCusker, C. D.; Yilmaz, T.; Rotello, V. M. Toxicity of Gold Nanoparticles Functionalized with Cationic and Anionic Side Chains. *Bioconjugate Chemistry*, 15 (2004), 897-900.
- Goodman, P. Current and future uses of gold in electronics. *Gold Bulletin*, 35 (2002), 21-26.
- Gorin, D. J.; Toste, F. D. Relativistic effects in homogeneous gold catalysis. *Nature*, 446 (2007), 395-403.
- Guo, Z.; Kim, G.-H.; Shin, I.; Yoon, J. A cyanine-based fluorescent sensor for detecting endogenous zinc ions in live cells and organisms. *Biomaterials*, 33 (2012), 7818-7827.
- Habib, A.; Tabata, M. Oxidative DNA damage induced by HEPES (2-[4-(2-hydroxyethyl)-1-piperazinyl]ethanesulfonic acid) buffer in the presence of Au(III). *Journal of Inorganic Biochemistry*, 98 (2004), 1696-1702.
- Hashmi, A. S. K.; Weyrauch, J. P.; Frey, W.; Bats, J. W. Gold Catalysis: Mild Conditions for the Synthesis of Oxazoles from N-Propargylcarboxamides and Mechanistic Aspects. *Organic Letters*, 6 (2004), 4391-4394.
- Haugland, R. P. S., M. T. Z.; Johnson, I. D.; Basey, A., . (2005). *The Handbook: A Guide to Fluorescent Probes and Labeling Technologies* (10th ed.).
- Herschel, J. F. W. On the Epipolic Dispersion of Light, Being a Supplement to a Paper Entitled, "On a Case of Superficial Colour Presented by a Homogeneous Liquid Internally Colourless. *Phil. Trans. R. Soc. London*, 133 (1845), 143-145.
- Hong, R.; Han, G.; Fernández, J. M.; Kim, B.-j.; Forbes, N. S.; Rotello, V. M. Glutathione-Mediated Delivery and Release Using Monolayer Protected Nanoparticle Carriers. *Journal of the American Chemical Society*, 128 (2006), 1078-1079.
- Isik, M.; Ozdemir, T.; Turan, I. S.; Kolemen, S.; Akkaya, E. U. Chromogenic and Fluorogenic Sensing of Biological Thiols in Aqueous Solutions Using BODIPY-Based Reagents. *Organic Letters*, 15 (2013), 216-219.

- Jiménez-Núñez, E.; Echavarren, A. M. Gold-Catalyzed Cycloisomerizations of Enynes: A Mechanistic Perspective. *Chemical Reviews*, 108 (2008), 3326-3350.
- Jung, H. S.; Chen, X.; Kim, J. S.; Yoon, J. Recent progress in luminescent and colorimetric chemosensors for detection of thiols. *Chemical Society Reviews*, 42 (2013), 6019-6031.
- Kambam, S.; Wang, B.; Wang, F.; Wang, Y.; Chen, H.; Yin, J.; Chen, X. A highly sensitive and selective fluorescein-based fluorescence probe for Au<sup>3+</sup> and its application in living cell imaging. *Sensors and Actuators B: Chemical*, 209 (2015), 1005-1010.
- Karakus, E.; Cakan-Akdogan, G.; Emrullahoglu, M. A guanidinium modified rhodamine-based fluorescent probe for in vitro/vivo imaging of gold ions. *Analytical Methods*, 7 (2015), 8004-8008.
- Karakus, E.; Ucuncu, M.; Emrullahoglu, M. A rhodamine/BODIPY-based fluorescent probe for the differential detection of Hg(ii) and Au(iii). *Chemical Communications*, 50 (2014), 1119-1121.
- Karakuş, E.; Üçüncü, M.; Emrullahoğlu, M. Electrophilic Cyanate As a Recognition Motif for Reactive Sulfur Species: Selective Fluorescence Detection of H<sub>2</sub>S. *Analytical Chemistry*, 88 (2016), 1039-1043.
- Kim, H. N.; Lee, M. H.; Kim, H. J.; Kim, J. S.; Yoon, J. A new trend in rhodamine-based chemosensors: application of spirolactam ring-opening to sensing ions. *Chemical Society Reviews*, 37 (2008), 1465-1472.
- Kowada, T.; Maeda, H.; Kikuchi, K. BODIPY-based probes for the fluorescence imaging of biomolecules in living cells. *Chemical Society Reviews*, 44 (2015), 4953-4972.
- Kwon, J. Y.; Jang, Y. J.; Lee, Y. J.; Kim, K. M.; Seo, M. S.; Nam, W.; Yoon, J. A Highly Selective Fluorescent Chemosensor for Pb<sup>2+</sup>. *Journal of the American Chemical Society*, 127 (2005), 10107-10111.
- Lakowicz, J. R. (2006). *Principles of fluorescence spectroscopy*. New York: Springer.
- Li, X.; Gao, X.; Shi, W.; Ma, H. Design Strategies for Water-Soluble Small Molecular Chromogenic and Fluorogenic Probes. *Chemical Reviews*, 114 (2014), 590-659.
- Li, Y.; Schluesener, H. J.; Xu, S. Gold nanoparticle-based biosensors. *Gold Bulletin*, 43 (2010), 29-41.
- Li, Z.; Brouwer, C.; He, C. Gold-Catalyzed Organic Transformations. *Chemical Reviews*, 108 (2008), 3239-3265.

- Liu, Z.; Wang, W.; Xu, H.; Sheng, L.; Chen, S.; Huang, D.; Sun, F. A “naked eye” and ratiometric chemosensor for cobalt(II) based on coumarin platform in aqueous solution. *Inorganic Chemistry Communications*, 62 (2015), 19-23.
- Lo, L.-C.; Chu, C.-Y. Development of highly selective and sensitive probes for hydrogen peroxide. *Chemical Communications*, (2003), 2728-2729.
- Loudet, A.; Burgess, K. BODIPY Dyes and Their Derivatives: Syntheses and Spectroscopic Properties. *Chemical Reviews*, 107 (2007), 4891-4932.
- Marks, K. M.; Nolan, G. P. Chemical labeling strategies for cell biology. *Nat Meth*, 3 (2006), 591-596.
- Martínez-Máñez, R.; Sancenón, F. Fluorogenic and Chromogenic Chemosensors and Reagents for Anions. *Chemical Reviews*, 103 (2003), 4419-4476.
- Messori, L.; Marcon, G. (2004). *Gold Complexes in the Treatment of Rheumatoid Arthritis Metal Ions in Biological Systems*: CRC Press.
- Mishra, A.; Behera, R. K.; Behera, P. K.; Mishra, B. K.; Behera, G. B. Cyanines during the 1990s: A Review. *Chemical Reviews*, 100 (2000), 1973-2012.
- Nam, S.-H.; Lee, W.-M.; Shin, Y.-J.; Yoon, S.-J.; Kim, S. W.; Kwak, J. I.; An, Y.-J. Derivation of guideline values for gold (III) ion toxicity limits to protect aquatic ecosystems. *Water Research*, 48 (2014), 126-136.
- Narayanan, N.; Patonay, G. A New Method for the Synthesis of Heptamethine Cyanine Dyes: Synthesis of New Near-Infrared Fluorescent Labels. *The Journal of Organic Chemistry*, 60 (1995), 2391-2395.
- Ni, Y.; Wu, J. Far-red and near infrared BODIPY dyes: synthesis and applications for fluorescent pH probes and bio-imaging. *Organic & Biomolecular Chemistry*, 12 (2014), 3774-3791.
- Noelting, E.; Dziewoński, K. Zur Kenntniss der Rhodamine. *Berichte der deutschen chemischen Gesellschaft*, 38 (1905), 3516-3527.
- Ott, I. On the medicinal chemistry of gold complexes as anticancer drugs. *Coordination Chemistry Reviews*, 253 (2009), 1670-1681.
- Patil, N. T.; Shinde, V. S.; Thakare, M. S.; Hemant Kumar, P.; Bangal, P. R.; Barui, A. K.; Patra, C. R. Exploiting the higher alkynophilicity of Au-species: development of a highly selective fluorescent probe for gold ions. *Chemical Communications*, 48 (2012), 11229-11231.

- Quang, D. T.; Kim, J. S. Fluoro- and Chromogenic Chemodosimeters for Heavy Metal Ion Detection in Solution and Biospecimens. *Chemical Reviews*, 110 (2010), 6280-6301.
- R. Martínez-Utrilla; Martín, M. E.; Amat-Guerri, F.; Sastre, R.; Botija, J. M. New halogenated succinylfluorescein dyes. synthesis and evaluation as singlet oxygen photosensitizers of their free and polymer-bound forms. *Dyes and Pigments*, 10 (1989), 47-61.
- Schulman, S. G.; Threatte, R. M.; Capomacchia, A. C.; Paul, W. L. Fluorescence of 6-methoxyquinoline, quinine, and quinidine in aqueous media. *Journal of Pharmaceutical Sciences*, 63 (1974), 876-880.
- Seo, H.; Jun, M. E.; Egorova, O. A.; Lee, K.-H.; Kim, K.-T.; Ahn, K. H. A Reaction-Based Sensing Scheme for Gold Species: Introduction of a (2-Ethynyl)benzoate Reactive Moiety. *Organic Letters*, 14 (2012), 5062-5065.
- Seo, H.; Jun, M. E.; Ranganathan, K.; Lee, K.-H.; Kim, K.-T.; Lim, W., . . . Ahn, K. H. Ground-State Elevation Approach To Suppress Side Reactions in Gold-Sensing Systems Based on Alkyne Activation. *Organic Letters*, 16 (2014), 1374-1377.
- Serin, J. M.; Brousmiche, D. W.; Fréchet, J. M. J. A FRET-Based Ultraviolet to Near-Infrared Frequency Converter. *Journal of the American Chemical Society*, 124 (2002), 11848-11849.
- Singha, S.; Kim, D.; Seo, H.; Cho, S. W.; Ahn, K. H. Fluorescence sensing systems for gold and silver species. *Chemical Society Reviews*, 44 (2015), 4367-4399.
- Sjöback, R.; Nygren, J.; Kubista, M. Absorption and fluorescence properties of fluorescein. *Spectrochimica Acta Part A: Molecular and Biomolecular Spectroscopy*, 51 (1995), L7-L21.
- Smalley, M. K.; Silverman, S. K. Fluorescence of covalently attached pyrene as a general RNA folding probe. *Nucleic Acids Research*, 34 (2006), 152-166.
- Stokes, G. G. On the Change of Refrangibility of Light. *Phil. Trans. R. Soc. London*, 142 (1852).
- Süßmeier, F.; Langhals, H. Novel Fluorescence Labels: The Synthesis of Perylene-3,4,9-tricarboxylic Imides. *European Journal of Organic Chemistry*, 2001 (2001), 607-610.
- Ulrich, G.; Ziesel, R.; Harriman, A. The Chemistry of Fluorescent Bodipy Dyes: Versatility Unsurpassed. *Angewandte Chemie International Edition*, 47 (2008), 1184-1201.



- Valeur, B.; Leray, I. Design principles of fluorescent molecular sensors for cation recognition. *Coordination Chemistry Reviews*, 205 (2000), 3-40.
- Vasimalai, N.; Rajalakshmi, K.; John, S. A. Economically viable sensitive and selective luminescent sensor for the determination of Au(III) in environmental samples. *RSC Advances*, 4 (2014), 38812-38819.
- Wang, J.; Lin, W.; Yuan, L.; Song, J.; Gao, W. Development of a reversible fluorescent gold sensor with high selectivity. *Chemical Communications*, 47 (2011), 12506-12508.
- Wechakorn, K.; Prabpai, S.; Suksen, K.; Piyachaturawat, P.; Kongsaree, P. Rhodol-based fluorescent probe for Au<sup>3+</sup> detection and its application in bioimaging. *RSC Advances*, 6 (2016), 24752-24755.
- Woodroffe, C. C.; Lim, M. H.; Bu, W.; Lippard, S. J. Synthesis of isomerically pure carboxylate- and sulfonate-substituted xanthene fluorophores. *Tetrahedron*, 61 (2005), 3097-3105.
- Wu, W.; Guo, H.; Wu, W.; Ji, S.; Zhao, J. Organic Triplet Sensitizer Library Derived from a Single Chromophore (BODIPY) with Long-Lived Triplet Excited State for Triplet-Triplet Annihilation Based Upconversion. *The Journal of Organic Chemistry*, 76 (2011), 7056-7064.
- Xiang, Y.; Tong, A.; Jin, P.; Ju, Y. New Fluorescent Rhodamine Hydrazone Chemosensor for Cu(II) with High Selectivity and Sensitivity. *Organic Letters*, 8 (2006), 2863-2866.
- Yang, Y.-K.; Lee, S.; Tae, J. A Gold(III) Ion-Selective Fluorescent Probe and Its Application to Bioimaging. *Organic Letters*, 11 (2009), 5610-5613.
- Yang, Y.-K.; Yook, K.-J.; Tae, J. A Rhodamine-Based Fluorescent and Colorimetric Chemodosimeter for the Rapid Detection of Hg<sup>2+</sup> Ions in Aqueous Media. *Journal of the American Chemical Society*, 127 (2005), 16760-16761.
- Yin, J.; Kwon, Y.; Kim, D.; Lee, D.; Kim, G.; Hu, Y., . . . Yoon, J. Preparation of a cyanine-based fluorescent probe for highly selective detection of glutathione and its use in living cells and tissues of mice. *Nat. Protocols*, 10 (2015), 1742-1754.
- Yuan, L.; Lin, W.; Yang, Y.; Song, J. A fast-responsive fluorescent probe for detection of gold ions in water and synthetic products. *Chemical Communications*, 47 (2011), 4703-4705.
- Zhao, X.; Wei, R.; Chen, L.; Jin, D.; Yan, X. Glucosamine modified near-infrared cyanine as a sensitive colorimetric fluorescent chemosensor for aspartic and glutamic acid and its applications. *New Journal of Chemistry*, 38 (2014), 4791-4798.

Zheng, H.; Zhan, X.-Q.; Bian, Q.-N.; Zhang, X.-J. Advances in modifying fluorescein and rhodamine fluorophores as fluorescent chemosensors. *Chemical Communications*, 49 (2013), 429-447.

## **APPENDIX A**

### **$^1\text{H-NMR}$ AND $^{13}\text{C-NMR}$ SPECTRA OF COMPOUNDS**

Acquisition Time (sec)	2.5559	Comment	EK-RH-HYDRAZIDE	Date	Apr 19 2017
File Name	C:\Users\IERMAN\Google Drive\TEZ.YAZIM\EK-RH-HYDRAZIDE_20170419_02\PROTON_01	Number of Transients	8	Frequency (MHz)	399.92
Nucleus	<sup>1</sup> H	Solvent	CHLOROFORM-D	Points Count	16384
Pulse Sequence	s2pul	Original Points Count	16384	Sweep Width (Hz)	6410.26
Temperature (degree C)	23.000				

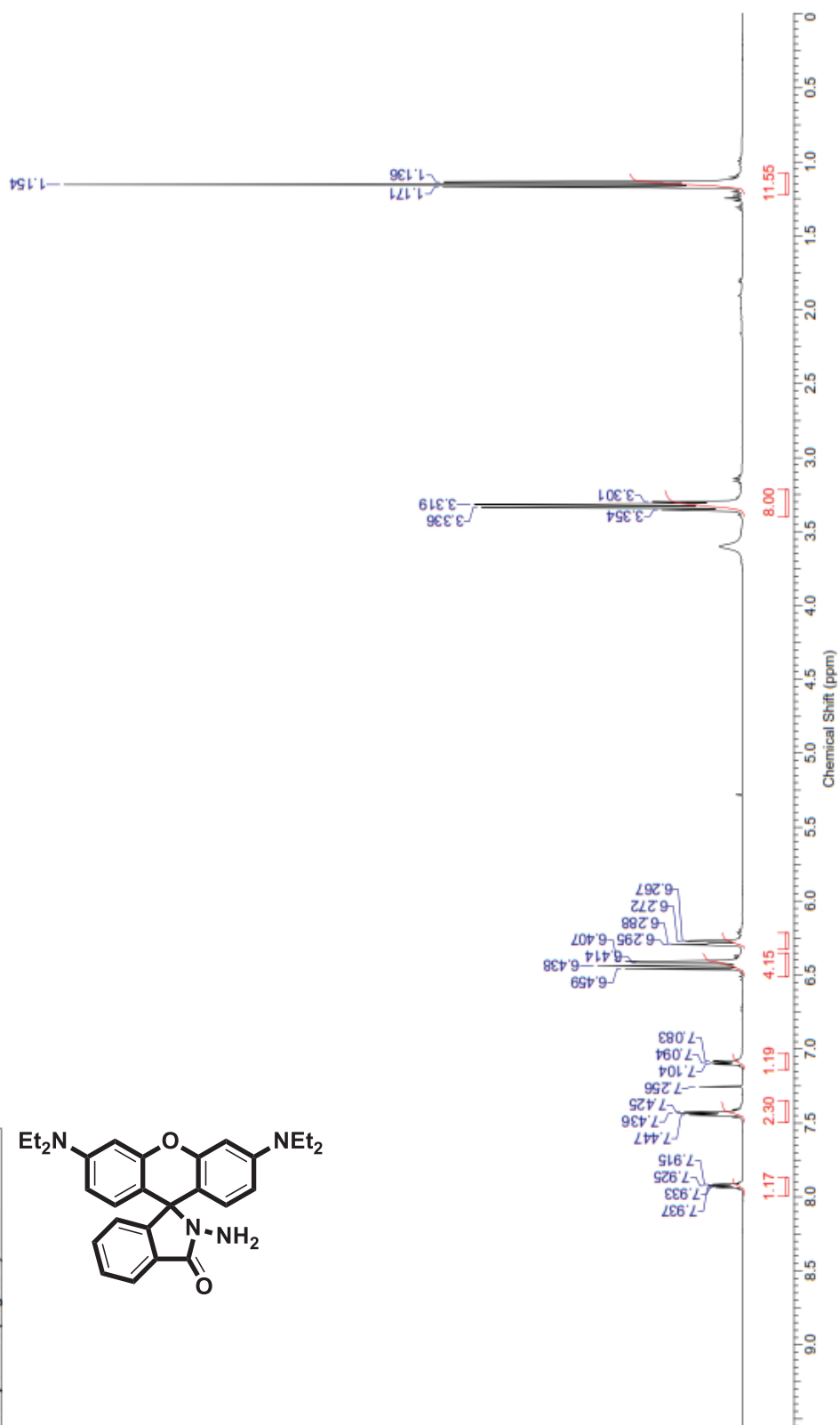
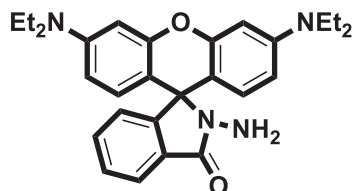


Figure A.1. <sup>1</sup>H NMR of 2-amino-3',6'-bis(diethylamino)spiro[isoindoline-1,9'-xanthen]-3-one

Acquisition Time (sec)	1.3107	Comment	EK-RH-HYDRAZIDE	Date	Apr 19 2017
File Name	C:\Users\ERMANI\Google Drive\TEZ YAZIM\EK-RH-HYDRAZIDE_20170419_02\CARBON_01	Number of Transients	256	Original Points Count	32768
Nucleus	<sup>13</sup> C	Solvent	CHLOROFORM-D	Frequency (MHz)	100.57
Pulse Sequence	s2pul			Points Count	32768
Temperature (degree C)	23.000			Sweep Width (Hz)	25000.00

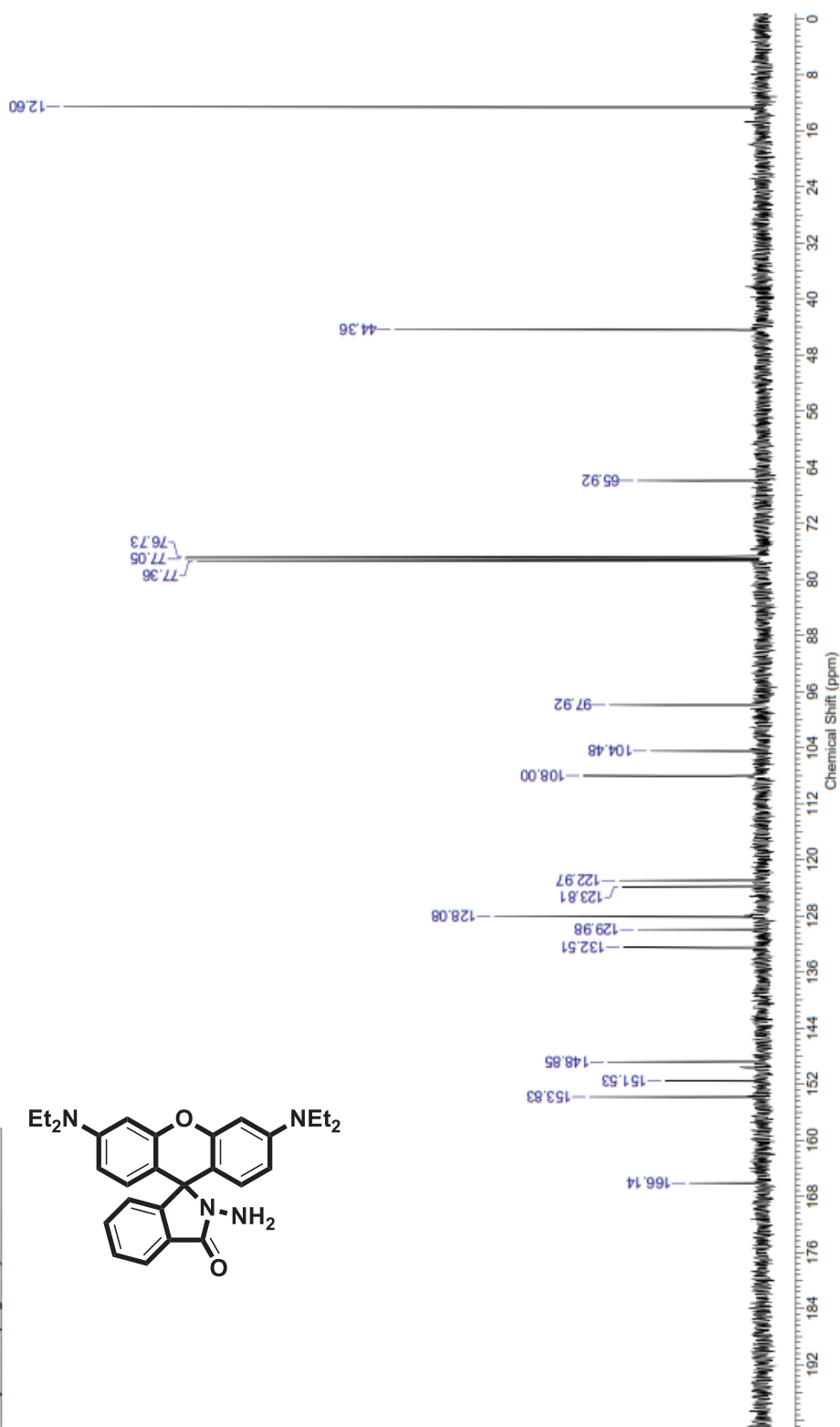
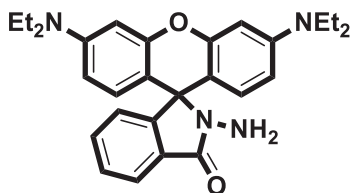


Figure A.2. <sup>13</sup>C NMR of 2-amino-3',6'-bis(diethylamino)spiro[isoindoline-1,9'-xanthen]-3-one

Acquisition Time (sec)	2.5559	Comment	Gradient Shimming	Date	Nov 16 2012
File Name	C:\Users\ERMAN\Desktop\MUSTAFA EMRULLAHOGLUEK-ER-64_20121116_01\PROTON_01			Frequency (MHz)	399.92
Nucleus	<sup>1</sup> H	Number of Transients	8	Original Points Count	16384
Pulse Sequence	s2pul	Solvent	CHLOROFORM-D	Sweep Width (Hz)	6410.26
Temperature (degree C)	25.000				

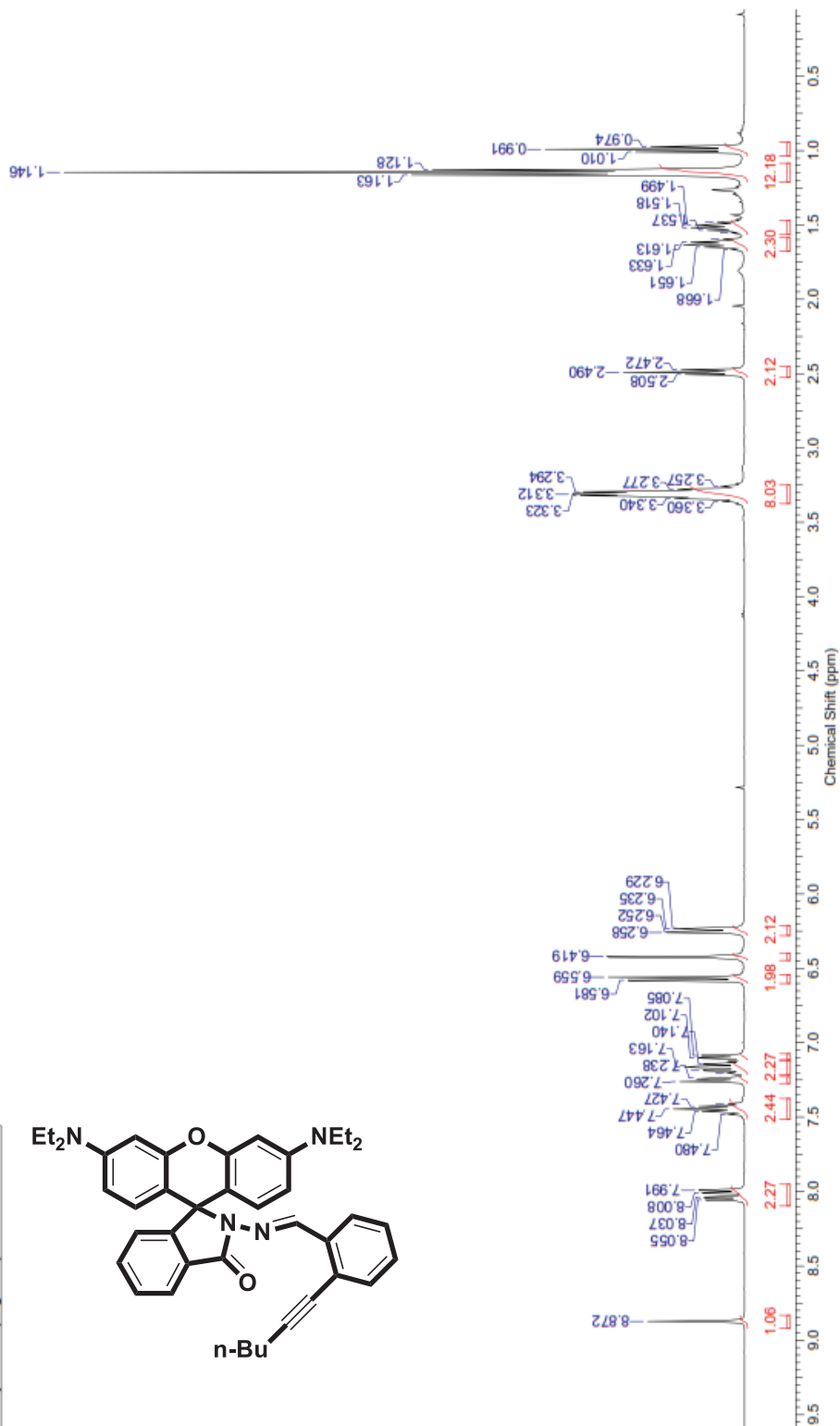
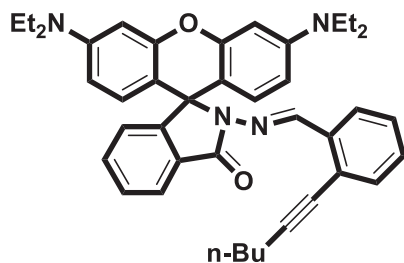


Figure A.3. <sup>1</sup>H NMR of (E)-3',6'-bis(diethylamino)-2-((2-(hex-1-yn-1-yl)benzylidene)amino)spiro[isindoline-1,9'-xanthen]-3-one

Acquisition Time (sec)	1.3107	Comment	Gradient Shimming	Date	Nov 16 2012
File Name	C:\Users\ERMANI\Desktop\MUSTAFA EMRULLAHOGLU\EK-ER-64_20121116_03\CARBON_01	Number of Transients	512	Frequency (MHz)	100.57
Nucleus	<sup>13</sup> C	Solvent	CHLOROFORM-D	Points Count	32768
Pulse Sequence	s2pul			Sweep Width (Hz)	25000.00
Temperature (degree C)	25.000				

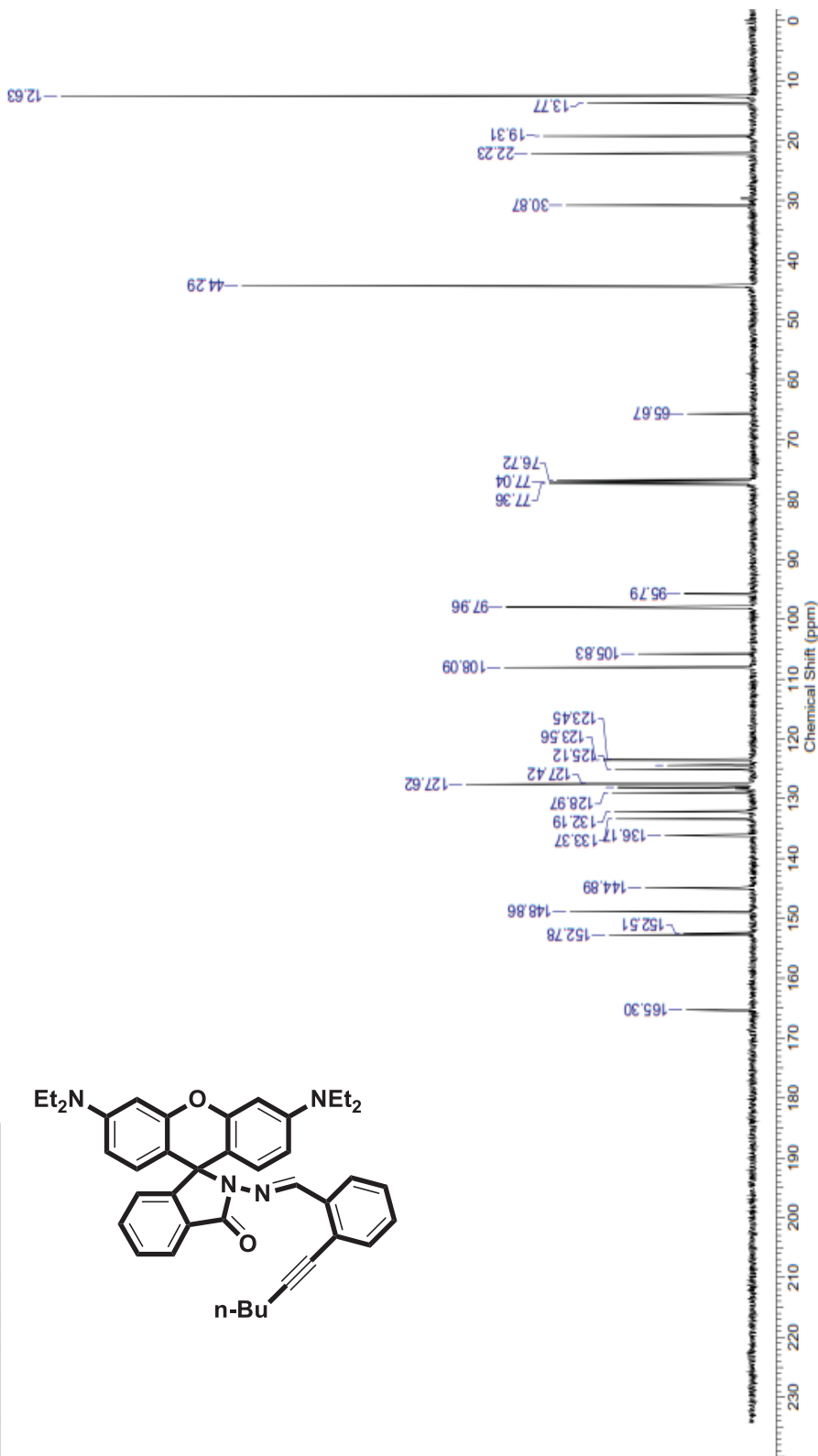


Figure A.4. <sup>13</sup>C NMR of (E)-3',6'-bis(diethylamino)-2-((2-(hex-1-yn-1-yl)benzylidene)amino)spiro[isindoline-1,9'-xanthen]-3-one

Acquisition Time (sec)	2.5559	Comment	Gradient Shimming	Date	Nov 7 2012
File Name	C:\Users\BERMAN\Desktop\MUSTAFA.EMR\LLAHOGLUEK-ER-60-FR3_20121107_01\PROTON_01	Number of Transients	8	Frequency (MHz)	399.92
Nucleus	<sup>1</sup> H	Original Points Count	16384	Points Count	16384
Pulse Sequence	s2pul	Solvent	CHLOROFORM-D	Sweep Width (Hz)	6410.26
Temperature (degree C)	25.000				

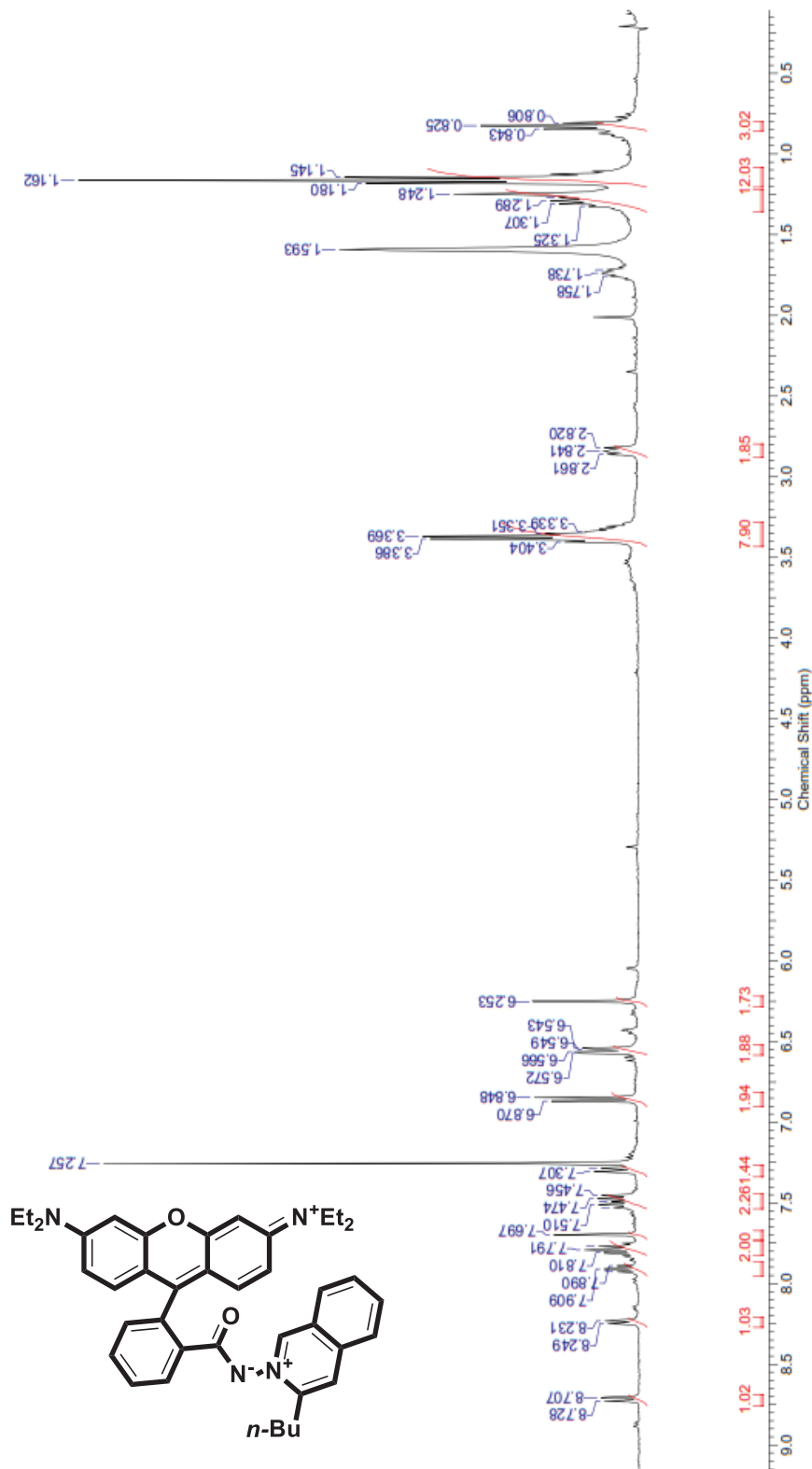


Figure A.5. <sup>1</sup>H NMR of (3-butylisoquinolin-2-ium-2-yl)(2-(6-(diethylamino)-3H-xanthen-9-yl)benzoyl)amide



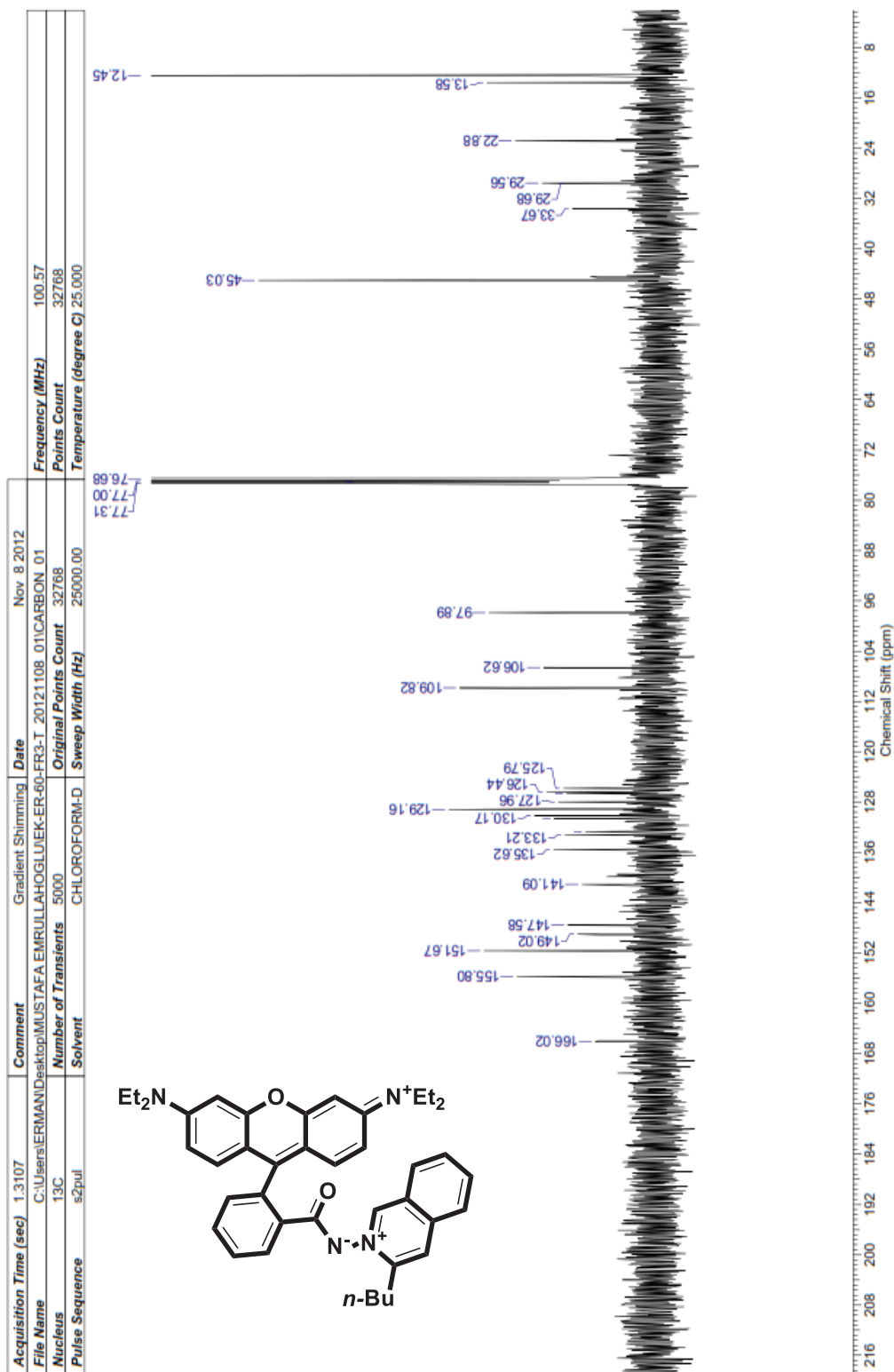


Figure A.6. <sup>13</sup>C NMR of (3-butylisoquinolin-2-ium-2-yl)(2-(6-(diethylamino)-3H-xanthen-9-yl)benzoyl)amide

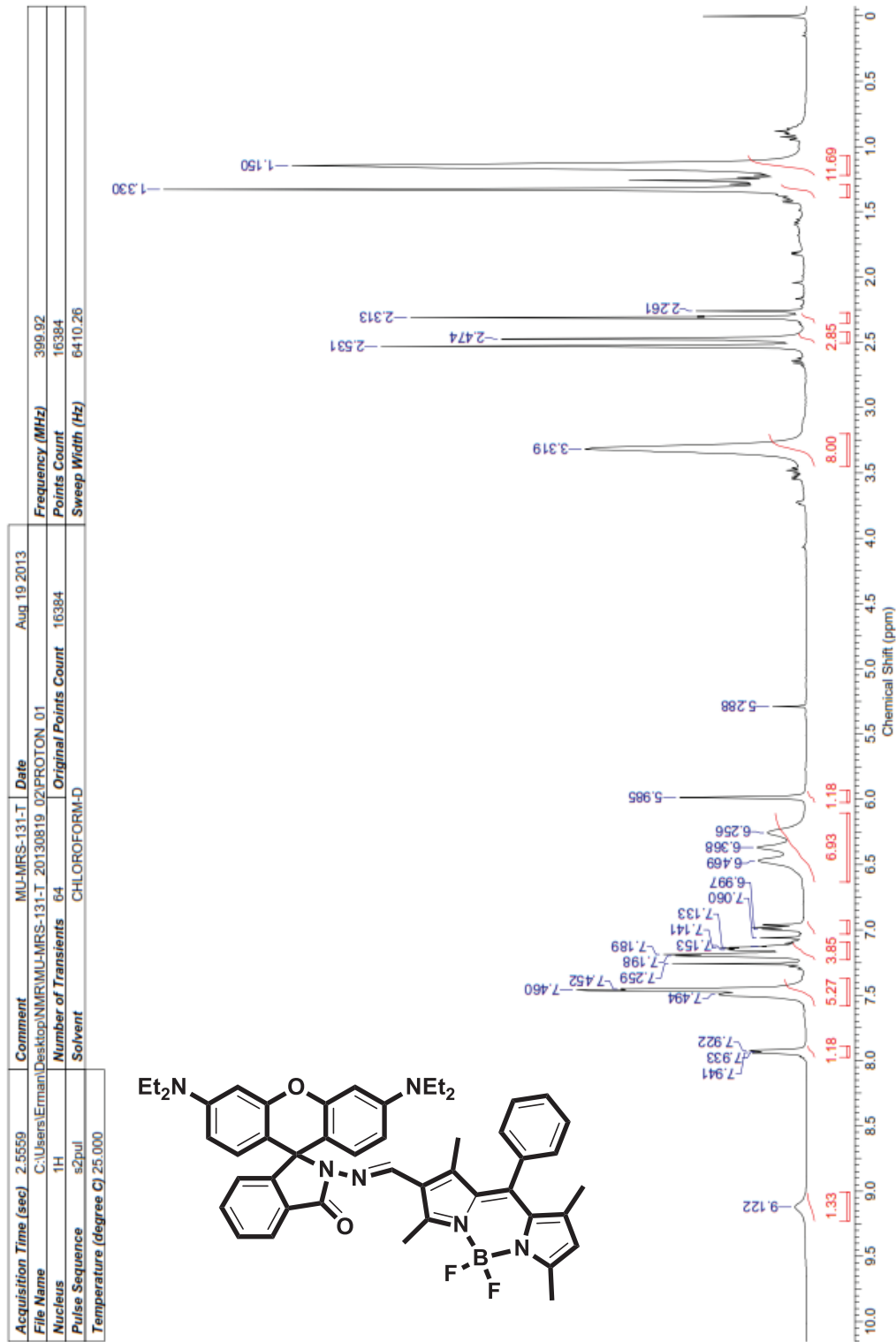


Figure A.7. <sup>1</sup>H NMR of (E)-2-(((3',6'-bis(diethylamino)-3-oxospiro[isoindoline-1,9'-xanthen]-2-yl)imino)methyl)-5,5-difluoro-1,3,7,9-tetramethyl-10-phenyl-5H-dipyrrolo[1,2-c:2',1'-f][1,3,2]diazaborinin-4-ium-5-uide

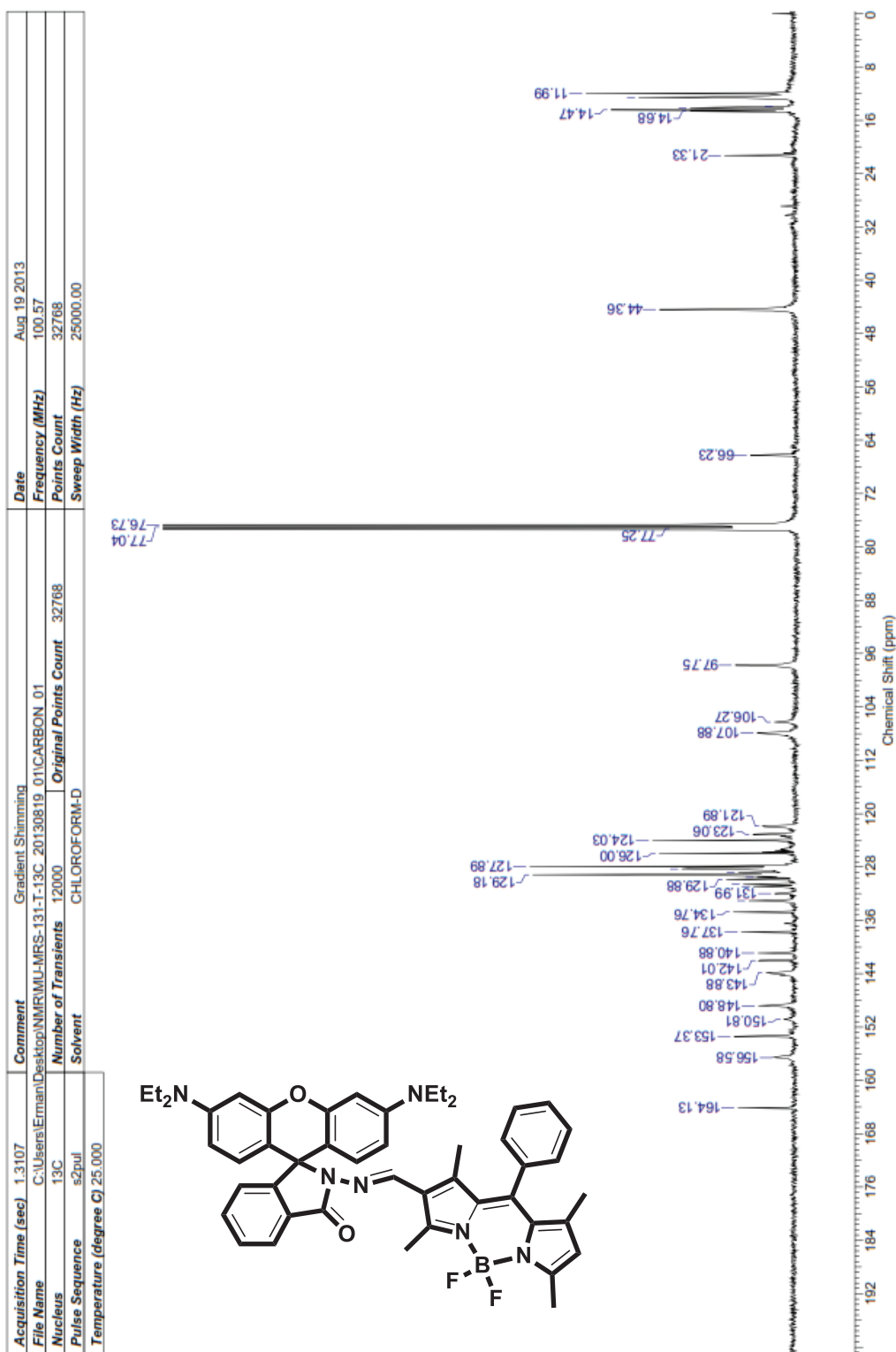


Figure A.8. <sup>13</sup>C NMR of (E)-2-(((3',6'-bis(diethylamino)-3-oxospiro[isoindoline-1,9'-xanthen]-2-yl)imino)methyl)-5,5-difluoro-1,3,7,9-tetramethyl-10-phenyl-5H-dipyrrolo[1,2-c:2',1'-f][1,3,2]diazaborinin-4-ium-5-uide

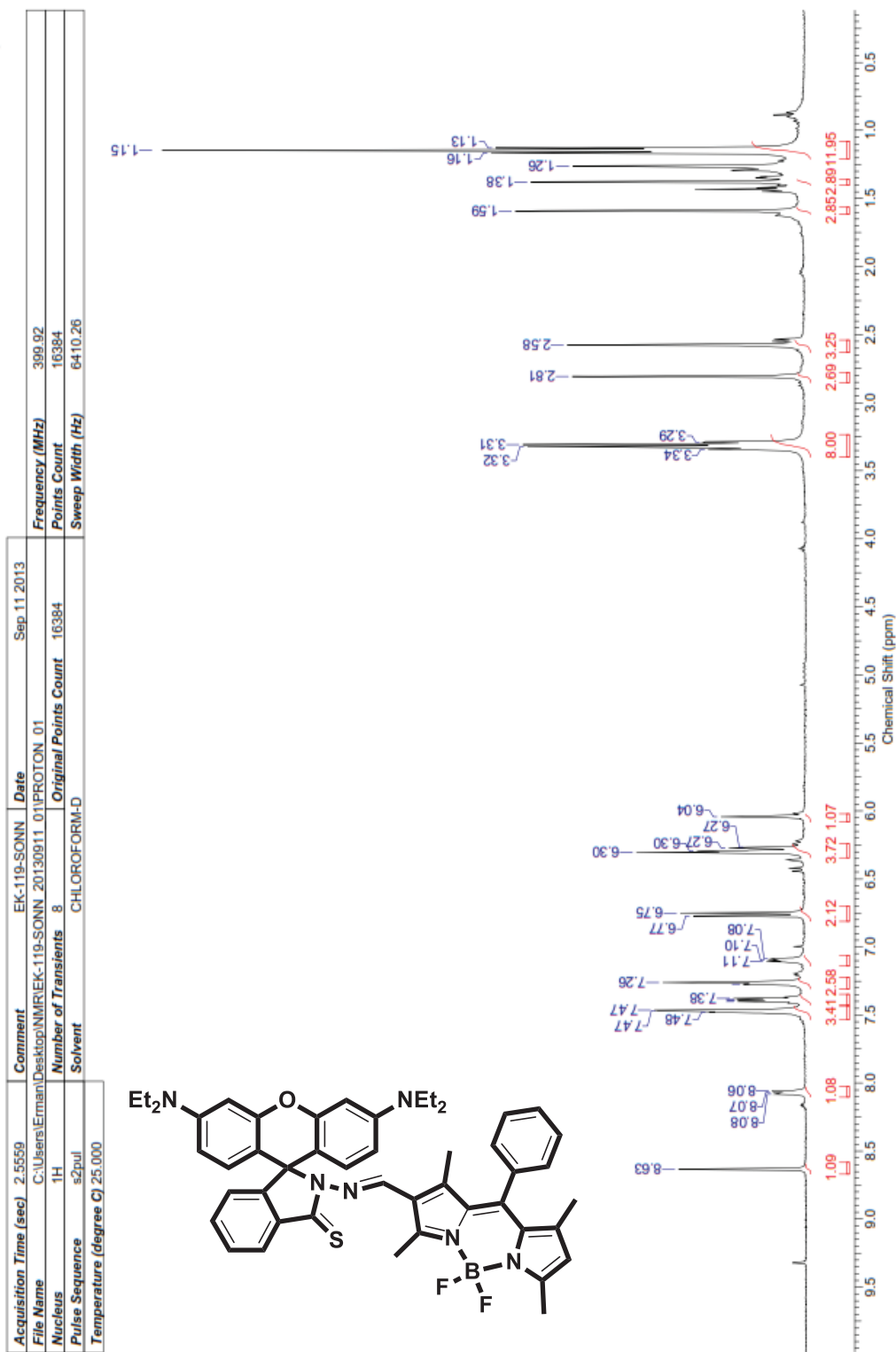


Figure A.9. <sup>1</sup>H NMR of (E)-2-(((3',6'-bis(diethylamino)-3-thioxospiro[isindoline-1,9'-xanthen]-2-yl)imino)methyl)-5,5-difluoro-1,3,7,9-tetramethyl-10-phenyl-5H-dipyrrolo[1,2-c:2',1'-f][1,3,2]diazaborinin-4-ium-5-uide

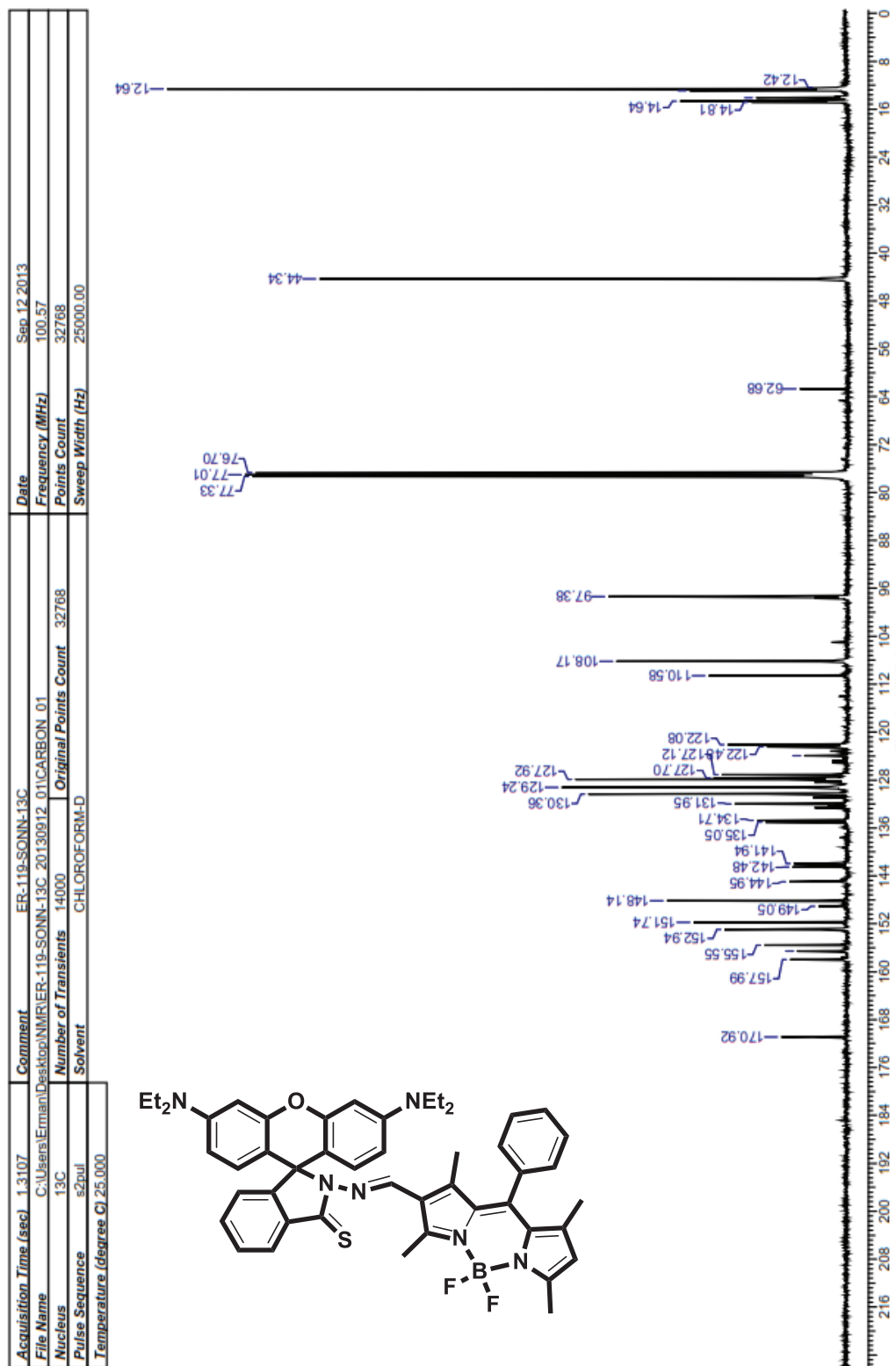


Figure A.10. <sup>13</sup>C NMR of (E)-2-(((3',6'-bis(diethylamino)-3-thioxospiro[isindoline-1,9'-xanthen]-2-yl)imino)methyl)-5,5-difluoro-1,3,7,9-tetramethyl-10-phenyl-5H-dipyrrolo[1,2-c:2',1'-f][1,3,2]diazaborinin-4-ium-5-uide

Acquisition Time (sec)	2.5659	Comment	Gradient Shimmo	Date	Jun.12.2013
File Name	C:\Users\jerman\karaku\Desktop\ERMAN PC\Belieken\Erman NMR\EK-ER-49_20130612_01\PROTON_01	Number of Transients	8	Original Points Count	16384
Nucleus	<sup>1</sup> H	Solvent	CHLOROFORM-D	Sweep Width (Hz)	6410.26
Pulse Sequence	s2pul	Frequency (MHz)	399.92	Points Count	16384
		Temperature (degree C)	25.000		

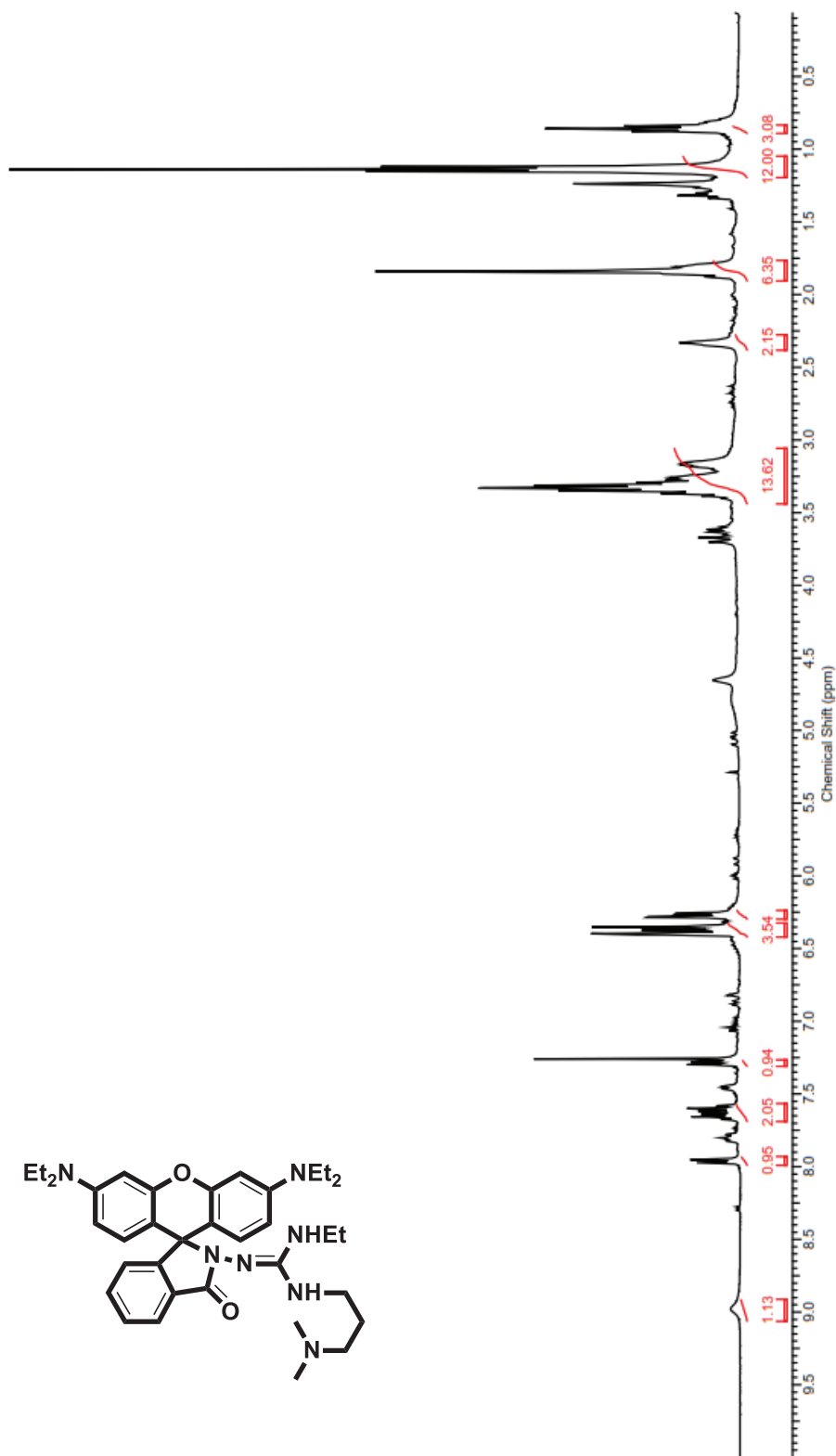


Figure A.11. <sup>1</sup>H NMR of (E)-2-(3',6'-bis(diethylamino)-3-oxospiro[isoindoline-1,9'-xanthen]-2-yl)-1-(3-(dimethylamino)propyl)-3-ethylguanidine

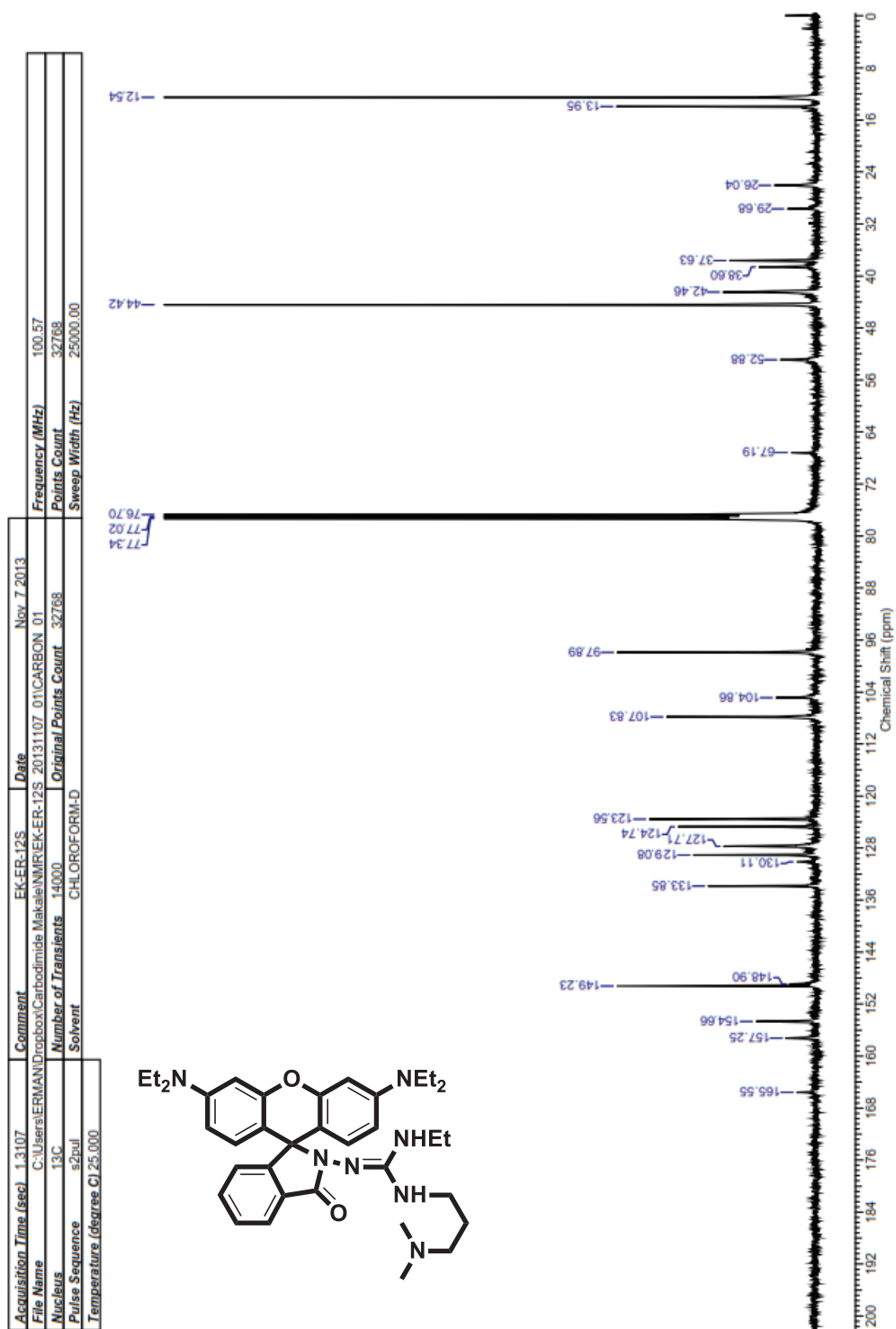


Figure A.12. <sup>13</sup>C NMR of (E)-2-(3',6'-bis(diethylamino)-3-oxospiro[isoindoline-1,9'-xanthen]-2-yl)-1-(3-(dimethylamino)propyl)-3-ethylguanidine

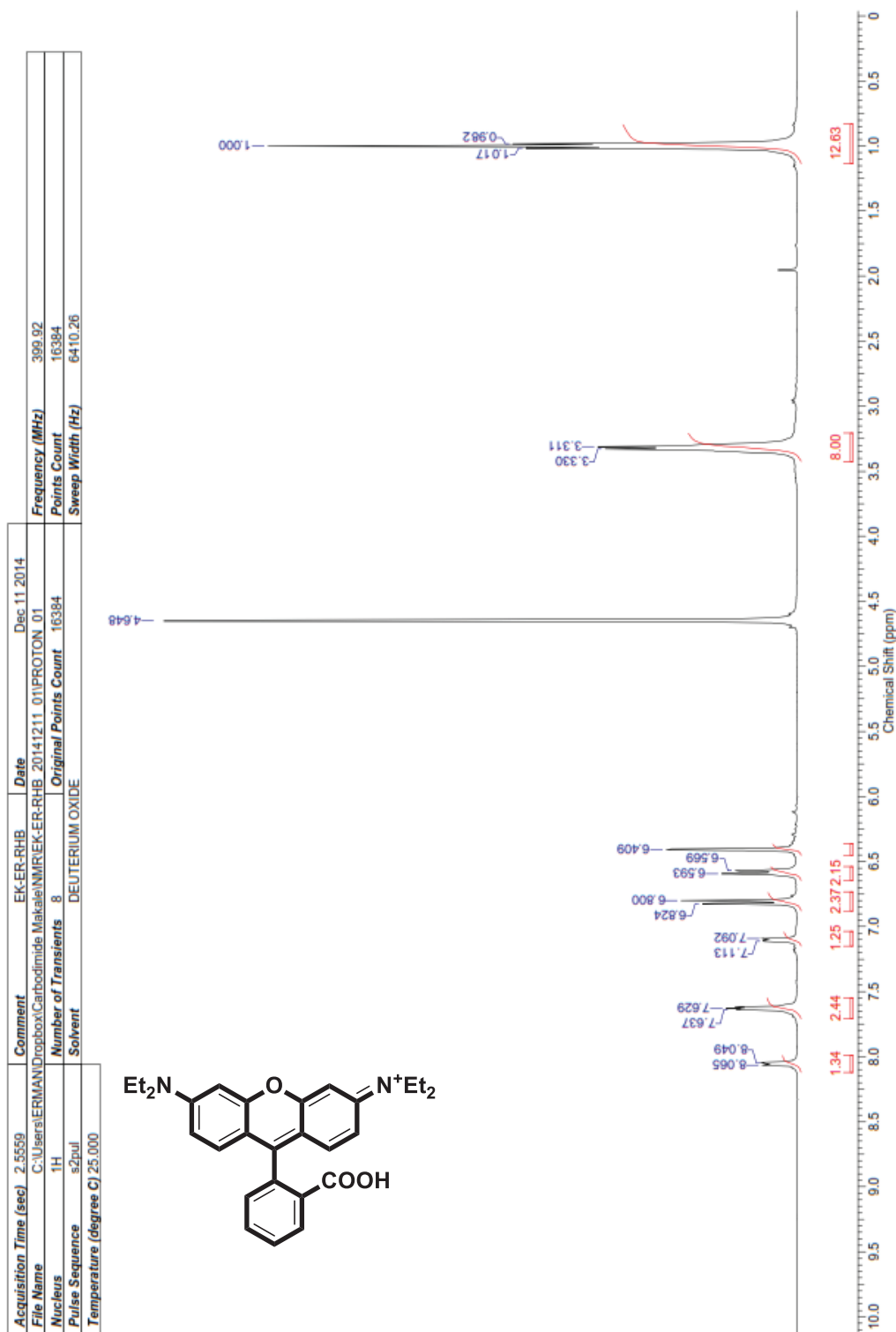


Figure A.13. <sup>1</sup>H NMR of N-(9-(2-carboxyphenyl)-6-(diethylamino)-3H-xanthen-3-ylidene)-N-ethylethanaminium



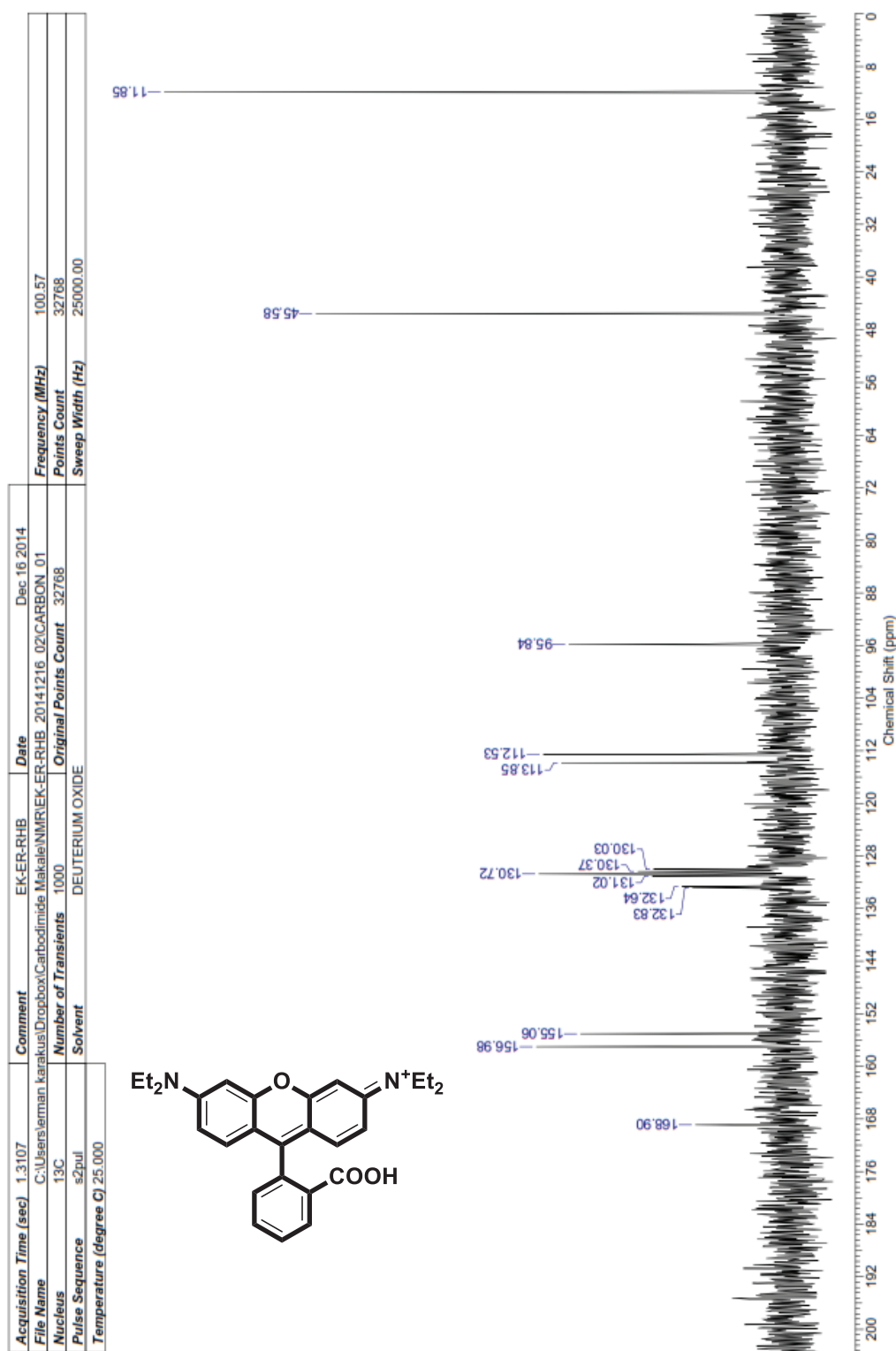


Figure A.14  $^{13}\text{C}$  NMR of N-(9-(2-carboxyphenyl)-6-(diethylamino)-3H-xanthen-3-ylidene)-N-ethylethanaminium

## **APPENDIX B**

### **MASS SPECTRA OF COMPOUNDS**

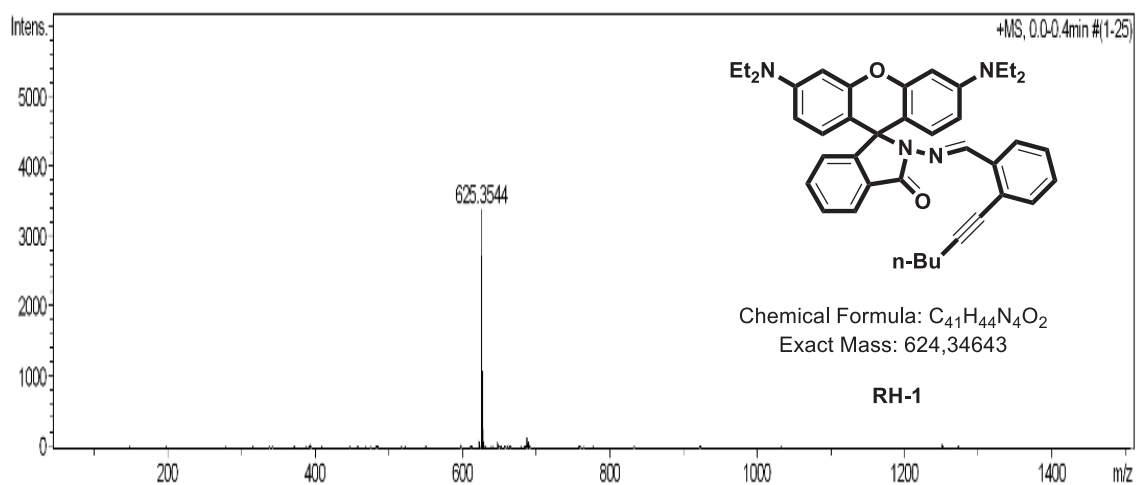


Figure B.1. ESI-TOF MS result of probe **RH-1**

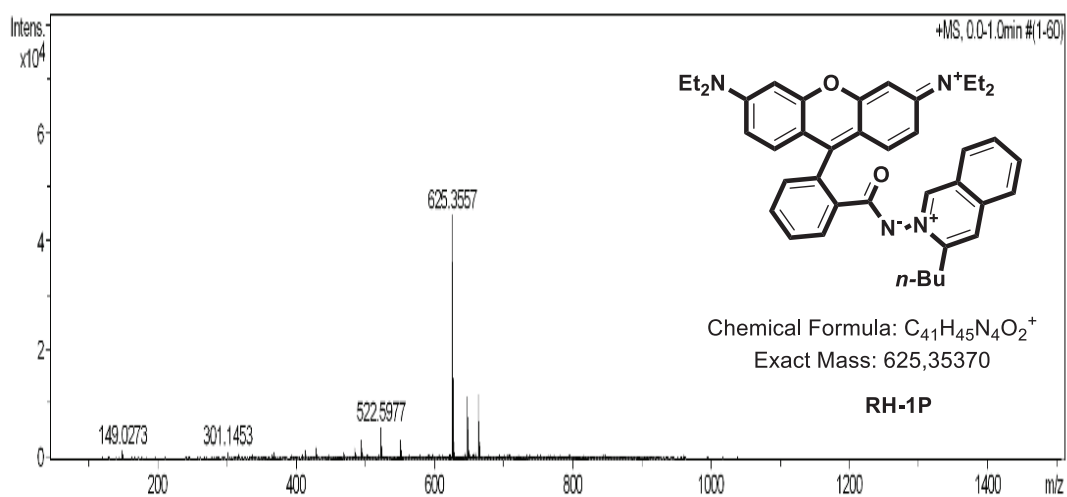


Figure B.2. ESI-TOF MS result of probe **RH-1P**

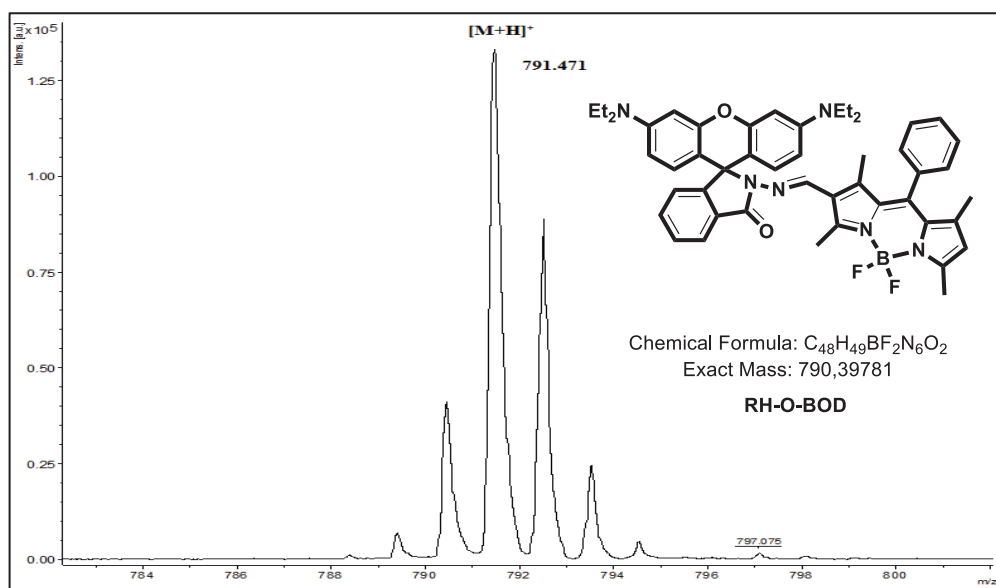


Figure B.3. MALDI-TOF MS result of probe **RH-O-BOD**

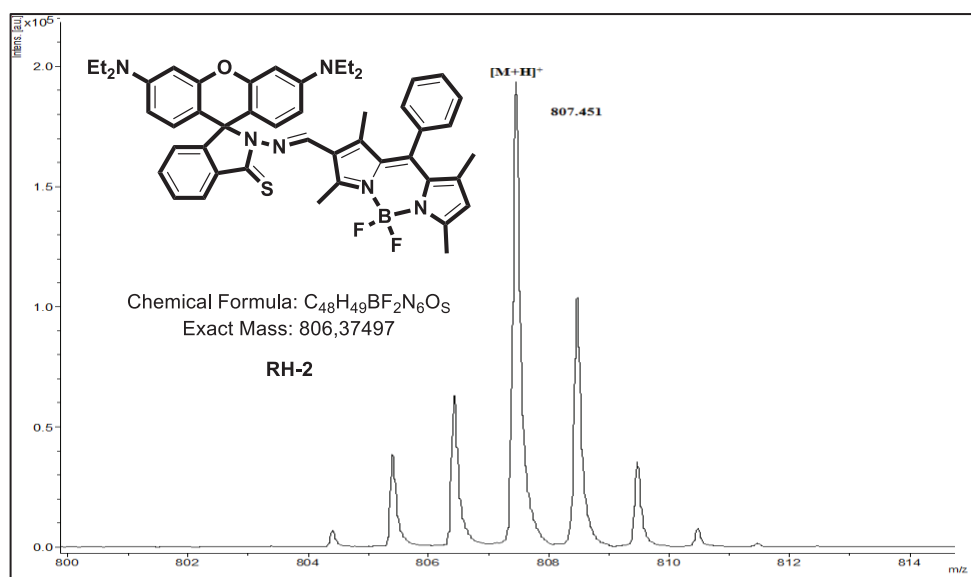


Figure B.4. MALDI-TOF MS result of probe **RH-2**

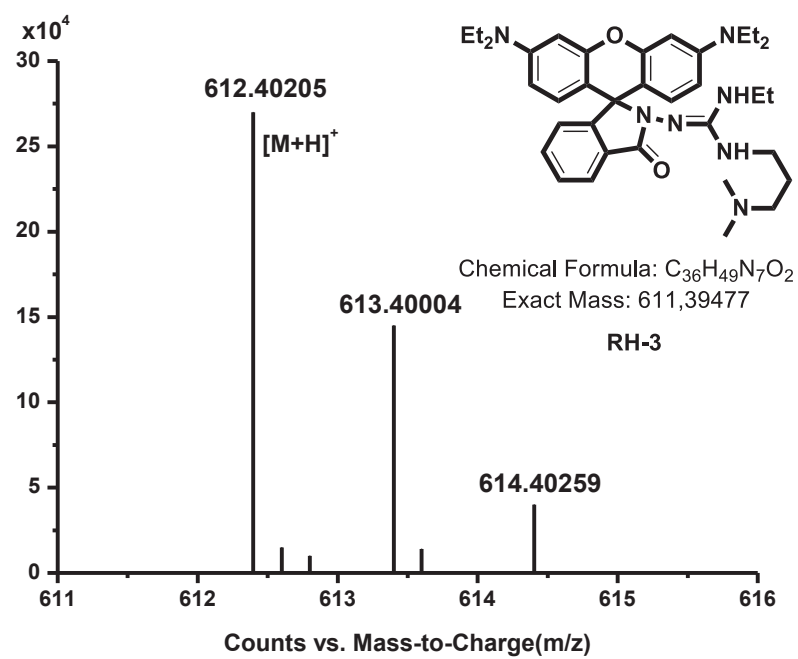


Figure B.5. HRMS result of probe **RH-3**

# VITA

## PERSONAL INFORMATION

**Surname, Name:** KARAKUŞ, Erman

**Nationality:** Turkish (T.C.)

**Date and Place of Birth:** 22.06.1987, Şarkışla/SİVAS

**Marital Status:** Married

**Phone:** (+90) 541 6397522

**E-mail:** [ermankarakus@gmail.com](mailto:ermankarakus@gmail.com)

## EDUCATION

**Degree, Institution, Year of Graduation**

PhD, İzmir Institute of Technology, 2017

MSc, İzmir Institute of Technology, 2011

BSc, İzmir Institute of Technology, 2009

## WORK EXPERIENCE

2009 – 2017 İzmir Institute of Technology Teaching and Research Assistant

2008 İzmir District Office/Laboratory National Hygiene Institute, Trainee

## FOREIGN LANGUAGE

English (Advanced)

## PUBLICATIONS

1. Üçüncü M., Karakuş E., Kuş M., Akpınar G. E., Aksın-Artok Ö., Karaca S., Elmacı N. and Artok L. *J. Org. Chem.*, 2011, 76, 5959.
2. Akpınar G. E., Kuş M., Üçüncü M., Karakuş E., Artok L. *Org. Lett.*, 2011, 13, 748.
3. Emrulloğlu M., Karakuş E. and Üçüncü M. *Analyst*, 2013, 138, 3638.
4. Emrulloğlu M., Üçüncü M. and Karakuş E. *Chem. Commun.*, 2013, 49, 7836.
5. Karakuş E., Üçüncü M., Eanes R. and Emrulloğlu M. *New J. Chem.*, 2013, 2632.
6. Karakuş E., Üçüncü M. and Emrulloğlu M. *Chem. Commun.*, 2014, 50, 1119.
7. Karakuş E., Çakan G. and Emrulloğlu M. *Anal. Methods*, 2015, 7, 8004.
8. Üçüncü M., Karakuş E. and Emrulloğlu M. *Chem. Eur. J.*, 2015, 21, 13201.
9. Üçüncü M., Karakuş E. and Emrulloğlu M. *New J. Chem.*, 2015, 39, 8337.
10. Karakuş E., Üçüncü M. and Emrulloğlu M. *Anal. Chem.*, 2016, 88, 1039.
11. Horzum N., Mete D., Karakuş E., Üçüncü M., Emrulloğlu M. and Demir M. M. *ChemistrySelect*, 2016, 1, 896.
12. Çetintaş C., Karakuş E., Üçüncü M. and Emrulloğlu M. *Sens. Actuators B*, 2016, 234, 109.
13. Üçüncü M., Karakuş E. and Emrulloğlu M. *Chem. Commun.*, 2016, 52, 8247.
14. Üçüncü M., Cantürk C., Karakuş E., Zeybek H. Bozyaka U., Soydaş E., Şahin E. and Emrulloğlu M. *Org. Biomol. Chem.*, 2016, 14, 7490.
15. Üçüncü M., Karakuş E., Demirci-Kurulgan E., Sayar M., Dartar S. and Emrulloğlu M. *Org. Lett.*, 2017, 19, 2522.
16. Kırpat İ., Göksel Y., Karakuş E., Emrulloğlu M., Akdoğan Y. *Materials Letters*, 2017, 205, 48.

## AWARDS

Honor Student of İzmir Institute of Technology (2009)

Second Highest-Ranking Student of the Department (2009)

TUBITAK National Scholarship Program for PhD Students (2012-2016)

Best Poster Awards at XIV European Symposium on Organic Reactivity- Prague (2013)